2011

DESIGN, VALIDATION AND NAVIGATION OF ANATOMIC POPULATION- BASED AND PATIENT-SPECIFIC RADIAL HEAD IMPLANTS

Simon Robert Deluce

DESIGN, VALIDATION AND NAVIGATION OF ANATOMIC POPULATION-BASED AND PATIENT-SPECIFIC RADIAL HEAD IMPLANTS

(Spine title: Design, Validation and Navigation of Anatomic Radial Head Implants)

(Thesis Format: Integrated-Article)

By

Simon R. Deluce

Graduate Program in Biomedical Engineering

2

A thesis submitted in partial fulfillment
Of the requirements for the degree of
Master of Engineering Science

The School of Graduate and Postdoctoral Studies
The University of Western Ontario
London, Ontario, Canada

THE UNIVERSITY OF WESTERN ONTARIO
SCHOOL OF GRADUATE AND POSTDOCTORAL STUDIES

CERTIFICATE OF EXAMINATION

Co-Supervisors

J.A. Johnson, PhD, PEng
Department of Mechanical and Materials Engineering
Biomedical Engineering Graduate Program
Department of Surgery

G.J.W. King, MD, Msc, FRCSC
Department of Surgery
Department of Medical Biophysics

Examiners

P.B. Canham, PhD

K.J. Faber, MD, MHPE, FRCSC

O.R. Tutunea-Fatan, PhD

This thesis by

Simon Robert Deluce

Entitled:

Design, Validation and Navigation of Anatomic Population-Based and Patient-Specific Radial Head Implants

is accepted in partial fulfillment of the
requirements for the degree of
Master of Engineering Science

Date_____

_____
Chair of the Thesis Examination Board

ABSTRACT

Radial head replacement for fractures and arthritis are commonly performed; however, most available implants do not accurately replicate the complex native anatomy. This work examines the creation and surgical implantation of an anatomic implant system. Radial head morphology was parameterized using ellipse fitting to allow reverse engineering of the shape (n=50). Using the derived parameters, anatomic implants were generated for both a population "average" and patient-specific designs. Mean surface mismatch between these implant models and the native morphology was compared to an existing axisymmetric implant (n=34). Anatomic designs showed reduced mismatch relative to the existing implant with the anatomic patient-specific design performing best. A surgical navigation system was developed and tested for implant alignment. The mean placement accuracy and standard deviation was 1.5±0.5mm in translation and 1.2±1.0°, 1.4±1.8°and 5.5±3.2° in rotation about the lateral, anterior and proximal axes respectively (n=7). These studies demonstrate the feasibility of anatomic radial head implant designs; however, further work is required to improve placement accuracy.

Keywords: elbow, radial head, arthroplasty, morphology, implant design, computer-assisted orthopaedic surgery, patient-specific

CO-AUTHORSHIP

Chapter 1:	Simon Deluce	-	sole author
Chapter 2:	Simon Deluce	-	study design, data collection, analysis, wrote manuscript
	Hannah Shannon	-	study design, data collection
	Louis Ferreira	-	study design
	James Johnson	-	study design, reviewed manuscript
	Graham King	-	study design, reviewed manuscript
Chapter 3:	Simon Deluce	-	study design, data collection, analysis, wrote manuscript
	Hannah Shannon	-	data collection
	James Johnson	-	study design, reviewed manuscript
	Graham King	-	study design, reviewed manuscript
Chapter 4:	Simon Deluce	-	study design, data collection, analysis, wrote manuscript
	Hannah Shannon	-	specimen preparation, data collection
	Emily Lalone	-	study design , data collection
	Louis Ferreira	-	study design, data collection
	James Johnson	-	study design, reviewed manuscript
	Graham King	-	study design, specimen preparation, performed surgeries, reviewed manuscript
Chapter 5:	Simon Deluce	-	sole author

ACKNOWLEDGEMENTS

Without the encouragement, assistance and support of many people this thesis would not have been completed. It was often noted the radial head team meetings grew to encompass almost everyone in the lab. This project was a true team-effort.

Foremost I would like to thank my supervisors Dr. Jim Johnson and Dr. Graham King. Their shared passion for research was a constant source of inspiration throughout these last two years. They ensured that the work was challenging but also that I was given the resources, time and assistance I needed to succeed. Thank you.

I would like to thank all of my colleagues who made working in the lab such an enjoyable experience. I could not have completed the work detailed in this thesis without the constant help of my research partner Hannah Shannon, my only company through some of our longer testing days. Louis Ferreira was an invaluable mentor when facing many challenges throughout this project and often the first sounding board for my ideas. Emily Lalone, our "registress" was responsible for helping me find my way in VTK, a daunting task. Josh Giles is the one responsible for introducing me, via our fourth year project, to the lab and has been a constant source of help and advice. Finally, Ryan Katchky completed the preliminary investigation which served as a starting point for my own work. Thank you all.

I would also like to thank the various residents with whom I have had the privilege of working: Bashar Alolabi, Sagar Desai, Brent Lanting, Alex Leclerc and Marlis Sabo. Also, thank you to Dr. George Athwal who was always eager to discuss my project and share his insight.

Thanks also to Chris Vandelaar and the other staff at UMS who provided valuable insight and assistance during the construction of the implant system.

I would like to thank my friends and family who have been a constant source of support over these last two years. My friends David Edey and CJ Vitanza are responsible for making sure that even when I did not think I had time to spend an evening out, I did, and I thank them for it. Thank you to my siblings for putting up with my busy schedule. I'm happy to be staying in London for the next four years so that I can (hopefully) make up for it! Thank you to my Mom and Dad who are constantly supportive, even if it meant a skype conversation in the wee hours of the morning or taking me across the country for my medical school interviews. I always had family dinners together on Sunday with all of you to look forward to at the end of the week which helped to keep me well balanced and well fed.

Lastly, I would like to thank my girlfriend Danielle Brewer who over the last two years has become an increasingly important person in my life. Danielle was the first to see these chapters and they were always improved with the help of her feedback, graphical prowess and diligent editing. For your encouragement, selflessness and support, especially over these last four months, I will always be grateful.

TABLE OF CONTENTS

LIST OF FIGURES

Appendices

LIST OF TABLES

LIST OF APPENDICES

CHAPTER 1 - Introduction

OVERVIEW:

The overall goal of this thesis is to develop a computer-assisted navigation system for radial head arthroplasty and assess the accuracy of implant placement using novel anatomic implants designed around measured morphologic parameters. This chapter provides an introduction to elbow anatomy and function with a particular focus on the radial head. An overview of radial head treatment options and implant designs are also presented. A description of Computer Assisted Orthopedic Surgery (CAOS) techniques and technology relevant to this thesis work is provided. The project objectives, hypotheses, rationale and thesis outline are also summarized.

1.1 THE ELBOW

The elbow is composed of three articulations which function to position the hand in space. The joint itself allows two degrees of freedom, flexion/extension and pronation/supination as shown in Figure 1.1. A combination of muscles, ligaments, bony restraints and highly congruous articular surfaces serve to ensure elbow stability. Loss of elbow mobility or stability "is extremely limiting to the activities of daily living"[1].

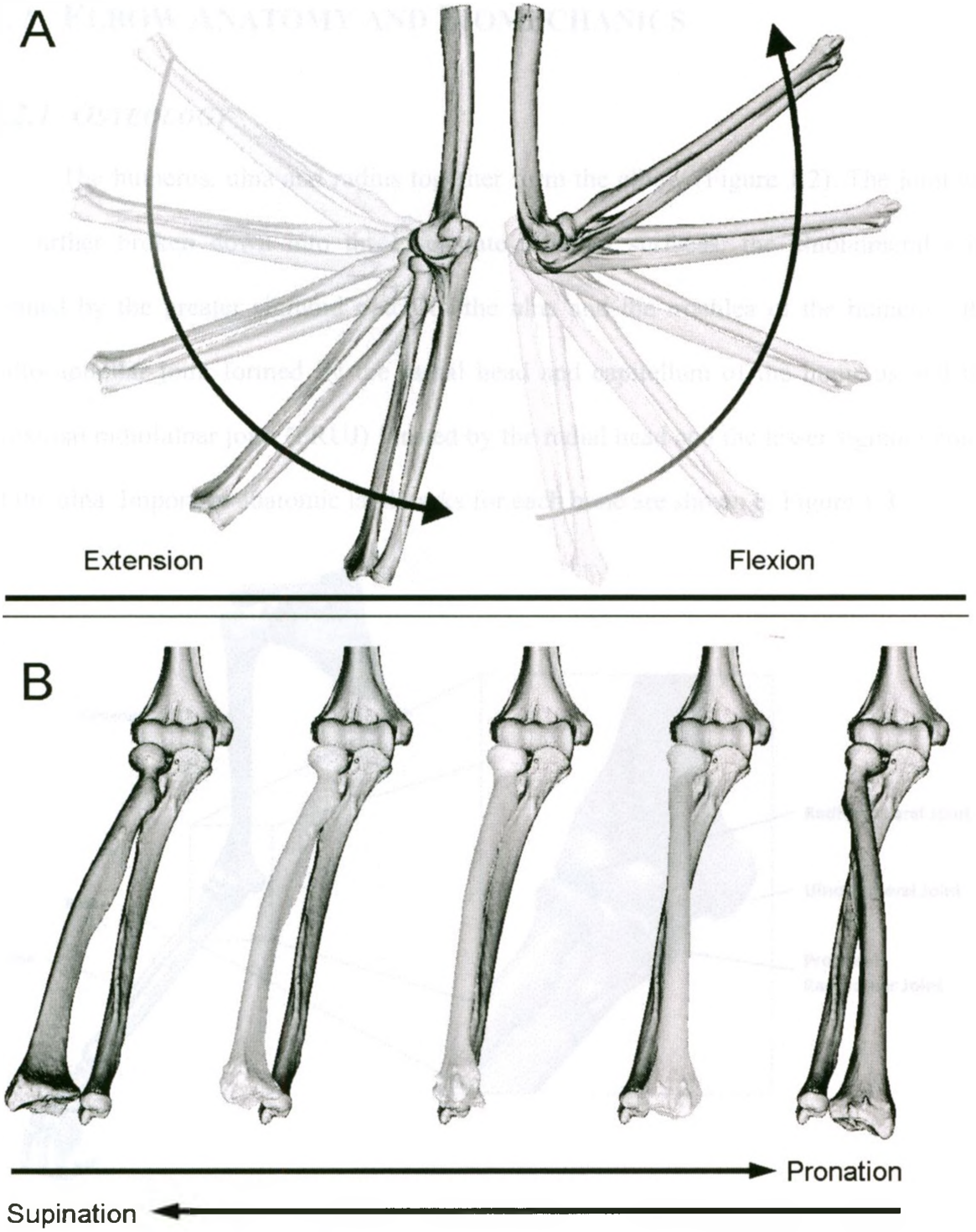

Figure 1.1: Motions of the Elbow

A) Elbow flexion and extension
B) Forearm supination and pronation
© HULC

1.2 Elbow Anatomy and Biomechanics

1.2.1 Osteology

The humerus, ulna and radius together form the elbow (Figure 1.2). The joint can be further broken down into three separate articular surfaces: the ulnohumeral joint formed by the greater sigmoid notch of the ulna and the trochlea of the humerus, the radiocapitellar joint formed by the radial head and capitellum of the humerus and the proximal radiolulnar joint (PRUJ) formed by the radial head and the lesser sigmoid notch of the ulna. Important anatomic landmarks for each bone are shown in Figure 1.3.

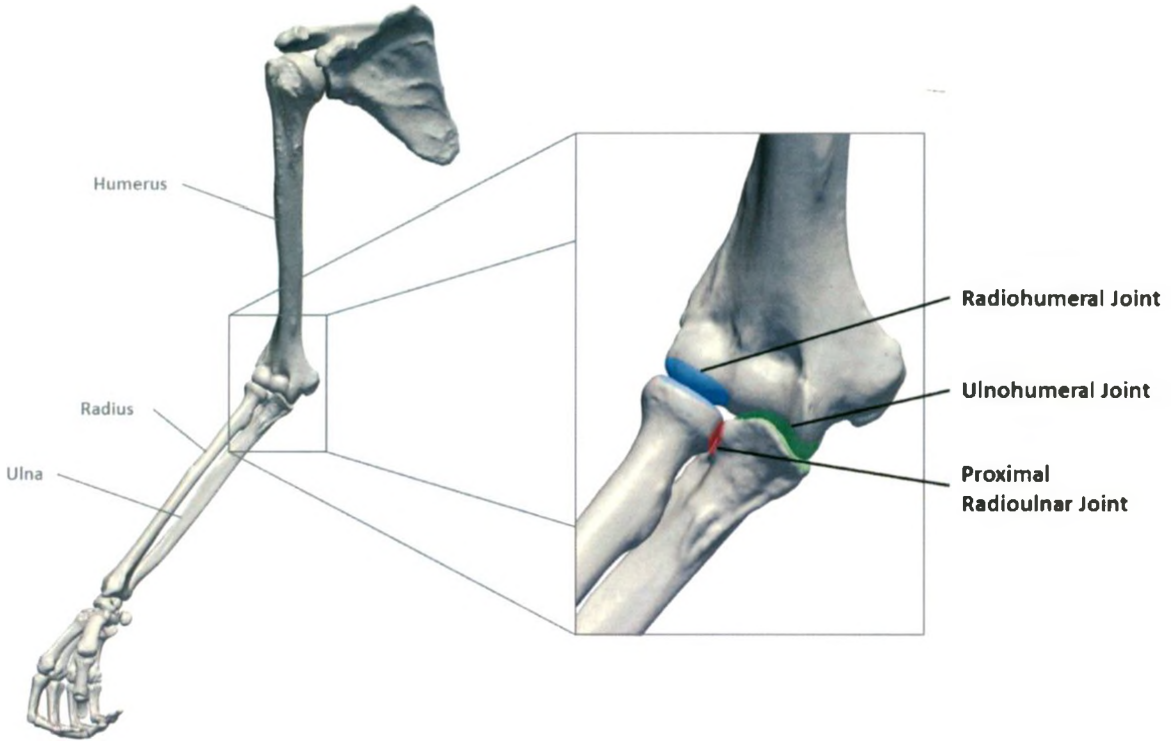

Figure 1.2: The Elbow

Overview of a right elbow showing the radiohumeral, ulnohumeral and proximal radioulnar articulations.

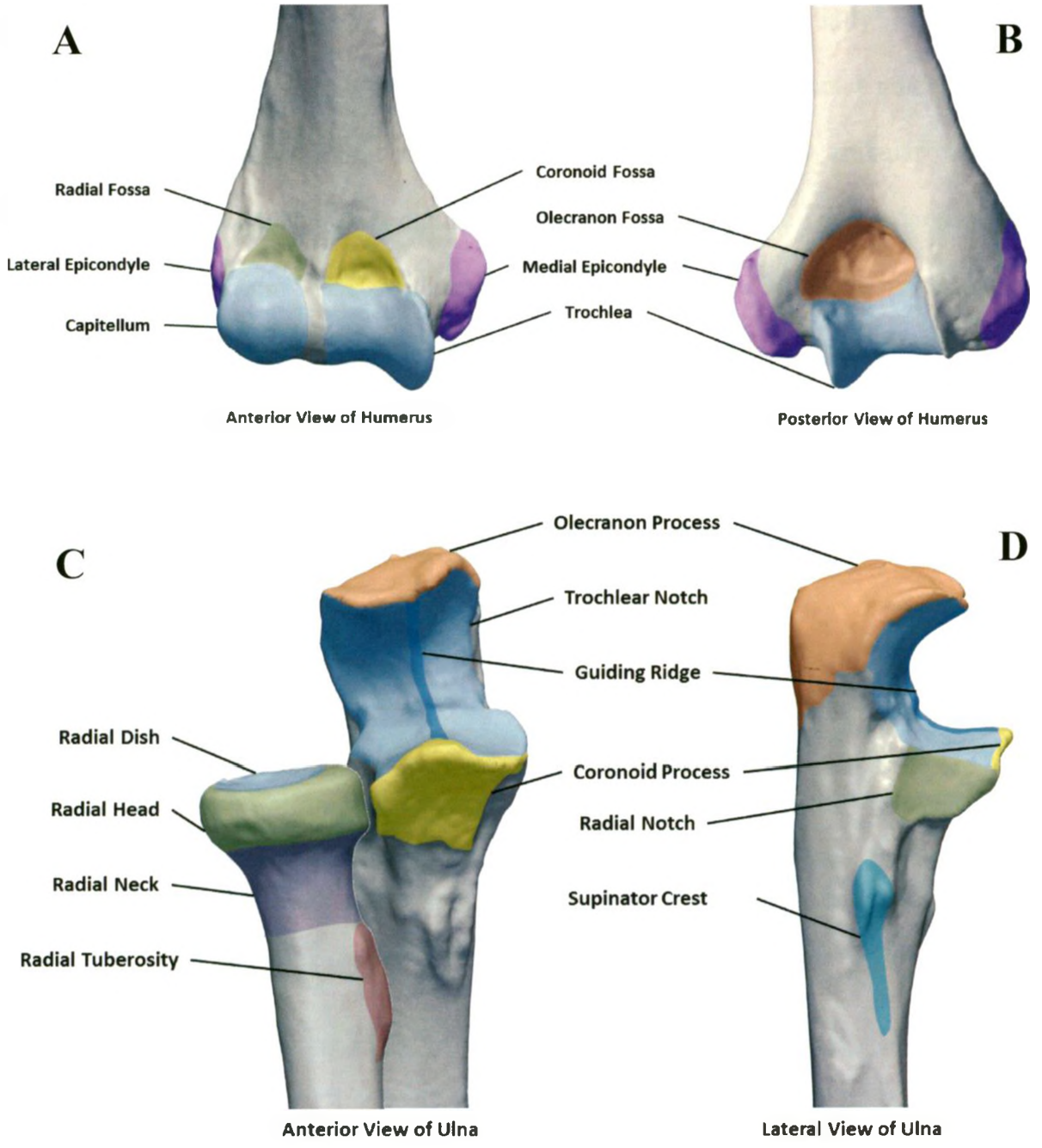

Figure 1.3: Osseous Structures of the Elbow

Significant features of the distal humerus showing an anterior (A) and posterior (B) views and the ulna and radius showing an anterior (C) and lateral (D, radius excluded) views.

The radial head is a complex structure as detailed in Figure 1.4. The circumference is non-circular and is both offset and tilted relative to the radial neck[2,3]. The mean tilt was

measured at 2.50° away from the radial tuberosity and 9.5° medially[3]. The radial circumference is broad and flattened where it articulates with the radial notch, and is more curved and narrow in the non-articular region. It is covered by articular cartilage over approximately 240°of its circumference corresponding to the contact area of the proximal radioulnar joint[4]. The radial dish is shifted in the direction of the major axis of the radial circumference leading to the translations observed during forearm rotation shown in Figure 1.5[2,5-7]. The capitellum, with which the radial dish articulates, has been shown to be ellipsoidal rather than spherical in shape[8]. Throughout the entire range of flexion the radial dish contacts the surface of the capitellum[9,10].

1.2.2 Capsules and Ligaments

The joint capsule encloses the elbow joint and contains synovial fluid to provide lubrication. Anteriorly the capsule extends from the annular ligament and the articular edge of the coronoid process to the proximal edge of the radial and ulnar fossae. Posteriorly it extends from both the annular ligament and the medial and lateral edges of the sigmoid notch to the proximal edge of the olecranon fossa. The major ligaments of the elbow joint are formed of thickenings of the joint capsule and can be divided into the medial and lateral collateral ligaments which are both shown in Figure 1.6.

The medial collateral ligament (MCL) is the primary elbow stabilizer against valgus forces[11]. It originates on the medial epicondyle and inserts into the medial margin of the coronoid at the sublime tubercle. The lateral collateral ligament (LCL) is subdivided into the radial collateral ligament (RCL), annular ligament and the lateral ulnar collateral ligament (LUCL). The LCL becomes slack if the radial head is excised increasing varus laxity[12].

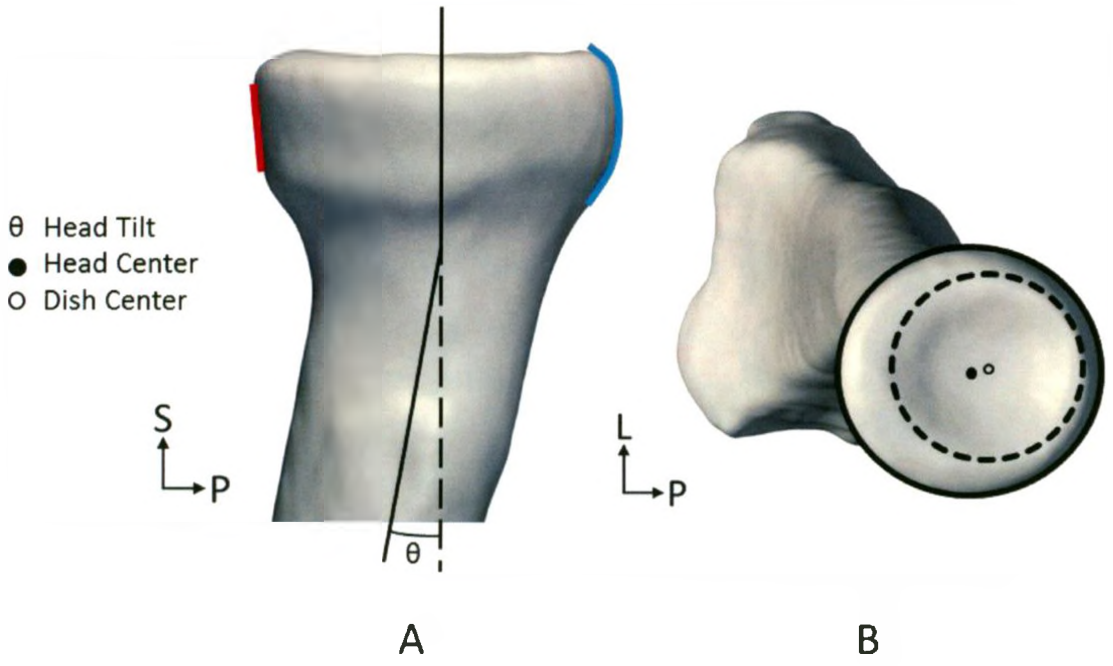

Figure 1.4: Features of the Radial Head

A) Medial view of radius showing the differences between the non-articular (blue) and articular (red) circumferential profile and the tilt (θ) between the head and the long axis of the radius.

B) Superior view showing the slight posterior offset of the dish center relative to the center of the head circumference at its widest point as well as the non-circular shape of the both the dish and head.

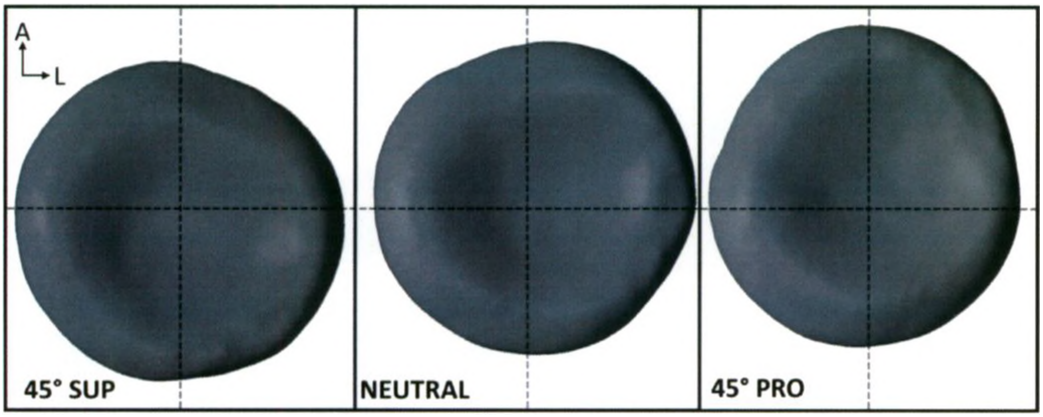

Figure 1.5: The Effect of Dish Offset

The radial head translates anteriorly during pronation and posteriorly during supination of the forearm. The dashed lines show the same fixed axes as the radial head is rotated.

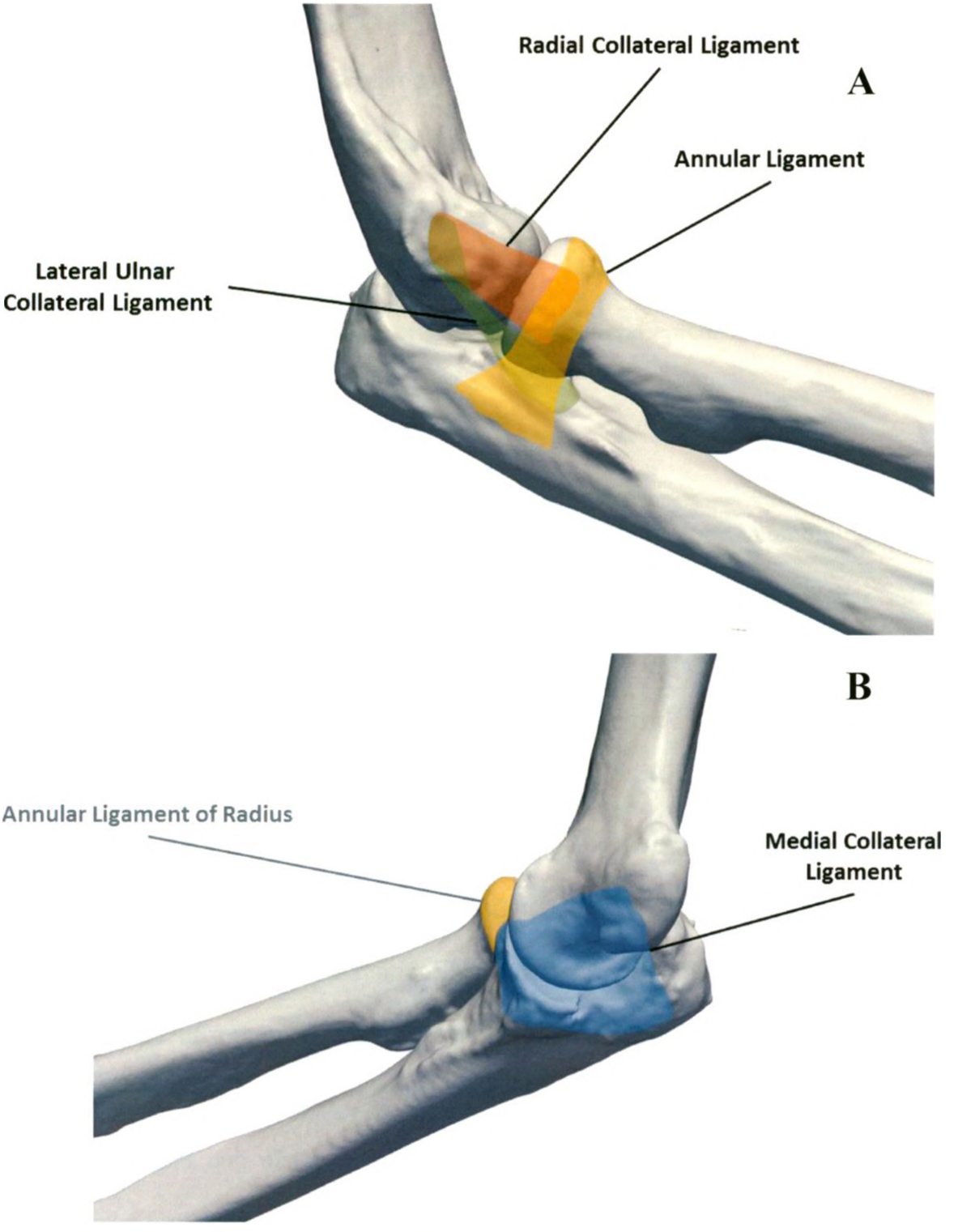

Figure 1.6: Ligaments of the Elbow

Lateral (A) and medial (B) views of the elbow and the respective collateral ligament complexes. The annular ligament (yellow) is shown in (b) for reference but is not part of the medial collateral ligament complex.

The annular ligament envelops the radial head[13,14] and maintains contact between the proximal radius and ulna. The radial collateral ligament (RCL) originates from a point on the lateral epicondyle in line with the flexion/extension axis of the elbow and inserts into the annular ligament[14,15]. It serves as a primary elbow stabilizer against varus forces[16]. The lateral ulnar collateral ligament (LUCL) serves as an important posterolateral rotational stabilizer[15]. It originates at the lateral epicondyle and inserts into the supinator crest of the ulna.

1.2.3 Kinematics And Load Transfer

The elbow joint is classified as a trochoginglymoid joint, combining hinge (ginglymus) and pivot joints (trochoid). The ulnohumeral and radiocapitellar joints function together as the hinge to allow elbow flexion and extension as shown in Figure 1.1. The flexion/extension axis of the elbow can be approximated by a line connecting the center of the trochlear groove and the center of the capitellum[17]. Although the flexion/extension axis is often described as a fixed line, studies have shown that the instantaneous joint axis varies across the flexion range, acting as a "sloppy hinge," especially at the extremes of the motion, and is affected by muscle forces across the joint[18]. The range of motion in extension and flexion is approximately 0° to 140-145° respectively[19].

The proximal and distal radioulnar joints allow the radius to rotate about the relatively fixed ulna enabling axial forearm rotation which is also shown in Figure 1.1. The rotation axis for the forearm can be approximated by a line connecting the center of the radial dish head and the ulnar styloid[20]. Earlier studies have shown that the ulna does rotate internally and externally at the extremes of pronation and supination respectively,

complicating the previously simplified model of the joint [21,22]. This finding has not been confirmed by more recent studies[7,23]. A screw-home mechanism has also been described in which the radius shifts 1-2mm proximally as it pronates[10]. The typical range of motion in pronation and supination is approximately 70° and 85° respectively[19].

It has been suggested that approximately 60% of the axial load along the forearm passes through the radius and the remainder through the ulna when statically loaded in full extension[24]. Using a load cell at the proximal radius, the maximum load measured at 90% bodyweight was determined to occur in full extension and pronation due to a combination of the poor mechanical advantage for flexion and the screw-home mechanism[10]. Load sharing patterns vary depending on the varus/valgus alignment from 7% to 88% of load passing through the radius[25]. The central band of the interosseous membrane between the ulna and radius plays a role in transferring load from the radius to the ulna, and as a secondary restraint in preventing proximal migration and maintaining the spacing of the forearm bones when under axial compression[26].

1.2.4 Elbow Stability

Highly congruous articular surfaces and soft-tissue constraints make the elbow one of the most stable joints in the body. The contribution of each soft-tissue and osseous structure in resisting varus and valgus forces has been studied through progressive sectioning/excision. The relative contributions of each structure in resisting varus and valgus forces are shown in Table 1.

The coronoid process is the most important articular constraint in the elbow especially if the radial head has been excised. During flexion and extension the coronoid

resists posterior displacement acting as a primary stabilizer. Loss of more than 50% of the coronoid may lead to elbow subluxation[27,28].

Table 1.1: Percent Contributions of Restraining Varus-Valgus Displacement[29]

Position	Component	Varus	Valgus
Extension	MCL	-	30
	LCL	15	-
	Capsule	30	40
	Articulation	55	30
Flexion (90 deg)	MCL	-	55
	LCL	10	-
	Articulation	75	35

The radial head serves as an important secondary valgus stabilizer, most notably in the presence of MCL injury[28]. As mentioned previously it also acts to tension the LCL and its excision contributes to the development of posterolateral rotary instability[30].

The olecranon is the least important osseous constraint from the perspective of elbow stability. As much as 50% may be excised before a clinically relevant change in function is present[28]. Stability decreases linearly with progressive removal of the olecranon[31].

1.3 RADIAL HEAD FRACTURE

The radial head is the site of approximately one third of elbow fractures[32]. Concomitant elbow injuries are present in a quarter of these fractures[33]. Radial head fractures occur at all ages, with a mean age between 40 and 50 years, and equal incidence in males and females[33]. Male patients have more severe fracture types and a higher incidence of associated injuries.

1.3.1 MECHANISM

The most common mechanism of radial head fractures is thought to be an axial load while the forearm is in full pronation [34]. Fractures are most frequently located in the anterior portion of the radial head. This mechanism may be further explained by the reduced density of bone on the non-articulating side of the radius which may increase its vulnerability to fracture[35,36]. In addition to failure of the radial head, concomitant injuries of the elbow and forearm ligaments are common. Disruption of the collateral ligaments or interosseous membrane should be suspected, particularly in more severe fractures caused by high-energy mechanisms where the incidence of associated injuries may be as high as 75-100%[33,37]. Associated osseous injuries are also more common for severe fractures of the radial head, specifically fractures of the coronoid, olecranon and capitellum[33,38].

1.3.2 CLASSIFICATION

Mason described a system for the classification of radial head fractures in 1954 which is the most common system in current use[39]. Fractures were described as marginal/fissure undisplaced (Type I) or displaced (Type II) or comminuted involving the whole head (Type III) (Figure 1.7). This classification was expanded by Johnston in 1962 to include fractures associated with an elbow dislocation (Type IV)[32].

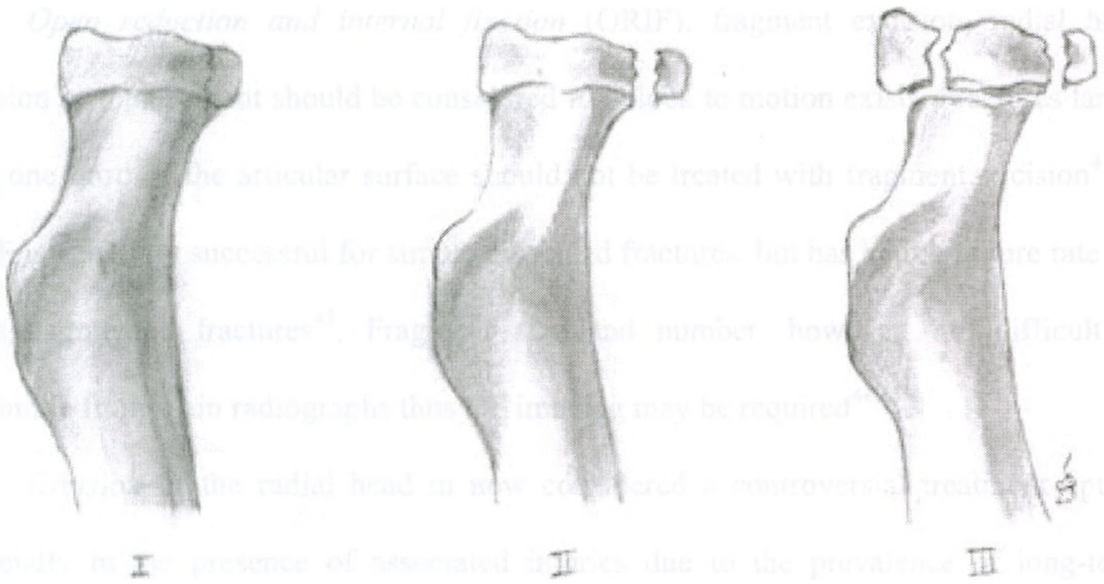

Figure 1.7: The Mason Classification System

I) Nondisplaced fracture
II) Displaced fracture
III) Comminuted fracture

1.3.3 TREATMENT OPTIONS

The treatment for radial head fractures has changed significantly over the previous century. In 1954 the axiom described by Mason was "If in doubt – resect" whereas Johnston in 1962 advised "If in doubt, treat conservatively"[32,39]. The current mindset advocates different treatment options based on the severity of the fractures and the associated injuries present. For operative treatment the current axiom would best be described as repair if possible - else replace.

Non-operative treatment is favored for Mason Type I fractures and Mason Type II fractures with minimal displacement as long as there is no block to motion[40]. Early active motion is advised in the treatment of these fractures in order to prevent elbow stiffness. For displaced and comminuted fractures with associated injuries, operative treatment should be considered to restore elbow stability and prevent further complications.

Open reduction and internal fixation (ORIF), fragment excision, radial head excision or replacement should be considered if a block to motion exists. Fractures larger than one third of the articular surface should not be treated with fragment excision[41,42]. ORIF is generally successful for simple displaced fractures, but has a high failure rate for multi-fragmented fractures[43]. Fragment size and number, however, are difficult to determine from plain radiographs thus CT imaging may be required[44,45].

Excision of the radial head in now considered a controversial treatment option especially in the presence of associated injuries due to the prevalence of long-term complications including instability, diminished strength, osteoarthritis of the ulnohumeral joint (likely due to increased loading), cubitus valgus and proximal radius migration with associated pain at the wrist[40,46,47]. Excision may be considered in the unusual case of an isolated but unrepairable comminuted fracture of the radial head; however, as discussed, this rarely occurs without damage to the surrounding soft-tissue and osseous structures.

Radial head arthroplasty has shown promising mid-term results in restoring normal joint function in the case of severely comminuted fractures with or without associated injuries. However few studies provide long-term follow-up. Some complications associated with radial head replacement with current designs include capitellar erosion, especially with over-lengthening of the prosthesis and degeneration of the ulnohumeral joint leading to late osteoarthritis[48-50]. Implant wear and failure have also been reported[51].

Radiographs showing each of these treatment options are shown in Figure 1.8.

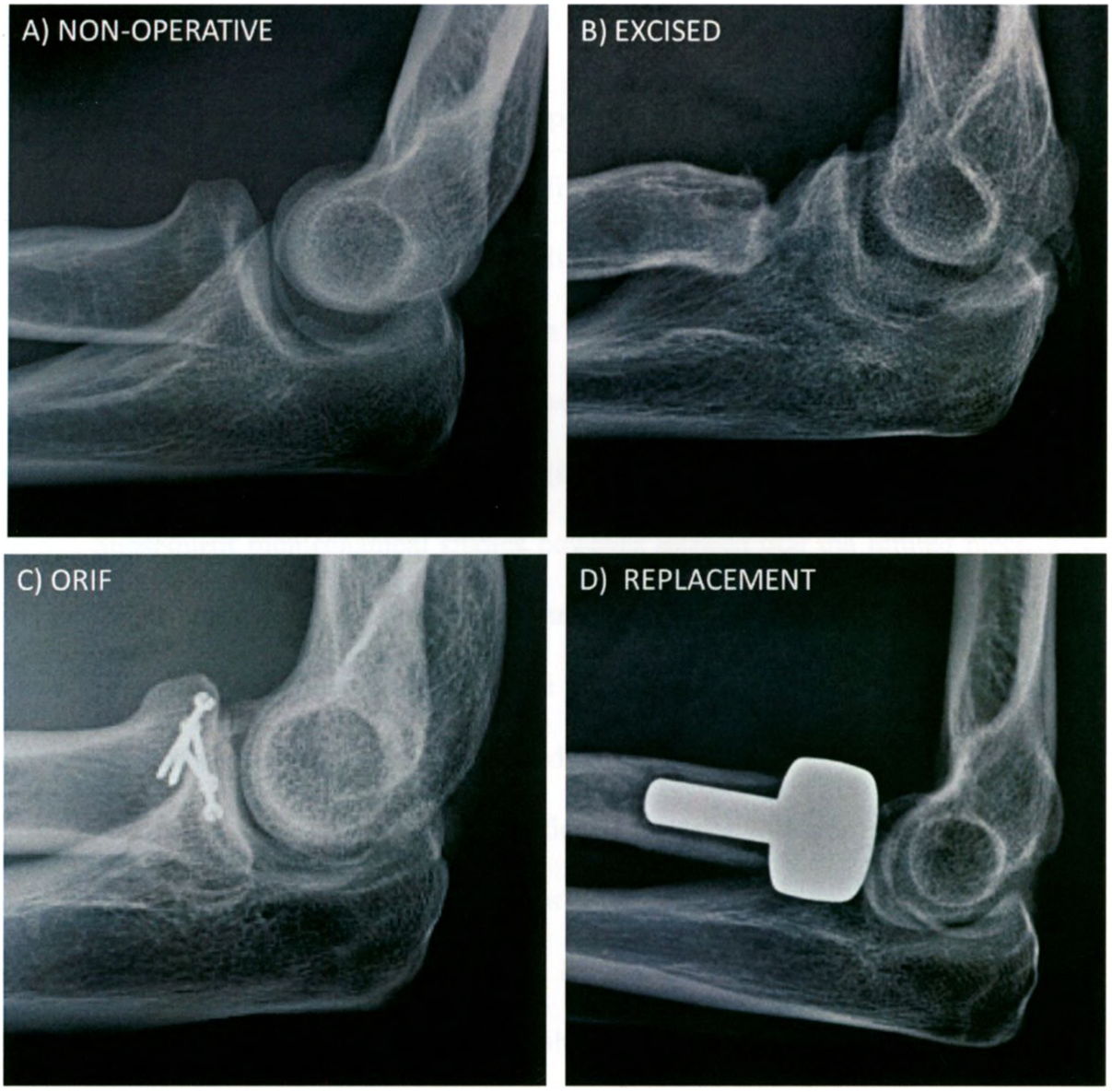

Figure 1.8: Radial Head Fracture Treatment Options

A) Fracture of the radial head without operative treatment
B) Radial head fracture treated with excision
C) Radial head repaired using open reduction and internal fixation
D) Replacement of the fractured radial head using a smooth stemmed axisymmetric implant

1.4 RADIAL HEAD IMPLANTS

The first radial head implant, developed by Speed in 1941, used casts of intact radii[52]. These vitallium ferrule caps were first tested in a canine model and in three patients. Cherry reported the use of an acrylic implant in 1953[53] though neither of these early implant models gained general adoption as a treatment option.

The first prosthesis to gain widespread use in the treatment of unreconstructible radial head fractures was a silicon-rubber (silastic) implant developed by Swanson in 1968[54]. Subsequent biomechanical studies however showed that the limited mechanical strength of the silicon material was inadequate in providing sufficient resistance to valgus forces[55]. This silastic implant was also prone to failure at the head-neck interface as well as synovitis and cartilage degeneration caused by wear debris[56,57].

The use of metal implants with sufficient material strength to resist valgus and axial forces was reported in the early 1990s by Knight et al.[77] and Judet et al.[60] using monoblock and bipolar designs respectively. Both of these implants use a circular profile for the radial head with a concentric dish. The monoblock implant, composed of vitallium, was designed with ribs and grooves on the head-neck interface to aid in fixation and was manufactured in three diameters and two heights. The bipolar design featured a long stem with a 15° neck shaft angle and a spherical joint connecting the stem and head which allowed up to 35° of tilt. The head was manufactured in two diameters using high density polyethylene enclosed in cobalt chrome. The stem was also cobalt-chrome and was manufactured in two different sizes. As the stem and head components were interchangeable, the Judet prosthesis could be considered the first modular design.

Gupta et al. [58] noted in 1997 that radial head implant designs were non-anatomic and that stems conformed poorly to the intramedullary canal. In 1999 Beredjiklian et al.[59] reported on the mismatch between an available titanium implant and the shape of the radius determined using MRI imaging. In approximately 40% of elbows, the intramedullary canal was too small for even the smallest implant model. Surprisingly, in all cases the length of the native radius would not be restored with an average shortening of 4mm. King et al. [5] further examined the radial head morphology and concluded that there was a poor correlation between radial head and medullary canal diameter and thus a modular implant system should be considered.

Current implant designs are variable in shape, material and fixation method although trends have emerged in the design of axisymmetric and anatomic implant systems. Axisymmetric implants may use a loose stem or a cemented bipolar design to allow implant movement during elbow motion to compensate for mal-alignment due to their non-anatomic shape as shown in Figure 1.9 (A,C) [2,5,60]. Anatomically shaped implants rely on precise positioning and either a press-fit or cemented stems to ensure the implant is fixed in the correct position as shown in Figure 1.9 (B).

Current designs are not without their limitations. A recent study has shown that bipolar implants have a reduced capacity to resist radiocapitellar subluxation when compared to other designs[61]. Radiolucencies surrounding the stem of smooth-stemmed implants have been observed but are uncorrelated to pain or reduced function[62]. Complications associated with implant height mismatch, particularly over-lengthening and corresponding capitellar erosion, have also been shown[63]. For anatomically shaped implants, poor correlation between the orientation of landmarks such as the biceps

tuberosity, distal radius and the radial head make precise positioning using these clinically available landmarks a challenging task[64,65].

Figure 1.9: Examples of Current Radial Head Implant Designs

A) Evolve Proline Radial Head System with axisymmetric head and smooth stem. (Wright Medical Technology Inc., Arlington, TN, USA)

B) Anatomic Radial Head System which is designed to allow for bone ingrowth. (Acumed, Hillboro, OR, USA)

C) RHS Radial Head System bipolar axisymmetric implant with short and long stem designs. (Tornier, Stafford, TX, USA)

Despite the variability among the design of current implant systems, no prosthesis is successful in restoring both contact properties and kinematics of the native joint[66-68]. This may, in part, be due to the inability of current implants to precisely match the native

morphology and height either due to shape mismatch in the case of axisymmetric implant designs, or poor alignment in the case of anatomic implant designs. Alternatively, the differing material properties of the articular cartilage and the various metals currently employed may be concerning[66]. Pyrocarbon, a material similar to graphite, may provide a closer match to the material properties of the native radial head compared to the titanium and cobalt chrome which are currently most commonly used[69].

In summary, while radial head replacement is generally a successful treatment with regard to pain reduction, restoring stability and motion, further advances in implant designs and surgical techniques will be beneficial

1.5 COMPUTER ASSISTED SURGERY

The development of Computer Assisted Surgery (CAS) techniques and systems is a rapidly growing research area in many medical specialties. CAS pairs preoperative medical imaging with computer guidance within the operating room (OR) to assist the surgeon during procedures.

1.5.1 HISTORY

The development of CAS systems initially focused on neurosurgery and stemmed from early stereotactic techniques in which a rigid frame was attached to the skull to establish a physical coordinate system[70]. With the invention of computed tomography scanners by Hounsfield[71] in 1973, stereotactic frames were equipped with simple radio-opaque markers to link the image and physical space significantly improving their precision. The final technological development crucial in the history of CAS was the availability of increasingly powerful computing systems. In the late 1980s several groups

realized that stereotactic techniques which allowed a tool to be guided to a target based on imaging could be reversed using a 3D localizer so that a tool's position could be displayed on pre-operative images allowing the physical stereotactic frame to be eliminated[72]. These first "frameless stereotaxic" systems are the origin of modern CAS techniques.

The initial application of CAS to orthopaedics was the development navigation systems for pedicle screw placement in the spine in 1995[73]. Subsequently, research into the field of Computer Assisted Orthopedic Surgery (CAOS) has seen significant growth, particularly with respect to surgical navigation systems which have been applied at the hip and knee to aid in joint replacement. CAOS promises advantages such as improved placement accuracy, decreased surgical invasiveness and a reduction in the likelihood of revision surgery. Additionally, CAOS paired with the proper training tools should allow a less experienced surgeon to perform procedures with increased accuracy and a lower incidence of complications. However, there is a paucity of long-term studies justifying its use in many procedures.

1.5.2 TECHNIQUES

Most, if not all CAOS systems employ at least one modality of pre-operative imaging. Typically for orthopedic procedures, CT is the modality of choice as bone is easily segmented from the surrounding tissue when making 3D models. Using this information, a pre-operative plan is established using custom software. Surgical navigation is often employed to allow the surgeon to visualize the instruments relative to the pre-operative imaging in real-time, thus image registration must be performed to establish the link between the pre-operative model and patient. This may be

accomplished using a variety of techniques including fiducial markers in the pre-operative imaging, landmark or surface-based algorithms or intra-operative imaging. Registration procedures in CAOS often assume that each bone acts as a rigid body and is not subject to any deformation. This drastically simplifies the process of matching pre-operative models to the geometry encountered operatively. The general steps in the application of computer-assisted techniques in orthopedics are shown in Figure 1.10.

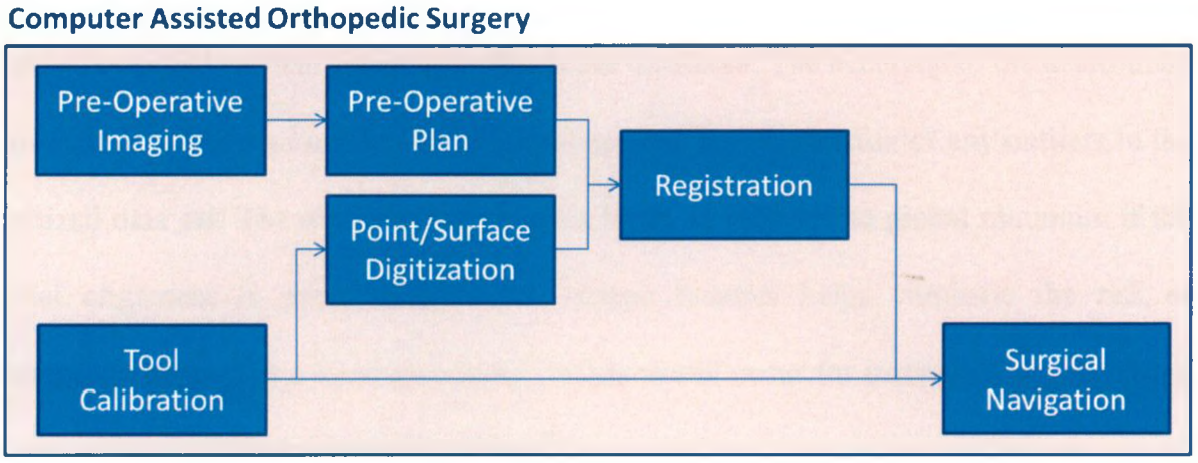

Figure 1.10: Overview of CAOS Tasks

This flowchart shows the typical workflow of a CAOS system. Some steps may be excluded from a particular system. For example pre-operative imaging may not be required if joint kinematics are used to determine the target implant location.

1.5.3 REGISTRATION

Registration is the process by which one dataset is aligned with another based on shared features. Registration is used between pre-operative CT imaging and points digitized using a tracking system (inter-modality) or pre-operative and post-operative CT imaging (intra-modality). This is the key step in linking pre-operative imaging to the operative field for the purpose of navigation. Ensuring an accurate registration is essential to the success of CAOS. For the purpose of this thesis, two registration methods will be discussed : landmark-based registration and surface-based registration.

Landmark-based or paired-point registration attempts to minimize the residual error between two sets of corresponding points. A minimum of three non-collinear points are required to determine the landmark transform.

The iterative closest point (ICP) algorithm is a common choice for surface-based registration of rigid bodies. The distance between a selection of points on the digitized surface and their nearest neighbor on the CT model is determined. A paired point registration is then calculated using each set of points. This process repeats until the residual error is less than a user specified input threshold. The accuracy of the determined minimum is dependent on the initial alignment and the elimination of any outliers in the digitized data set. The algorithm may find a local, as opposed to global minimum if the initial alignment is poor. Inclusion of unique features helps eliminate the risk of becoming "trapped in a local minimum" which would occur for instance if the algorithm was used to match two spherical surfaces[74].

1.5.4 Registration Accuracy

Fiducial registration error (FRE) and target registration error (TRE) are typically used to describe registration accuracy. FRE measures the root-mean-square of residual error between homologous points in the registration. This can be a deceptive measure of error as it may be poorly correlated to error in the region of interest. TRE is calculated by determining the error between a measured point in the region of interest not involved in the registration and its location determined using the registration transform. By choosing a large number of widely spread and reproducible points surrounding the target area in the registration the TRE may be minimized.

These measures of registration error are well suited to landmark based methods where paired points are easily identified. In the case of surface-based registration, for example using the ICP algorithm, it is not innately known which points should be paired between the virtual model and the digitized surfaces. Unless additional landmarks which can be reliably identified in both digitized and virtual models are present, FRE and TRE cannot be determined. In order to quantify the error in this case, it may be necessary to use another "gold-standard" registration method with a known high accuracy to enable error to be calculated through comparison to this datum.

Errors during the collection of surface digitizations can affect the registration accuracy. Surgeon familiarity with both the navigation system and the procedure itself would likely have some impact on the accuracy of digitizations obtained in a clinical setting. Attempting to use the digitizing probe at too great an angle to the surface of interest is an example of error stemming from a lack of experience with the navigation system. A lack of familiarity with the anatomical landmarks leading to digitization error is an example of how a surgeon's inexperience with the procedure could lead to error. Additionally cartilage, which is not present in the CT derived models, may lead to an offset between digitizations and the model surfaces furthering increasing registration error.

1.5.5 Tracking Systems

Tracking systems provide the fundamental technology for surgical navigation. They allow the location and orientation of objects within the working volume to be measured in real-time. Thus, the accuracy of image guided surgery is heavily dependent on the accuracy of the tracking system employed for guidance[75]. Most current systems

are classified as electromagnetic or optical - the former using magnetic fields and the latter infrared cameras to determine the location of "markers" within the measurement volume. Both systems have limitations. Electromagnetic systems have lower accuracy and suffer from interference caused by metal within their working volume. Optical systems must maintain a line-of-sight with each marker and only the position (not orientation) of each marker may be measured.

Optical systems may be further classified as active or passive based respectively on whether the markers generate their own light (LEDs) or are merely reflective. Regardless of the type, at least three non-collinear markers must be present on an object for orientation to be determined. The configuration of the markers must be defined through a calibration process for the rigid body to be recognized by the tracking program. Adding extra markers to an object ensures that even if some markers are covered the object's location and orientation can still be determined as long as at least three remain visible, minimizing line of sight issues. Increasing the number of markers has been shown to improve accuracy[76], although in this case, when only the minimum three markers may be visible at any one time, error increases based on the accuracy of the calibration used to define the configuration of the markers.

The work presented herein was conducted using the Optotrak Certus (Northern Digital Inc., Waterloo, ON, Canada) which is an active optical tracking system. The major advantage of active over passive markers is that each can be identified by its frequency rather than itsconfiguration, eliminating the risk of tracker confusion. This system has manufacturer specified accuracy of up to 0.1 mm.

1.5.6 NAVIGATION

For the purpose of surgical navigation, markers are affixed to tools and the patient so that their position and orientation can be measured. Pre-operative imaging is registered to the markers affixed to the patient so that the position of each tool is properly referenced to the host structure. This is displayed on a screen using application specific software. A digitizing system is typically included which allows for points to be measured with respect to the tracking system or relative to other trackers.

1.5.7 NAVIGATION ERROR

Total error, which relates to the actual position relative to the desired position, is dependent on the registration accuracy, tool calibration accuracy, tracking accuracy and finally, placement accuracy. Navigation accuracy describes how closely the user can physically align an object to the target location using the feedback provided by the software. Tracking accuracy is dependent on the tracking modality and specific system used. This may be variable throughout the working volume of the tracking system. Since the registration error is typically performed using data provided by the tracking system, which includes this source of error, post-operative imaging to determine the final position relative to the target may be used to measure this error.

Tool calibration error can be minimized through proper tool design and calibration procedures. Depending on the methods used, another registration may be involved in the calibration process which is subject to the corresponding registration errors. Registration accuracy between pre-operative imaging and the tracked space is the final factor affecting navigation accuracy.

1.6 STUDY RATIONALE

It has been identified in the literature that current axisymmetric radial head prostheses do not adequately match the morphology of the native radial head [59]. van Riet et al. [65] concluded that "even with a perfectly anatomical prosthesis, restoration of the anatomical situation can only be achieved when the implant is placed in the correct position", and commented that "instrumentation should be developed to allow accurate and reproducible implantation". Bipolar and smooth stemmed implants allow for implant adjustment to ensure proper tracking with the capitellum in an effort to compensate for the effects of poor surface matching and implant misalignment. Other implants strive to be correct morphologically but small errors in alignment may be easily incurred when only visual landmarks are used, potentially leading to complications and later surgical revision. Morphologically correct and accurately placed radial head prostheses may help improve the outcome of patients who require radial head arthroplasty.

1.7 OBJECTIVES AND HYPOTHESES

The specific objectives of this research were:

1. To develop a system for measuring the morphological parameters of the radial head using CT modeling and reverse engineering techniques.
2. To design both patient-specific and population-based anatomical radial head implants using relevant morphological parameters, and to compare their geometric match relative to a commercially available axisymmetric implant.
3. To validate surface based registration using pre-operative CT imaging of the radial head and assess the accuracy compared to a gold standard method.

4. To develop and evaluate a computer-assisted navigation system for radial head arthroplasty.

The hypotheses are:

1. Patient-specific radial head prosthesis can be reverse engineered from CT imaging using a fixed number of parameters to represent the native surface within 0.25mm.
2. Anatomic implant designs will show significant reduction in mean surface mismatch from the radial head when compared to current axisymmetric design.
3. Low registration errors can be achieved through the use of accessible radial head surface landmarks.
4. Implant navigation error with image guidance will be equal to or less than (a) 0.25mm in translation and (b) 2° in rotation about each of the anatomic axes.

1.8 THESIS OVERVIEW

Chapter 2 details the methods used to parameterize proximal radius morphology from CT imaging. Each step of the implant design process for both the patient-specific and population-based prostheses are described in Chapter 3 and the resulting implant models are assessed using calculated mean shape mismatch between implant and CT models. The creation and performance of a computer- and image-assisted radial head guidance system are detailed in Chapter 4 including the accuracy of surface-based registration. Chapter 5 provides general discussion, conclusions and summarizes future work.

1.9 REFERENCES

1. Fornalski S, Gupta R, Lee TQ. Anatomy and biomechanics of the elbow joint. *Techniques in Hand & Upper Extremity Surgery*. 2003;7(4):168-78.

2. van Riet RP, van Glabbeek F, Neale PG, et al. The noncircular shape of the radial head. *The Journal of Hand Surgery*. 2003;28(6):972-978.

3. Swieszkowski W, Skalski K, Pomianowski S, Kedzior K. The anatomic features of the radial head and their implication for prosthesis design. *Clinical Biomechanics*. 2001;16(10):880-7.

4. Caputo AE, Mazzocca AD, Santoro VM. The nonarticulating portion of the radial head: anatomic and clinical correlations for internal fixation. *The Journal of Hand Surgery*. 1998;23(6):1082-90.

5. King GJW, Zarzour ZD, Patterson SD, Johnson JA. An anthropometric study of the radial head: implications in the design of a prosthesis. *The Journal of Arthroplasty*. 2001;16(1):112-6.

6. Captier G, Canovas F, Mercier N, Thomas E, Bonnel F. Biometry of the radial head: biomechanical implications in pronation and supination. *Surgical and Radiologic Anatomy*. 2002;24(5):295-301.

7. Cone R, Szabo R, Resnick D. Computed tomography of the normal radioulnar joints. *Investigative Radiology*. 1983;18(6):541-545.

8. Sabo MT, McDonald CP, Ng J, et al. A morphological analysis of the humeral capitellum with an interest in prosthesis design. *Journal of Shoulder and Elbow Surgery*. 2011:ARTICLE IN PRESS.

9. Goodfellow JW, Bullough PG. The pattern of ageing of the articular cartilage of the elbow joint. *Journal of Bone and Joint Surgery - British Volume*. 1967;49(1):175.

10. Morrey B, An K, Stormont T. Force transmission through the radial head. *The Journal of Bone and Joint Surgery*. 1988;70(2):250-56.

11. Floris S, Olsen BS, Dalstra M, Skujbjerg JO, Sneppen O. The medial collateral ligament of the elbow joint: anatomy and kinematics. *Journal of Shoulder and Elbow Surgery*. 1998;7(4):345–351.

12. Jensen SL, Olsen BS, Søjbjerg JO. Elbow joint kinematics after excision of the radial head. *Journal of Shoulder and Elbow Surgery*. 1999;8(3):238-41.

13. Martin BF. The annular ligament of the superior radio-ulnar joint. *Journal of Anatomy*. 1958;92(3):473-82.

14. Seki A, Olsen BS, Jensen SL, Eygendaal D, Søjbjerg JO. Functional anatomy of the lateral collateral ligament complex of the elbow: configuration of Y and its role. *Journal of Shoulder and Elbow Surgery*. 2002;11(1):53-9.

15. Takigawa N, Ryu J, Kish V, Kinoshita M, Abe M. Functional anatomy of the lateral collateral ligament complex of the elbow: morphology and strain. *Journal of Hand Surgery (British and European Volume)*. 2005;30(2):143-47.

16. Olsen BS, Vsel MT, Sojbjerg JO, Helmig P, Sneppen O. Lateral collateral ligament of the elbow joint: Anatomy and kinematics. *Journal of Shoulder and Elbow Surgery*. 1996;5(2):103–112.

17. Brownhill JR, Furukawa K, Faber KJ, Johnson JA, King GJW. Surgeon accuracy in the selection of the flexion-extension axis of the elbow: an in vitro study. *Journal of Shoulder and Elbow Surgery*. 2006;15(4):451-6.

18. Duck TR, Dunning CE, King GJW, Johnson JA. Variability and repeatability of the flexion axis at the ulnohumeral joint. *Journal of Orthopaedic Research*. 2003;21(3):399-404.

19. Boone DC, Azen SP. Normal range of motion of joints in male subjects. *Journal of Bone and Joint Surgery - American Volume*. 1979;61(5):756-9.

20. Hollister a M, Gellman H, Waters RL. The relationship of the interosseous membrane to the axis of rotation of the forearm. *Clinical Orthopaedics and Related Research*. 1994;(298):272-6.

21. Ray R, Johnson R, Jameson RM. Rotation of the forearm: an experimental study of pronation and supination. *The Journal of Bone and Joint Surgery*. 1951;33(4):993.

22. Dwight T. The movements of the ulna in rotation of the fore-arm. *Journal of Anatomy and Physiology*. 1885;19(Pt 2):186.

23. Morrey BF, Chao E. Passive motion of the elbow joint. *The Journal of Bone and Joint Surgery*. 1976;58(4):501.

24. Halls AA, Travill A. Transmission of Pressures Across the Elbow Joint. *The Anatomical Record*. 1964;150:243-7.

25. Markolf KL, Lamey D, Yang S, Meals ROY, Hotchkiss R. Radioulnar Load-Sharing in the Forearm. *The Journal of Bone and Joint Surgery*. 1998;80-A(6):879-888.

26. McGinley JC, Kozin SH. Interosseous membrane anatomy and functional mechanics. *Clinical Orthopaedics and Related Research*. 2001;(383):108-22.

27. Beingessner DM, Dunning CE, Stacpoole RA, Johnson JA, King GJW. The effect of coronoid fractures on elbow kinematics and stability. *Clinical Biomechanics*. 2007;22(2):183-90.

28. Morrey BF, An K-N. Stability of the elbow: osseous constraints. *Journal of Shoulder and Elbow Surgery*. 2005;14(1 Suppl S):174S-178S.

29. Morrey BF, Sanchez-Sotelo J. *The Elbow and Its Disorders*. 4th ed. Elsevier Health Sciences; 2009:1211.

30. Charalambous CP, Stanley JK. Posterolateral rotatory instability of the elbow. *Journal of Bone and Joint Surgery - British Volume*. 2008;90(3):272-9.

31. Bell T, King G, Johnson J, Ferreira L. Contribution of the Olecranon to Elbow Stability: An In-Vitro Biomechanical Study. *The Journal of Bone and Joint Surgery*. 2010;92-A(4):949-57.

32. Johnston GW. A follow-up of one hundred cases of fracture of the head of the radius with a review of the literature. *The Ulster Medical Journal*. 1962;31:51-6.

33. van Riet RP, Morrey BF, O'Driscoll SW, van Glabbeek F. Associated Injuries Complicating Radial Head Fractures. *Clinical Orthopaedics and Related Research*. 2005;441:351-355.

34. Thomas TT. A contribution to the mechanism of fractures and dislocations in the elbow region. *Annals of Surgery*. 1929;89(1):108-121.

35. Bartz B, Tillmann B, Schleicher A. Stress in the human elbow joint. *Anatomy and Embryology*. 1984;169(3):309–318.

36. Haverstock JP, Katchky RN, Lalone EA, et al. Regional variations in radial head bone density - implications for fracture pattern and fixation. In: *COA/CORS Annual Meeting Abstract Supplement*. 2011:169-170.

37. Davidson PA, Moseley BK, Tullos HS. Radial Head Fracture A Potentially Complex Injury. *Clinical Orthopedics and Related Research*. 1993;(297):224-230.

38. Itamura J, Roidis N, Mirzayan R, et al. Radial head fractures: MRI evaluation of associated injuries. *Journal of Shoulder and Elbow Surgery*. 2005;14(4):421-4.

39. Mason M. Some observations on fractures of the head of the radius with a review of one hundred cases. *British Journal of Surgery*. 1954.

40. van Beek C, Levine WN. Radial Head—Resect, Fix, or Replace. *Operative Techniques in Orthopaedics*. 2010;20(1):2-10.

41. Beingessner DM, Dunning CE, Beingessner CJ, Johnson JA, King GJW. The effect of radial head fracture size on radiocapitellar joint stability. *Clinical Biomechanics*. 2003;18(7):677-681.

42. Beingessner DM, Dunning CE, Gordon KD, Johnson JA, King GJW. The effect of radial head fracture size on elbow kinematics and stability. *Journal of Orthopaedic Research*. 2005;23(1):210-7.

43. Ring D, Quintero J, Jupiter JB. Open reduction and internal fixation of fractures of the radial head. *The Journal of Bone and Joint Surgery*. 2002;84-A(10):1811-15.

44. Morgan SJ, Groshen SL, Itamura JM, et al. Reliability evaluation of classifying radial head fractures by the system of Mason. *Bulletin Hospital for Joint Diseases*. 1997;56(2):95-8.

45. Matsunaga FT, Tamaoki MJS, Cordeiro EF, et al. Are classifications of proximal radius fractures reproducible? *BMC Musculoskeletal Disorders*. 2009;10(1):120.

46. Stuffmann E, Baratz ME. Radial head implant arthroplasty. *The Journal of Hand Surgery*. 2009;34(4):745-54.

47. Leppilahti J, Jalovaara P. Early excision of the radial head for fracture. *International Orthopaedics*. 2000;24(3):160-2.

48. Burkhart KJ, Mattyasovszky SG, Runkel M, et al. Mid- to long-term results after bipolar radial head arthroplasty. *Journal of Shoulder and Elbow Surgery*. 2010;19(7):965-72.

49. Popovic N, Lemaire R, Georis P, Gillet P. Midterm results with a bipolar radial head prosthesis: radiographic evidence of loosening at the bone-cement interface. *Journal of Bone and Joint Surgery - American Volume*. 2007;89(11):2469-76.

50. Harrington IJ, Sekyi-Otu A, Barrington TW, Evans DC, Tuli V. The functional outcome with metallic radial head implants in the treatment of unstable elbow fractures: a long-term review. *The Journal of Trauma*. 2001;50(1):46-52.

51. Herald J, O'Driscoll S. Complete dissociation of a bipolar radial head prosthesis: a case report. *Journal of Shoulder and Elbow Surgery*. 2008;17(6):e22-3.

52. Speed K. Ferrule caps for the head of the radius. *Surgery Geynecology and Obstetrics*. 1941;73.

53. Cherry J. Use of acrylic prosthesis in the treatment of fracture of the head of the radius. The *Journal of Bone and Joint Surgery - British Volume*. 1953;35(1):70.

54. Swanson A, Jaeger S, La Rochelle D. Comminuted fractures of the radial head. The role of silicone-implant replacement arthroplasty. *The Journal of Bone and Joint Surgery*. 1981;63(7):1039.

55. Carn RM, Medige J, Curtain D, Koenig A. Silicone rubber replacement of the severely fractured radial head. *Clinical Orthopaedics and Related Research*. 1986;209:259.

56. Bohl WR, Brightman E. Fracture of a silastic radial-head prosthesis: diagnosis and localization of fragments by xerography. A case report. *The Journal of Bone andJjoint Surgery*. 1981;63(9):1482-3.

57. Vanderwilde R, Morrey B, Melberg M, Vinh T. Inflammatory arthritis after failure of silicone rubber replacement of the radial head. The *Journal of Bone and Joint Surgery - British Volume*. 1994;76(1):78.

58. Gupta G, Lucas G. Biomechanical and computer analysis of radial head prostheses. *Journal of Shoulder and Elbow Surgery*. 1997;6(1):37-48.

59. Beredjiklian PK, Nalbantoglu U, Potter HG, Hotchkiss RN. Prosthetic radial head components and proximal radial morphology: a mismatch. *Journal of Shoulder and Elbow Surgery*. 1999;8(5):471–475.

60. Judet T, Garreau de Loubresse C, Piriou P, Charnley G. A floating prosthesis for radial-head fractures. The *Journal of Bone and Joint Surgery - British Volume*. 1996;78(2):244-9.

61. Chanlalit C, Shukla DR, Fitzsimmons JS, et al. Radiocapitellar stability: the effect of soft tissue integrity on bipolar versus monopolar radial head prostheses. *Journal of Shoulder and Elbow Surgery*. 2011;20(2):219-25.

62. Fehringer EV, Burns EM, Knierim A, et al. Radiolucencies surrounding a smooth-stemmed radial head component may not correlate with forearm pain or poor elbow function. *Journal of Shoulder and Elbow Surgery*. 2009;18(2):275-8.

63. van Glabbeek F, van Riet RP, Baumfeld JA, et al. Detrimental effects of overstuffing or understuffing with a radial head replacement in the medial collateral-ligament deficient elbow. *Journal of Bone and Joint Surgery*. 2004;86-A(12):2629-35.

64. Katchky RN, Johnson JA, King GJW, Athwal GS. Anatomic radial head arthroplasty: A lack of reliable landmarks for alignment. In: *COA/CORS Annual Meeting Abstract Supplement*.; 2011:164-165.

65. van Riet RP, van Glabbeek F, Neale PG, et al. Anatomical considerations of the radius. *Clinical Anatomy*. 2004;17(7):564-9.

66. Liew VS, Cooper IC, Ferreira LM, Johnson JA, King GJW. The effect of metallic radial head arthroplasty on radiocapitellar joint contact area. *Clinical Biomechanics (Bristol, Avon)*. 2003;18(2):115-8.

67. Pomianowski S, Morrey BF, Neale PG, et al. Contribution of monoblock and bipolar radial head prostheses to valgus stability of the elbow. *Journal of Bone and Joint Surgery*. 2001;83-A(12):1829-34.

68. King GJW, Zarzour ZD, Rath DA, et al. Metallic radial head arthroplasty improves valgus stability of the elbow. *Clinical Orthopaedics and Related Research*. 1999;(368):114-25.

69. Allieu Y, Winter M, Pequignot JP, Mourgues P. Radial head replacement with a pyrocarbon head prosthesis: preliminary results of a multicentric prospective study. *European Journal of Orthopaedic Surgery & Traumatology*. 2005;16(1):1-9.

70. Horsley V, Clarke RH. The Structure and Function of the Cerebellum Examined by a New Method. *Brain*. 1908;31(1):45-124.

71. Hounsfield GN. Computerized transverse axial scanning (tomography): Part 1. Description of system. *British Journal of Radiology*. 1973;46(552):1016.

72. Peters T, Cleary K eds. *Image-Guided Interventions: Technology and Applications*. Springer; 2008:560.

73. Amiot L, Labelle H, DeGuise J, Sati M. Computer-assisted pedicle screw fixation-a feasibility study. *Spine*. 1995;20(10):1208-1212. 74. Besl P, McKay N. A method for registration of 3-D shapes. *IEEE Transactions on Pattern Analysis and Machine Intelligence*. 1992.

75. Fitzpatrick JM, West JB, Maurer CR. Predicting error in rigid-body point-based registration. *IEEE Transactions on Medical Imaging*. 1998;17(5):694-702.

76. Wiles AD. Accuracy assessment and interpretation for optical tracking systems. *Proceedings of SPIE*. 2004:421-432.

77. Knight DJ, Rymaszewski LA, Amis AA. Primary replacement of the fractured radial head with a metal prosthesis. *Journal of Bone and Joint*. 1993;75-B(4):572-576.

CHAPTER 2 - Radial Head Morphology

OVERVIEW:

Radial head morphology has been previously studied; however the documented parameters are insufficient for the development and design of an accurate anatomic implant. This chapter describes how radial head cross sections derived from CT imaging models were fitted as ellipses to quantify radial head geometry for use in future anatomic implant designs.

2.1 INTRODUCTION

Current radial head prostheses are either axisymmetric (circular) or anatomically shaped (non-circular). Circular implants rely on bipolar designs or loose fitting stems that allow implant movement to compensate for their non-anatomic shape[1-4]. It has been suggested that the use of an anatomically correct prosthesis may provide superior results[5].

There is currently little consensus on the most appropriate techniques to describe the geometry of the radial head. Both roughly circular and elliptical shapes have been reported[4-11]. Cadaver-based studies by van Riet et al.[5] and Swieszkowski et al.[11] have shown that the major and minor rim and outer (circumferential) diameters are statistically different and highly correlated, although the difference was small averaging between 1 and 2 mm'. The major and minor outer diameters have been described as roughly orthogonal and oriented perpendicular to the center of the proximal radial ulnar articulation[5].

The articular region of the radial head circumference features a relatively flat profile to engage the proximal radial ulnar joint (PRUJ), while the non-articular side is

more rounded, likely to allow constraint by the annular ligament as shown in Figure 2.1[12]. Regional differences in cartilage appearance between the articular and non-articular circumference of the radial head have been documented but variations in thickness have not been quantified[13].

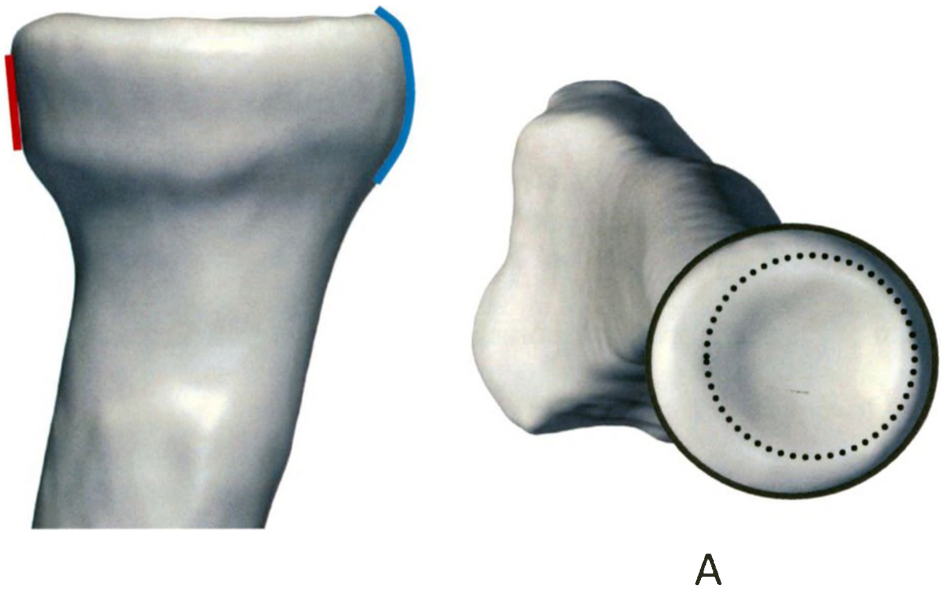

Figure 2.1: Radial Head Morphology

A) The variance in the articular profile between the articular (red) and non-articular (blue) sides as viewed from the medial aspect.
B) The lateral offset of the dish relative to the radial circumference in neutral rotation viewed from the superior aspect.

The articular dish is eccentric and shifted laterally away from the ulna when in the neutral position (or posteriorly in the anatomic position) as shown in Figure 2.1[5]. This may explain the translations observed during forearm rotation, where the radial head shifts posteriorly and distally with supination and anteriorly and proximally with pronation[14,15]. The edge of the dish has a major and minor diameter indicating the dish is not spherical but rather ellipsoidal[5,11].

Significant differences have been reported between male and female radial head dimensions[4,5]. Comparisons between sides however have shown no significant difference, supporting the use of measurements obtained from contralateral imaging for implant sizing[4,11]. Gupta, who examined 725 radii for differences based on age, side, gender and race found that only gender showed statistical differences in radial head shape[28]. The methods used however were not thoroughly documented.

Koslowsky et al.[6] measured 3mm slices of optosil imprints taken from cadaveric radial heads in order to quantify the diameter variation with respect to both height and orientation. They concluded that the radial head increases in size from the radiocapitellar joint surface to the middle of the proximal radioulnar joint and that the minor diameter was consistently perpendicular to the major. However, the shape of the dish was examined in only one plane. Mahaisavariya[7] et al. conducted some preliminary work on the use of reverse engineering techniques and fitting algorithms in defining radial head morphology. Although these techniques were highly effective in parameterizing shape, the concept was not extended further to use the reverse engineered data to construct a radial head implant model.

Current studies do not include sufficient parameters to fully define the variable shape of the radial circumference and dish. Thus, the objective of this study was to better define the normal anatomy of the radial head using CT and automated ellipse fitting to assist with the development of improved anatomic radial head implant designs. Correctly defining the shape of the articular circumference and dish is important in radial head prosthesis design, as a correctly shaped anatomic implant may mitigate complications

observed with current implant systems including increased radiocapitellar joint contact pressure and altered joint kinematics[16-18].

2.2 MATERIAL AND METHODS

2.2.1 MODEL CREATION AND ELLIPSE FITTING

Computed tomography images of 50 normal cadaveric upper extremities (34 male, 16 female) were obtained using a 64-slice scanner (GE Lightspeed VCT 64 Slice CT Scanner, New Berlin, WI). A 512x512 reconstruction matrix was used for all specimens. Pixel size and slice thickness ranged from 0.26-0.98mm and 0.625-1.25mm respectively. Tube current and voltage ranged from 73-292mA and 120-140KV. The images were segmented and a surface model reconstructed using medical image processing software (Mimics, Materialize NV, Leuven, Belgium). The 14 left sided specimens were mirrored into right handed digital models to simplify the measurement process.

Each model was imported into a custom program created using the Visualization Toolkit (VTK). The measurement process is shown in detail in Figure 2.2. A coordinate system was defined using manually selected bony landmarks. Twenty user defined points were chosen along the rim of the radial dish and a best-fit plane determined using least squares fitting. The deepest point, used as the origin, was found by searching the points in the dish to determine which point was furthest from the best-fit plane. The normal vector of the plane pointing proximally was defined as the z-axis direction.

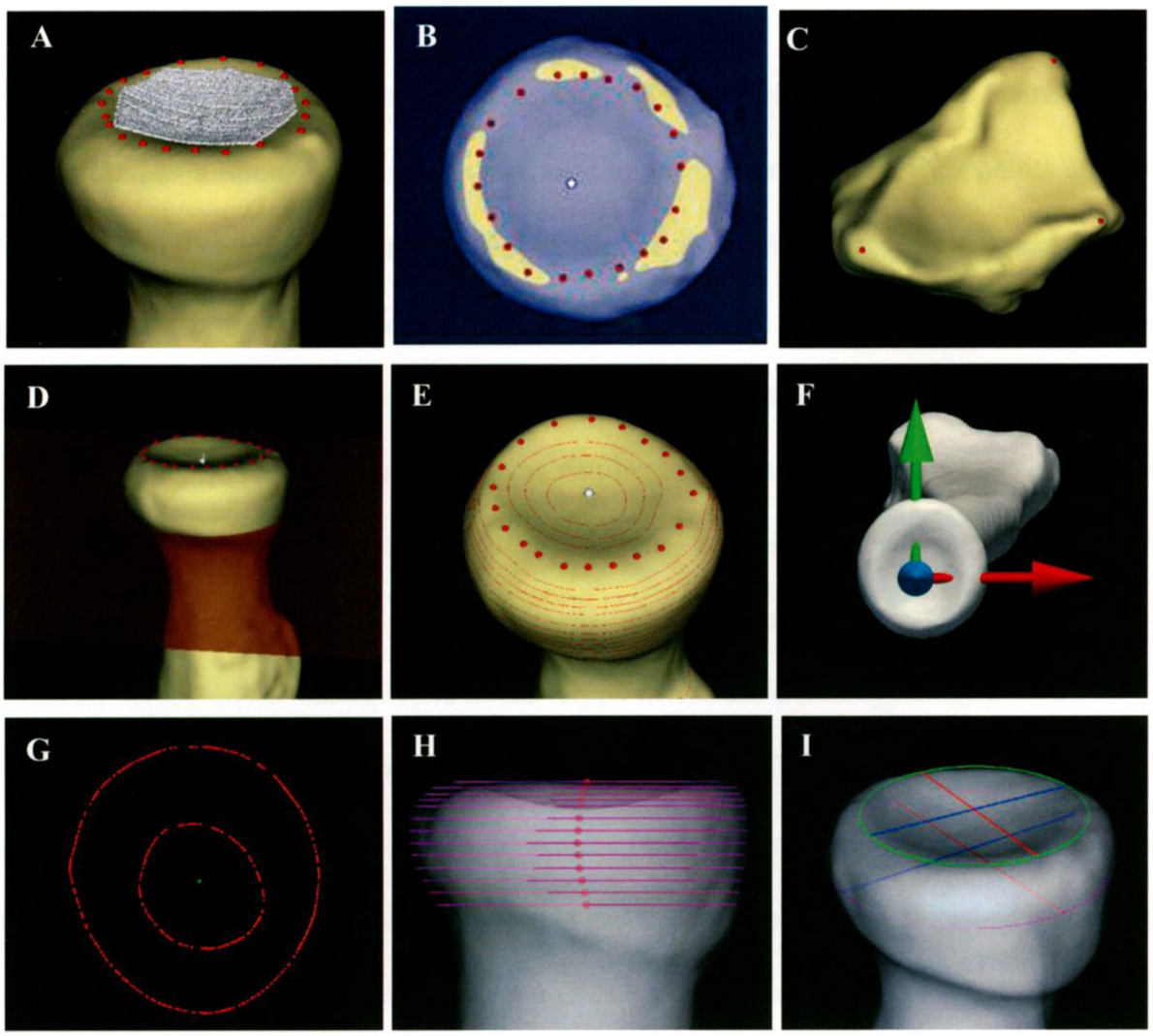

Figure 2.2: Overview of the Radial Head Measurement Process

A) Twenty rim points (red) are selected and points in the dish generated (white).
B) The best-fit plane (blue) is determined and the deepest point found (white).
C) Distal points (red) are selected by the user.
D) Height is measured using a plane (red) parallel to the best-fit plane.
E) Cross sections are generated at known height intervals.
F) Radial head coordinate system is determined (X,Y,Z = Red, Green, Blue).
G) An example cross section showing both outer (circumferential) and dish points.
H) Ellipses (purple) are fit to each of the radial head cross sections and their centers determined (red).
I) Major (red) and minor (blue) diameters are shown for the rim (green) and maximum outer (purple) cross sections.

The radial styloid, dorsal aspect and volar aspect of the distal radioulnar joint (DRUJ) were marked with points and projected onto the best-fit plane. The lateral X-axis was defined as a line connecting the midpoint of the two projected DRUJ points and the projected radial styloid. The anterior Y-axis (for our right handed specimens) was defined using the cross product of the Z and X vectors.

Once the coordinate system had been created, the height of the radial head was defined by moving a plane parallel to the rim best-fit plane distally until the head-neck interface was reached. After these input parameters had been chosen, the cross section at each slice were outputted as a list of points. The dish and outer cross sections were manually separated for the top 15% of the radius where the dish is typically present.

Our ellipse fitting method utilized available MATLAB (The Mathworks Inc., Natick, MA, USA) code based on a non-linear least squares approach which minimizes the orthogonal distance between input points and the fitted ellipse as described by Gander et al.[19,20]. Using this algorithm the dish and outer cross sections were fitted as ellipses. Additionally, the rim points initially selected by the user were fitted after projection onto their best-fit plane. For each ellipse the major and minor diameters, center position (Δx, Δy) and orientation about the Z axis (θ) were determined for a total of five parameters per cross section as shown in Figure 2.3. The Z coordinate of each ellipse center could also be determined using the height percentage of each cross section.

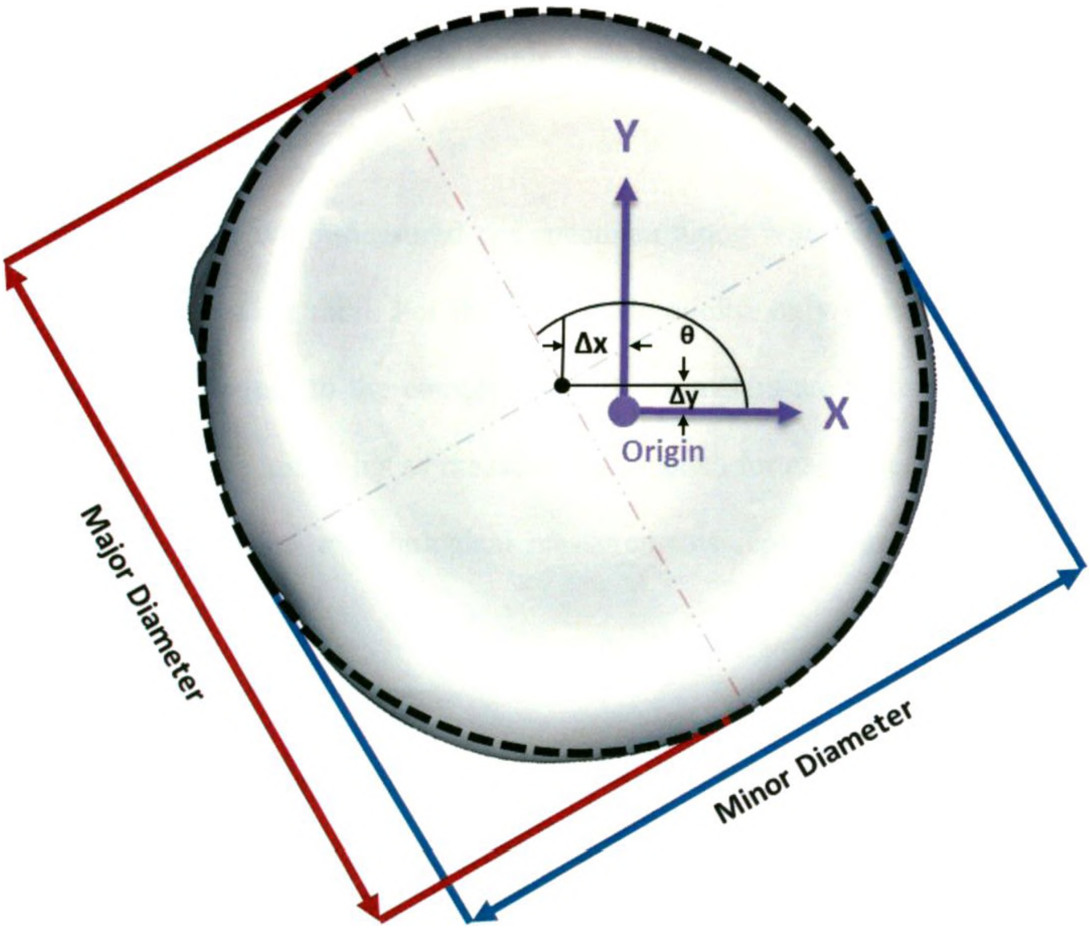

Figure 2.3: Ellipse-Fit Parameters for a Single Cross Section

Major Diameter = widest diameter of the ellipse
Minor Diameter = diameter orthogonal to the major diameter
Δx = x offset of ellipse center from the origin (at deepest point)
Δy = y offset of ellipse center from the origin (at deepest point)
θ = angle offset of the major diameter from the X-axis going CCW
Note: Δx and Δy exaggerated for clarity

To ensure that the slice thickness was fine enough to accurately capture the maximum major outer diameter of the radial head, ten specimens were measured using both 1% and 10% slices and the results compared. The average difference in maximum diameter was 0.02 mm (range 0-0.05mm), confirming that 10% slices are adequate to detect the peak transverse diameter. As the profile of the radius changes quickly as it

approaches the proximal end, 5% slices were used for the proximal 20% of the radius in order to capture this detail. The details of this comparison can be seen in Appendix C.

2.2.2 MEASUREMENTS

Sixteen ellipses were measured per specimen along with height and depth for a total of 82 parameters per radii. For the sake of simplicity, only general morphological measurements as opposed to the complete list of parameters are featured in the results and discussion. The complete list of measured parameters for each specimen is shown in Appendix D. The general morphological measurements reported are listed below and shown in Figure 2.4.

Major Outer Diameter – largest overall major diameter

Minor Outer Diameter – minor paired diameter with above

Major Rim Diameter – determined from fit of user selected rim points

Minor Rim Diameter – minor diameter paired with above

Height – measured between best-fit plane of rim to the head-neck interface

Depth – distance from best-fit plane of rim to deepest point (origin)

Lat. Dish Offset – distance in X from the origin to the center of the largest ellipse

Ant. Dish Offset – distance in Y from the origin to the center of the largest ellipse

Outer Angle – angle between X-axis and the Major Outer Diameter

Rim Angle – angle between X-axis the Major Rim Diameter

The major and minor diameters of both the manually selected rim points and the largest outer cross section along with height and depth are presented to compare with

previous studies on radial morphology. The orientation of both the outer and rim ellipses were determined to confirm that they were roughly aligned to each other and perpendicular to the PRUJ articulation (i.e. lateral) when in the neutral position as shown in previous studies. The offset of the deepest point of the dish relative to the center of the largest outer ellipse was determined in the lateral and anterior directions to quantify the dish offset.

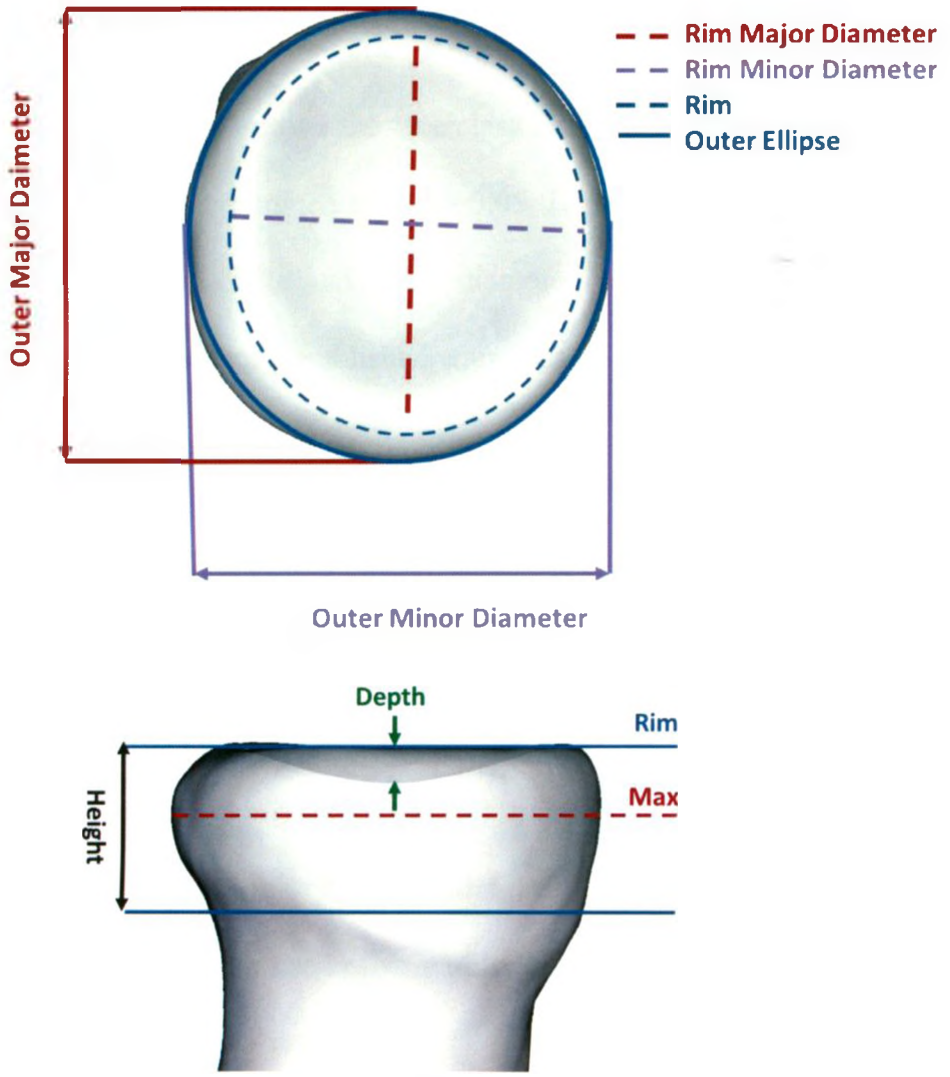

Figure 2.4: Overview of Reported Radial Head Measurements

Top – Major and minor diameter measurements. Angle and dish offset not shown. Bottom – Height and dish depth measurements. Also shown are the cross section planes for the rim and maximum outer ellipses.

2.2.3 Statistical Analyses

Significant correlations between measured variables were determined using two-tailed Pearson Correlation Coefficients. The male (n=34) and female (n=16) specimens were compared using an unpaired t-test for each of the reported parameters to determine which parameters showed significant gender-specific differences. The intra- and inter-observer reliability was determined using a separate set of eight specimens. Each specimen was measured twice by one researcher at different times and again by another. The reliability of each measurement was calculated using SPSS (IBM Corporation, Armonk, NY, USA) to determine the Interclass Correlation Coefficients (ICC). For this study significance was determined using α=0.05. Linear regressions were used to model the relationship between major and minor diameters at the rim and outer cross sections for comparison with previously published equations.

2.3 Results

The mean and standard deviation (SD) of all 50 specimens for each of the morphological measurements are shown below in Table 2.1. Table 2.2 shows the range of values for the same set of measurements. Both the rim and outer major and minor diameters were significantly different ($p<0.01$). The average difference in diameters was 1.3±0.5mm for the largest outer ellipse and 1.4±0.8mm for the rim. The outer and rim angle were compared to both each other and to 90° and in all cases were not statistically different ($p = 0.88, 0.31, 0.41$ respectively).

Linear regressions showing the relationship between major vs. minor outer and major vs. minor rim diameters were determined with $p<0.001$ as $y=-0.39+0.96x$ and $y=1.44+0.84x$ respectively as shown in Figure 2.5. Pearson correlations between each of

the variables which were significant at $\alpha = 0.05$ are shown in Table 2.3. Plots of relevant correlations are shown in Figure 2.6.

Comparison between the male (n=34) and female (n=16) specimens for each of the reported parameters and showed statistically significant differences for all four of the measured diameters as well as height, depth and lateral dish offset (α=0.05).

Table 2.1: Mean and SD of Selected Radial Head Measurements

	All (50)	Male (34)	Female (16)
Major Outer Diameter	24.7±2.3 mm*	26.0±1.5 mm	22.0±1.1 mm
Minor Outer Diameter	23.4±2.3 mm*	24.7±1.6 mm	20.8±0.8 mm
Major Rim Diameter	18.3±2.0 mm*	19.2±1.7 mm	16.5±0.9 mm
Minor Rim Diameter	16.9±1.8 mm*	17.6±1.6 mm	15.3±1.0 mm
Height	8.9±0.8 mm*	9.1±0.7 mm	8.4±0.6 mm
Depth	2.0±0.4 mm*	2.1±0.4 mm	1.8±0.2 mm
Lateral Dish Offset	-0.1±0.8 mm*	0.0±0.8 mm	-0.4±0.6 mm
Anterior Dish Offset	-1.4±0.8 mm	-1.5±0.9 mm	-1.0±0.5 mm
Outer Angle	93.0±20.6°	94.7±23.5°	89.4±12.0°
Rim Angle	93.6±30.5°	98.5±28.9°	83.3±32.2°

*Indicates statistically significant difference between male and female measured values ($\alpha = 0.05$)

Table 2.2: The Range of Selected Radial Head Measurements

	All	Male	Female
Major Outer	20.5-28.8 mm	22.5-28.8 mm	20.5-24.0 mm
Minor Outer	19.3-28.4 mm	20.3-28.4 mm	19.3-22.0 mm
Major Rim	15.0-24.1 mm	15.8-24.1 mm	15.0-17.9 mm
Minor Rim	12.4-20.8 mm	14.3-20.8 mm	12.4-16.9 mm
Height	7.5-10.5 mm	7.8-10.5 mm	7.5-10.3 mm
Depth	1.4-3.5 mm	1.6-3.5 mm	1.4-2.2 mm
X Outer	-1.7-1.6 mm	-1.7-1.6 mm	-0.9-1.4 mm
Y Outer	-0.8-3.0 mm	-0.8-3.0 mm	-0.1-1.8 mm
Outer Angle	33.5-157.4°	33.5-157.4°	53.4-104.6°
Rim Angle	6.5-152.8°	18.9-152.8°	6.5-114.9°

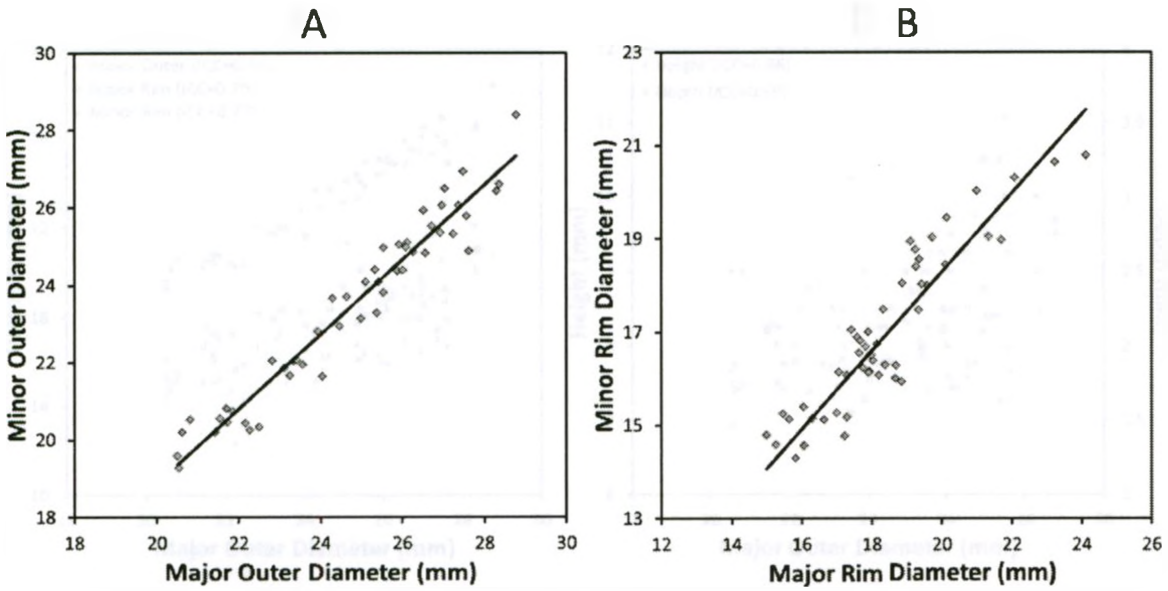

Figure 2.5: Regression Plots ($p<0.001$)

Regression showing relationship between major and minor:
A) outer diameters.
B) rim diameters.

Table 2.3: Table of Significant Pearson Correlation Coefficients ($p<0.05$)

	Major Outer	Minor Outer	Major Rim	Minor Rim	Height	Depth	Outer Angle	Rim Angle
Major Outer	x							
Minor Outer	0.97	x						
Major Rim	0.79	0.81	x					
Minor Rim	0.77	0.81	0.91	x				
Height	0.66	0.66	0.41	0.45	x			
Depth	0.50	0.57	0.77	0.71	0.40	x		
Outer Angle	-	-	0.43	-	-	0.38	x	
Rim Angle	-	-	-	-	-	-	0.47	x

Note: No significant correlations exist with respect to either direction of dish offset.

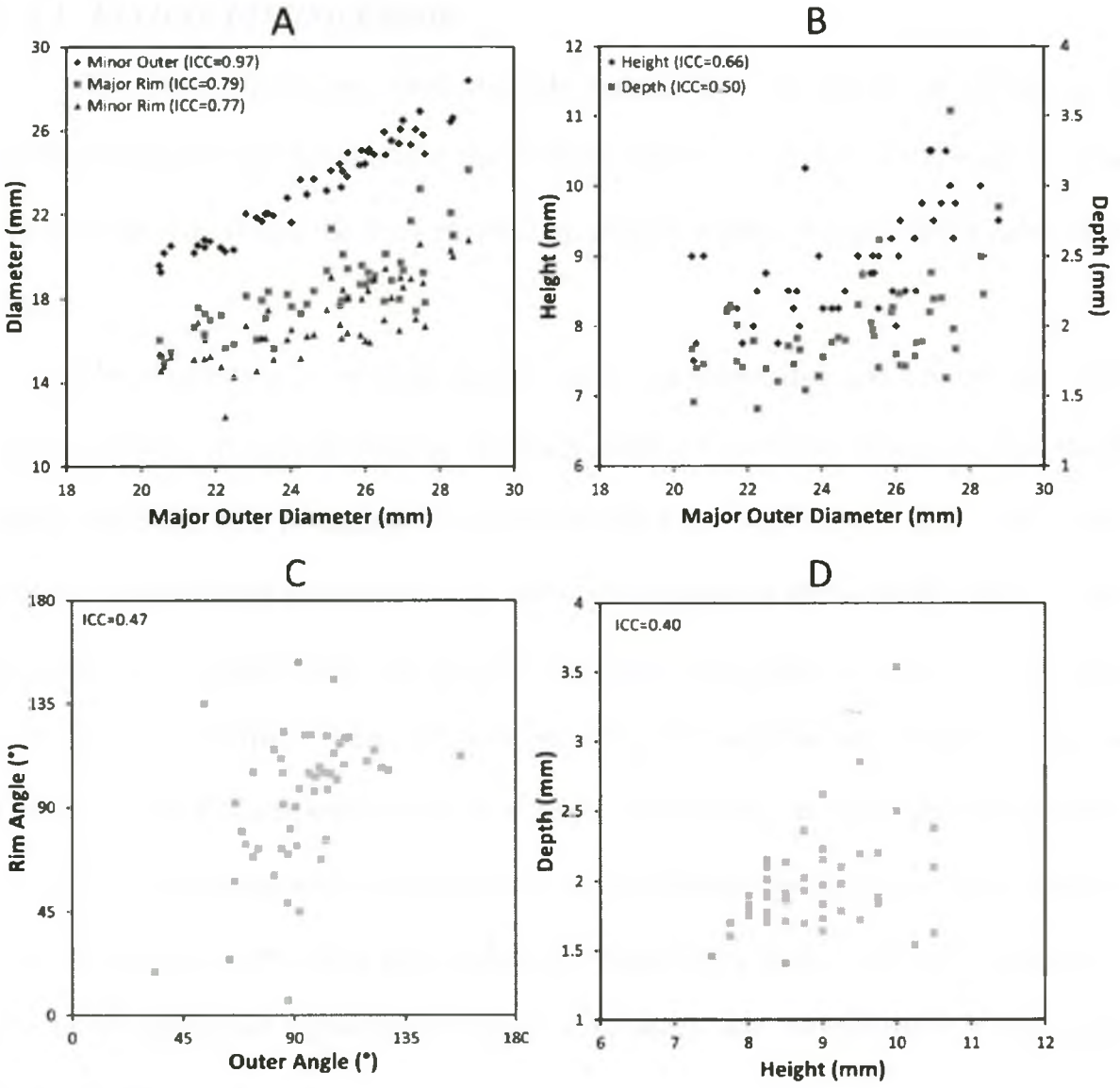

Figure 2.6: Correlation Plots ($p<0.05$)

A) Correlation between each of the measured radial head diameters with respect to the maximum outer head diameter.
B) Correlation between height and major outer head diameter and between depth and major outer diameter.
C) Correlation between rim angle and outer angle.
D) Correlation between height and depth.

2.3.1 *Ellipse Fitting Error*

The orthogonal distance between each point on the cross section and the ellipse-fit was measured for each fitted ellipse for all 50 specimens using MATLAB code[21,22]. This served as an indicator of the error incurred by using an ellipse to approximate radial head shape.

The ellipse fitting error was determined for the outer, dish and rim ellipses. The "outer" ellipses are each defined by the depth of the cross section relative to the best-fit plane expressed as a percentage of overall height (ie. 5%,10%,etc.). The "dish" cross sections are similarily defined but only up to 15% height (ie D5%, D10%, D15%). The twenty points selected by the user along the rim projected on the best-fit plane were used to fit the "rim" ellipse. These different group of cross sections are sorted by color in Figure 2.7 which corresponds to the color used to differentiate the same groups in Figures 2.8 and 2.9. The mean and standard deviation of the fitting error are shown in Figure 2.8. The average maximum fitting error and the maximum error range is shown in Figure 2.9. The mean orthogonal distance error was 0.13±0.06mm and the maximum error ranged from 0.01mm to 1.45mm.

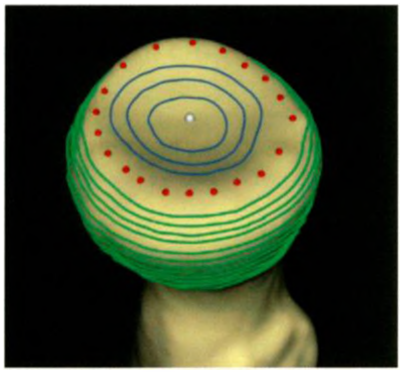

Figure 2.7: Color Legend for Error Plots

Red – Rim ellipse determined from user selected points shown above
Green – Outer ellipses determined from cross sections shown above
Blue – Dish ellipses determined from cross sections shown above

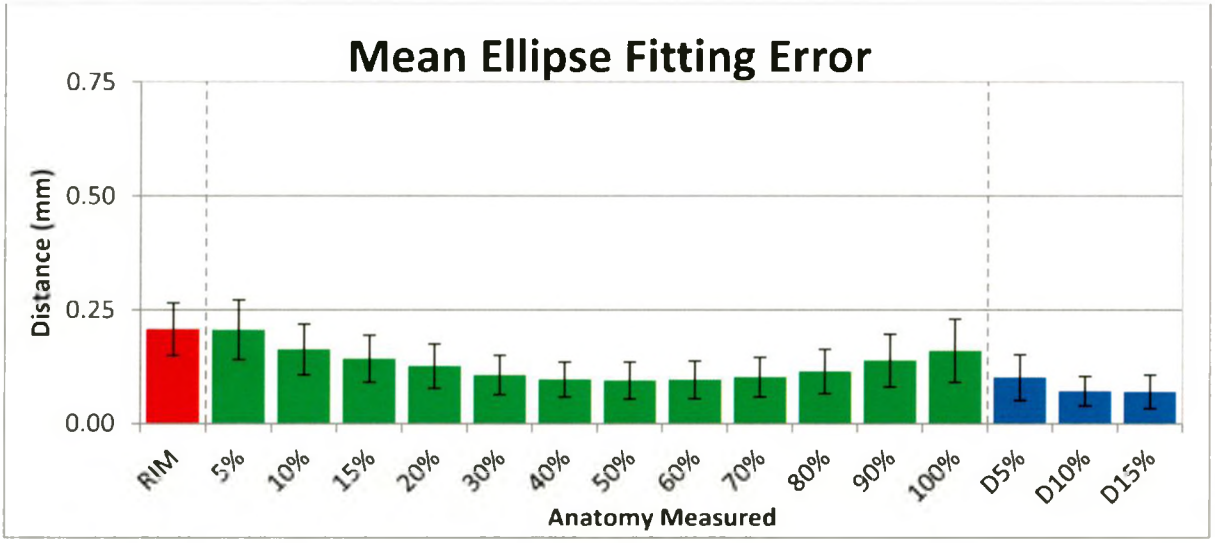

Figure 2.8: The mean ± 1SD of the ellipse fitting error for each of the sixteen fitted ellipses (n=50).

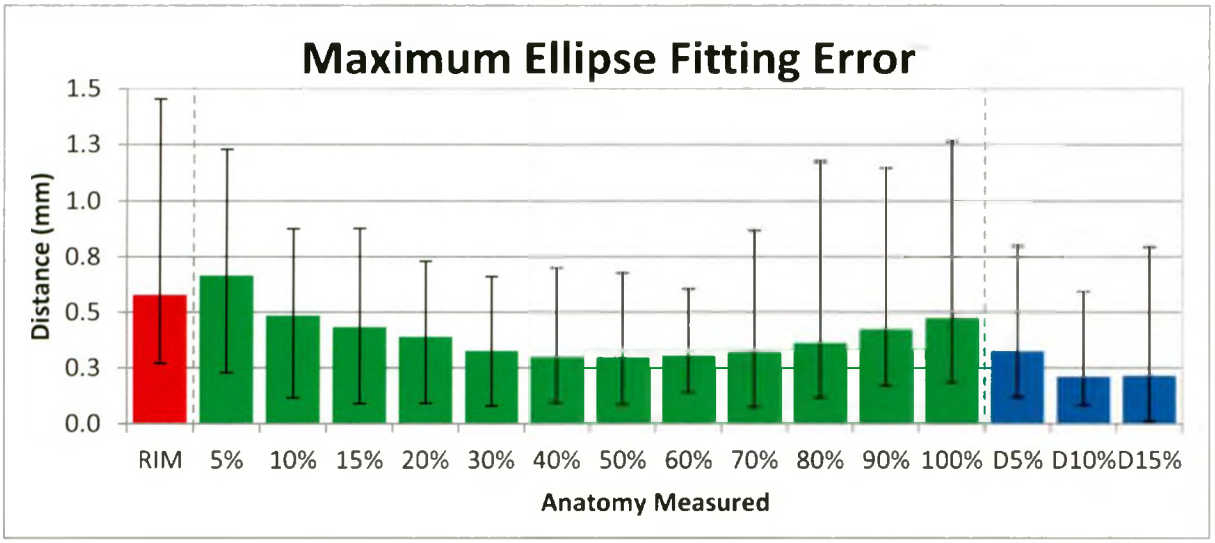

Figure 2.9: The mean maximum ellipse fitting error for each of the sixteen fitted ellipses (n=50).

Range of the maximum error across all specimens is shown by the error bars.

2.3.2 *Inter-Observer and Intra-Observer Reliability*

The ICC were calculated using SPSS and are shown in Figure 2.10. The measurement of radial head height showed poor inter and intra-observer reliability. Measurements of rim major diameter, minor diameter and angle showed less reliability compared to the rest of the measurements as reflected in the ICC values.

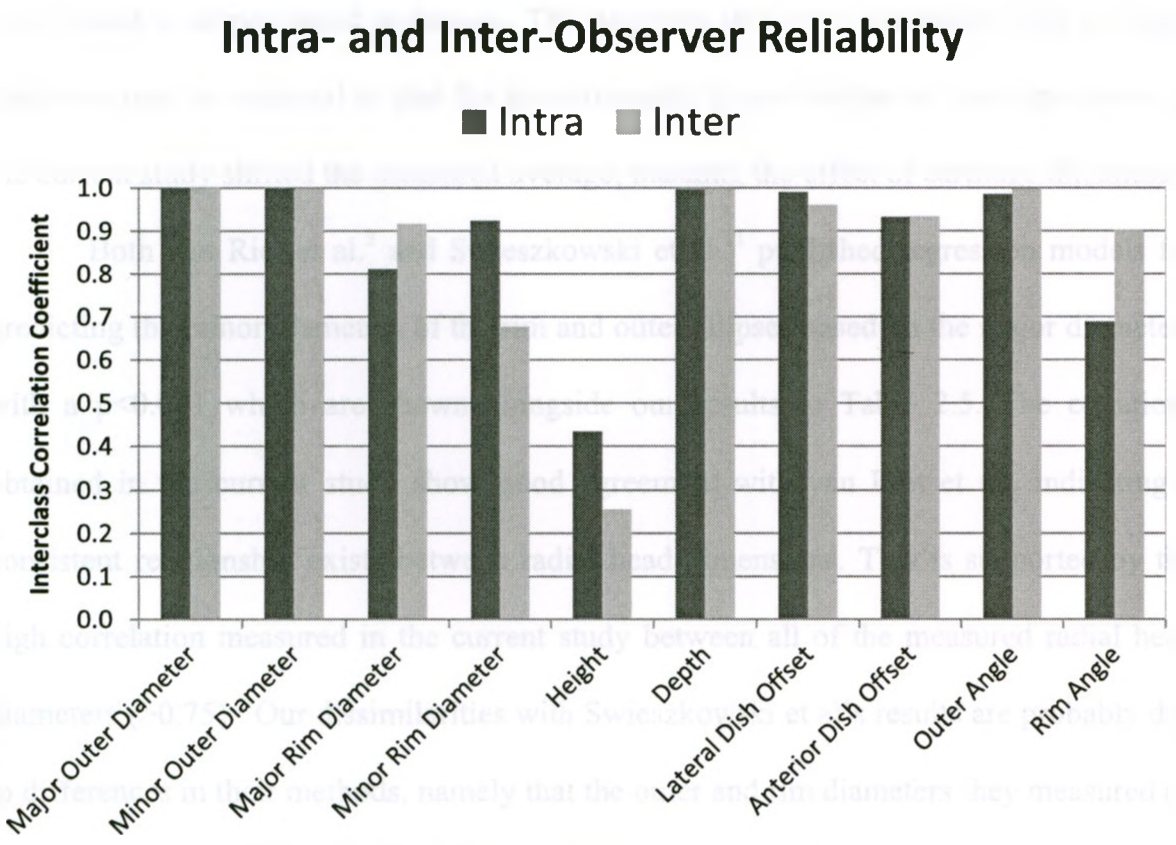

Figure 2.10: The intra and inter-observer reliability for each of the reported radial head measurements. (n=8)

2.4 DISCUSSION

Ellipse fitting can approximate the cross sections of the radial head and dish with minimal error across the height of the radial head. Results obtained using our automated ellipse fitting methods are consistent with those reported by others as shown in Table 2.4. In particular, the results closely matched those published by van Riet et al.[5] in 2003 which used a caliper-based technique. This suggests that error associated with cartilage thickness may be minimal or that the proportionally larger number of male specimens in the current study shifted the measured average, masking the effect of cartilage thickness.

Both van Riet et al.[5] and Swieszkowski et al.[11] published regression models for predicting the minor diameters of the rim and outer ellipses based on the major diameters with a $p<0.001$ which are shown alongside our results in Table 2.5. The equations obtained in the current study show good agreement with van Riet et al., indicating a consistent relationship exists between radial head dimensions. This is supported by the high correlation measured in the current study between all of the measured radial head diameters (>0.75). Our dissimilarities with Swieszkowski et al's results are probably due to differences in their methods, namely that the outer and rim diameters they measured do not appear to be orthogonal and the outer diameters were both measured at the level of the radial head concavity, as opposed to at the widest cross section as in the current investigation.

Table 2.4: Comparison of Results to Previous Morphological Studies

Study	Modality	n	M:F	Outer Max	Outer Min	Rim Max	Rim Min	Height	Depth
Current Study (2011)	CT	50	34:16	24.7 ± 2.3	23.4 ± 2.3	18.3 ± 2.0	16.9 ± 1.8	8.9 ± 0.8	2.0 ± 0.4
Koslowsky et al. (2007)	Image	18	8:10	24.1	22.7	16.7	x	10.53	1.95
Popovic et al. (2005)	CT	51	28:23	22.9 ± 1.9	21.9 ± 1.9	x	x	9.9 ± 1.6	2.4 ± 0.6
van Riet et al. (2003)	Caliper	27	14:13	25.1 ± 2.1	23.4 ± 2.3	17.8 ± 1.6	16.8 ± 1.5	x	2.4 ± 0.5
Captier et al. (2002)	Caliper	96	x	21.7 ± 2.7	20.2 ± 2.7	12.1 ± 1.6	x	9.1 ± 1.7	x
King et al. (2001)	CMM	28	x	24.3 ± 2.4	22.6 ± 2.4	x	x	x	2.4 ± 0.5
Swieszkowski et al. (2001)	CMM	8	Male	23.4 ± 1.1	22.5 ± 1.1	16.6 ± 1.0	14.8 ± 0.8	10.2 ± 1.4	2.0 ± 0.4

Table 2.5: Comparison of Regression Models Used to Predict Radial Head Minor Diameters

Regression	Current Study	van Riet et al.	Swieszkowski et al.
Outer Major to Minor	y= -0.39+0.96x	y = -0.53+0.96x	y = 4.57 + 0.73x
Rim Major to Minor	y = 1.44+0.84x	y = 1.98+0.85x	y = 3.180 + 0.73x

Although the diameters are significantly different between male and female specimens (Table 2.1), it is likely that both can be predicted using the same regression as diameters were correlated and may simply be proportionally larger when comparing male to female specimens. This may explain why the slopes of van Riet's regressions were similar to our results, despite differences in the male/female ratio. The best-fit line would be similar although the point distribution would be biased toward larger diameters.

The major and minor diameters were shown to be statistically different, although the magnitude of the differences was small, for both the circumferential and rim ellipses, confirming that the radial head is non-circular as reported by previous studies[5,6]. The rim and outer ellipse orientations were similar and close to the expected 90°, which indicates that in the neutral position their major axes are oriented medial-laterally or roughly perpendicular to the PRUJ articulation. The dish is offset in the posterior direction approximately 1-2mm from the center of the maximum outer ellipse while in the anatomic position. The dish is not consistently shifted medially or laterally. This agrees with observations reported previously[5,10].

Currently, there is some debate over the magnitude at which the difference between the maximum and minimum diameter indicate a non-circular shape, with a threshold of 1mm being used in multiple studies[10,11]. It has been suggested by Captier et al. [10] that this may be the result of two distinct radial head shapes within the population, approximately 60% "elliptical" and 40% "circular", with a corresponding change in the head neck angle. In the current study approximately 30% of specimens had a diameter difference less than 1 mm and would be considered "circular" using this threshold. These "circular" specimens were not significantly different in any measured diameter compared

to the "elliptical" heads and were distributed amongst the male and female specimens. The mean difference between the major and minor outer diameter was only 0.7±0.2 mm in this group compared to 1.6±0.4 in the remaining specimens which was statistically significant at α=0.05. However, based on the results of the current study, it appears that an ellipse provides a good descriptor of the radial head shape at all cross sections and that the difference between maximum and minimum diameters is proportional and statistically significant.

Another study suggested that the radial head circumference also presented in two distinct variations; uneven and even circumference height, in an approximate 2:1 ratio which may support the concept of different modes of radial head shape[23]. Evaluation of a larger and more variable pool of specimens with the techniques employed in the current study may provide further insight into this theory. However, new method of measuring height which included its variation about the radial head would be needed to evaluate this specific theory.

The different techniques used to measure shape, in particular the exclusion of articular cartilage in CT and radiography based morphology studies, may also explain the differences among published findings. Cartilage may be of non-uniform thickness altering the cross sectional profile of the radial head. Methods for determining regional variations in cartilage thickness have been described for other joints[24] and should be applied at the radial head.

The major advantage of the current measurement methods relative to previous studies is that radial head dimensions can be measured at known height intervals in a semi-automated fashion. The major and minor diameters are always perpendicular and at

the same height. The large number of measured cross sections should allow for highly accurate patient specific or population-based implant models to be generated using computer assisted design (CAD) software.

The method presented is not without weaknesses. Specimens used in this study were older, and therefore likely more osteoporotic, than the average patient suffering from a radial head fracture who typically has a mean age of 45 years[25]. The measured parameters do not account for the variable height of the dish rim as the rim points were first projected onto their best-fit plane before obtaining measurements. The variable height of the dish rim likely plays a role in resisting subluxation of the radial head[26]. Intra and inter-observer measurements were less consistent for the rim as this feature was defined manually by the observer. An automated technique for determining the rim points and their height variation would be a worthwhile addition to the current method.

While the intra and inter-observer reliability is generally very good the reliability is much lower in measuring radial head height. . This is a well-known problem which has been reported in previous morphology studies, primarily due to the fact that the height of the articular circumference varies significantly depending on orientation in many specimens [6,27]. A difference in the height measurement effects the creation of cross sections as they are based on fixed height percentages. However, reported values such as the maximum major and minor outer diameter are still consistent despite these issues, as their cross section height may change but their magnitude does not. Possible solutions to this problem include using a fixed percentage of the overall radial length to determine height or measuring height in a consistent orientation.

In conclusion, this study has shown that: (a) the radial head can be accurately modeled using elliptical cross sections with minimal error; (b) the diameters of both the outer and rim ellipses are correlated; (c) the outer and rim major diameters are aligned and oriented medial-laterally, or roughly perpendicular to the PRUJ; and (d) the dish is slightly offset in the posterior direction in the anatomic position. The measured parameters capture the variable shape of the radial dish and circumference with respect to a consistent anatomically derived coordinate system, and are expected to provide suitably accurate data for use in the design of a more anatomically correct radial head prosthesis.

2.5 REFERENCES

1. Judet T, Garreau de Loubresse C, Piriou P, Charnley G. A floating prosthesis for radial-head fractures. The *Journal of Bone and Joint Surgery - British Volume*. 1996;78(2):244-9.

2. King GJW, Zarzour ZD, Patterson SD, Johnson JA. An anthropometric study of the radial head: implications in the design of a prosthesis. *The Journal of Arthroplasty*. 2001;16(1):112-6.

3. Beredjiklian PK, Nalbantoglu U, Potter HG, Hotchkiss RN. Prosthetic radial head components and proximal radial morphology: a mismatch. *Journal of Shoulder and Elbow Surgery*. 1999;8(5):471–475.

4. Popovic N, Djekic J, Lemaire R, Gillet P. A comparative study between proximal radial morphology and the floating radial head prosthesis. *Journal of Shoulder and Elbow Surgery*. 2005;14(4):433-40.

5. van Riet RP, van Glabbeek F, Neale PG, et al. The noncircular shape of the radial head. *The Journal of Hand Surgery*. 2003;28(6):972-978.

6. Koslowsky TC, Germund I, Beyer F, et al. Morphometric parameters of the radial head: an anatomical study. *Surgical and Radiologic Anatomy*. 2007;29(3):225-30.

7. Mahaisavariya B, Saekee B, Sitthiseripratip K, et al. Morphology of the radial head: a reverse engineering based evaluation using three-dimensional anatomical data of radial bone. *Proceedings of the Institution of Mechanical Engineers. Part H: Journal of Engineering in Medicine*. 2004;218(1):79-84.

8. Skalski K, Swieszkowski W, Pamianowski S, Kedzior K, Kowalik S. Radial head prosthesis with a mobile head. *Journal of Shoulder and Elbow Surgery*. 2004;13(1):78-85.

9. van Riet RP, van Glabbeek F, Neale PG, et al. Anatomical considerations of the radius. *Clinical Anatomy*. 2004;17(7):564-9.

10. Captier G, Canovas F, Mercier N, Thomas E, Bonnel F. Biometry of the radial head: biomechanical implications in pronation and supination. *Surgical and Radiologic Anatomy*. 2002;24(5):295-301.

11. Swieszkowski W, Skalski K, Pomianowski S, Kedzior K. The anatomic features of the radial head and their implication for prosthesis design. *Clinical Biomechanics (Bristol, Avon)*. 2001;16(10):880-7.

12. Spinner M, Kaplan EB. The quadrate ligament of the elbow--its relationship to the stability of the proximal radio-ulnar joint. *Acta Orthopaedica Scandinavica.* 1970;41(6):632-47.

13. Caputo AE, Mazzocca AD, Santoro VM. The nonarticulating portion of the radial head: anatomic and clinical correlations for internal fixation. *The Journal of Hand Surgery.* 1998;23(6):1082-90.

14. Weiss A, Hastings I. The anatomy of the proximal radioulnar joint. *Journal of Shoulder and Elbow Surgery.* 1992.

15. Morrey B, An K, Stormont T. Force transmission through the radial head. *The Journal of Bone and Joint Surgery.* 1988;70(2):250.

16. King GJW, Zarzour ZD, Rath DA, et al. Metallic radial head arthroplasty improves valgus stability of the elbow. *Clinical Orthopaedic and Related Research.* 1999;(368):114-25.

17. Liew VS, Cooper IC, Ferreira LM, Johnson JA, King GJW. The effect of metallic radial head arthroplasty on radiocapitellar joint contact area. *Clinical Biomechanics (Bristol, Avon).* 2003;18(2):115-8.

18. Pomianowski S, Morrey BF, Neale PG, et al. Contribution of monoblock and bipolar radial head prostheses to valgus stability of the elbow. *Journal of Bone and Joint Surgery.* 2001;83-A(12):1829-34.

19. Gander W, Golub GH, Strebel R. Least-squares fitting of circles and ellipses. *BIT.* 1994;34(4):558-578.

20. Brown R. fitellipse.m. 2007. Available at: http://www.mathworks.fr/matlabcentral/fileexchange/15125-fitellipse-m.

21. Kim I-sung. An algorithm for finding the distance between two ellipses. *Communications of the Korean Mathematical Society.* 2006;21(3):559-567.

22. Arthington M. Distance from points to an ellipse. 2010. Available at: http://www.mathworks.com/matlabcentral/fileexchange/26261-distance-from-points-to-an-ellipse.

23. Bartz B, Tillmann B, Schleicher A. Stress in the human elbow joint. *Anatomy and Embryology.* 1984;169(3):309–318.

24. Trinh NH, Lester J, Fleming BC, Tung G, Kimia BB. Accurate measurement of cartilage morphology using a 3D laser scanner. *Measurement.* 2006:37-48.

25. van Riet RP, Morrey BF, O'Driscoll SW, van Glabbeek F. Associated Injuries Complicating Radial Head Fractures. *Clinical Orthopaedic and Related Research*. 2005;441(&NA;):351-355.

26. Jensen SL, Olsen BS, Seki A, Ole Søjbjerg J, Sneppen O. Radiohumeral stability to forced translation: an experimental analysis of the bony constraint. *Journal of Bone and Joint Surgery - American Volume*. 2002;11(2):158-65.

27. Itamura JM, Roidis NT, Chong AK, et al. Computed tomography study of radial head morphology. *Journal of Shoulder and Elbow Surgery*. 2008;17(2):347-54.

28. Gupta G. Differences in radial head dimensions based on gender, race, age and side. *Orthop Trans*. 1992.

CHAPTER 3 - Design of Patient-Specific and Population-Based Radial Head Implants With Comparison of Surface Fit to a Current Implant Design

OVERVIEW:

The surface mismatch between radial head prostheses and the native anatomy has not been reported. This chapter details the design and analysis of both a population-based quasi-anatomic implant series and three distinct patient-specific designs using a novel distance mapping approach with comparison to an existing axisymmetric implant.

3.1 INTRODUCTION

Comparisons of existing radial head implant shapes to the native morphology have been reported in previous studies by matching individual implant parameters to measured values. In 1999, using MRI imaging, Beredjiklian et al.[1] showed that available radial head implant designs overestimated the medullary canal diameter, resulting in a number of specimens which were unable to accommodate the implant stem when the head size was optimal. Studies by Popovic et al.[2] and King et al.[3] further confirmed that the size of the radial head and the medullary canal were poorly correlated. As a result of these findings, commercially available modular implant systems were developed allowing for increased variability between the implant stem and head size.

The radial head is known to have a complex and variable shape which is difficult to replicate[2,4]. In spite of this, the majority of currently available implant systems have an axisymmetric design. These implants compensate for their non-anatomic shape by

allowing implant motion using either an unfixed stem or a bipolar implant design[5,6]. There is currently one commercially available implant with a non-axisymmetric design[7]. As implants become available that are designed to match the anatomical shapes of the radial head, the accuracy with which they match the shape of the native radial head must be quantified. During surgical implantation, asymmetric prostheses are aligned to best match the native anatomy and are then fixed to bone. This represents an important difference from axisymmetric designs which typically allow motion of the stem in the radial neck or incorporate a bipolar articulation.

Studies examining the effect of prosthesis mal-positioning have been conducted on the radial head using current axisymmetric designs. Over or under-lengthening of the implant by as little as 2.5mm alters joint kinematics and laxity[8]. Over-lengthening in particular is problematic as radio-capitellar contact pressure has been shown to increase significantly, which may lead to complications including capitellar erosion and restricted motion[8]. There are currently no reported studies that have evaluated the effect of anatomic vs. axisymmetric implant shapes on elbow kinematics.

Finite element analysis (FEA) has been employed in numerous joints to investigate and optimize implant design with respect to their shape, material properties and wear resistance. Gupta et al.[9] examined the effect of implant material on load transfer and deformation as compared to the native radial head anatomy. They designed an implant based on a previous morphology study to minimize and distribute the joint contact force across the articular surface. However, their proposed implant design contradicts the findings detailed in Chapter 2 which showed the radius is non-circular and that the articular dish is non-concentric.

The current study sought to refine the techniques used to develop radial head implants using semi-automated ellipse fitting of radial head cross sections based on the morphological parameters measured in Chapter 2. Both population-based quasi-anatomic and patient-specific implants were designed using these measured parameters to represent currently emerging implant types which as of yet have not been reported in the literature[7,10]. Methods to ensure ideal placement may be important in ensuring the success of these asymmetric anatomic implant designs, as noted in previous studies, and will be the focus of a subsequent chapter[11].

In order to determine the success of these implant designs we quantified overall surface mismatch between proposed implant designs and the native morphology, as opposed to quantifying specific parameters. Using this approach, implant performance was assessed and compared by calculating the distance between nearest points on the implant and bone surfaces; these can then be displayed visually and quantified numerically.

In order to provide a reference for comparison, surface mismatch was also used to assess the difference between an existing axisymmetric implant and the native morphology. Given the elliptical shape of the radial head, the optimal diameter of an axisymmetric implant is not known in spite of the fact that these are widely used clinically. It is not clear whether the minor diameter, major diameter or dish diameter is the best dimension for the surgeon to choose. By determining the existing axisymmetric implant with the lowest mismatch and comparing its diameter to the measured diameters of the radial head, the relationship between these measurements and the optimal implant size could be determined as well.

3.2 METHODS

3.2.1 MORPHOLOGY MEASUREMENTS

Fifty radial head specimens were measured using cross section ellipse fitting to determine their morphological parameters (outlined in Chapter 2). Each ellipse cross section was described with five parameters: major and minor diameters, lateral and anterior planar offsets of its center relative to the deepest point of the dish and the orientation angle of its major diameter relative to the lateral direction (described in Figure 2.3). The following 82 parameters were measured for each specimen.

- Head height and dish depth
- 5 ellipse parameters for the rim
- 12x5 ellipse parameters for the circumferential cross sections (at 5,10,15,20,30,40…100% of the radial head height)
- 3x5 ellipse parameters for the dish cross section (at 5,10 and 15% of the radial head height)

For the current study, 34 male left or right specimens were used to simplify the design of a population-based quasi-anatomic implant series. Female specimens were excluded as they are statistically different in size (Chapter 2). As anatomic implants are side-specific, left sided specimens were mirrored digitally before measurements were obtained.

3.2.2 *Existing Axisymmetric Implant*

For comparison to the surface mismatch data obtained from the quasi-anatomic implant series, the same measurements were performed using CAD models of an existing axisymmetric implant (Evolve Modular Radial Head System, Wright Medical, Arlington, TN, USA) to provide a datum. In order to ensure that the best sized implant from the existing series was used for each specimen, the mean mismatch was computed for all available sizes of the implant series which are shown in Figure 3.1. The iterative closest point (ICP)[12] algorithm was used to determine the ideal implant alignment for each size. The difference between ICP and manual alignment was examined for the quasi-anatomic implants in Appendix B. From these results the implant size with the lowest mean surface mismatch for each particular specimen was then used in determining the overall mean for the existing implant series. The optimal implant size was compared to the measured outer major and minor diameters and the rim major and minor diameters to determine the measurements closest to the optimal implant size.

3.2.3 *Quasi-Anatomic Implant Design*

The specimens were initially sorted based on the magnitude of their maximum major outer diameter as shown in Figure 3.2. This served as a simple method to group similarly sized specimens together using the correlation shown between radial head diameters in Chapter 2. The first group (Quasi Mean or QM) included specimens within one standard deviation of the mean diameter (n=24). The other two groups included specimens above (Q+, n=5) and below (Q-, n=5) this range. All specimens were within three standard deviations of the mean.

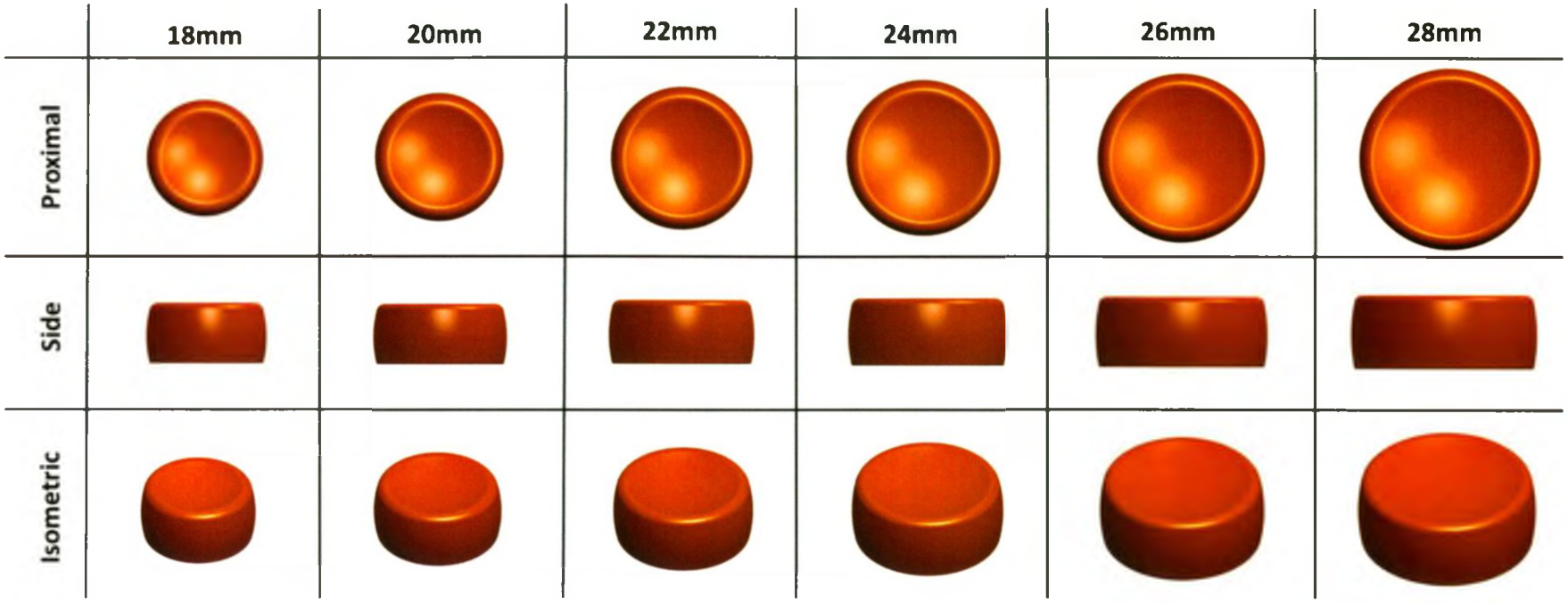

Figure 3.1: Existing axisymmetric implant series showing all sizes.

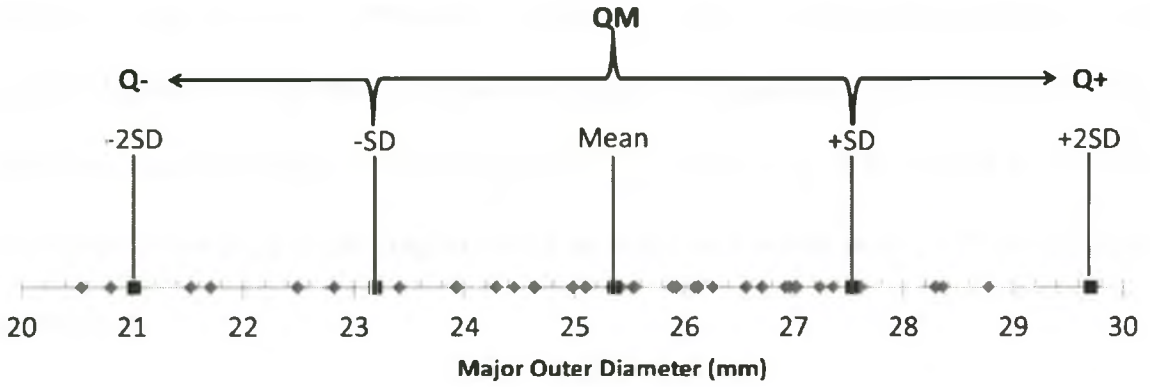

Figure 3.2: Quasi-Anatomic Implant Groups

Graphical depiction of the method used to sort the specimens (blue diamonds) into the Q-, QM and Q+ implant groups based on the mean and standard deviation of their major outer head diameter.

To determine the shapes of the quasi-anatomic implant series, the major and minor diameters, generated by ellipse-fitting each of the head and dish cross sections, were averaged along with overall height and dish depth across the specimens within each group. These measures were chosen as they were shown to be correlated with head size in Chapter 2. The orientation of each fitted ellipse was not correlated to radial head diameter, as shown in Chapter 2, so this parameter was averaged across all three groups. To ensure accurate measurements of orientation, any cross section in which the difference between the major and minor ellipse diameter was less than 0.5mm was eliminated from the average, as nearly-circular cross sections tended to have highly variable orientations. Three dimensional models of each quasi-anatomic implant are shown in Figure 3.3.

To determine ideal placement, the surface model of the quasi-anatomic implant with the closest major outer diameter was aligned to the CT model using the ICP algorithm after an initial coarse alignment of the deepest dish point on both models. ICP

alignment was used as it provided a quick, less biased and automated alternative to manual alignment of the three dimensional model. Comparison between manual and ICP alignment was conducted for seven specimens to ensure the ICP method was reliable. The results showed a slight improvement in alignment when using ICP as detailed in Appendix B.

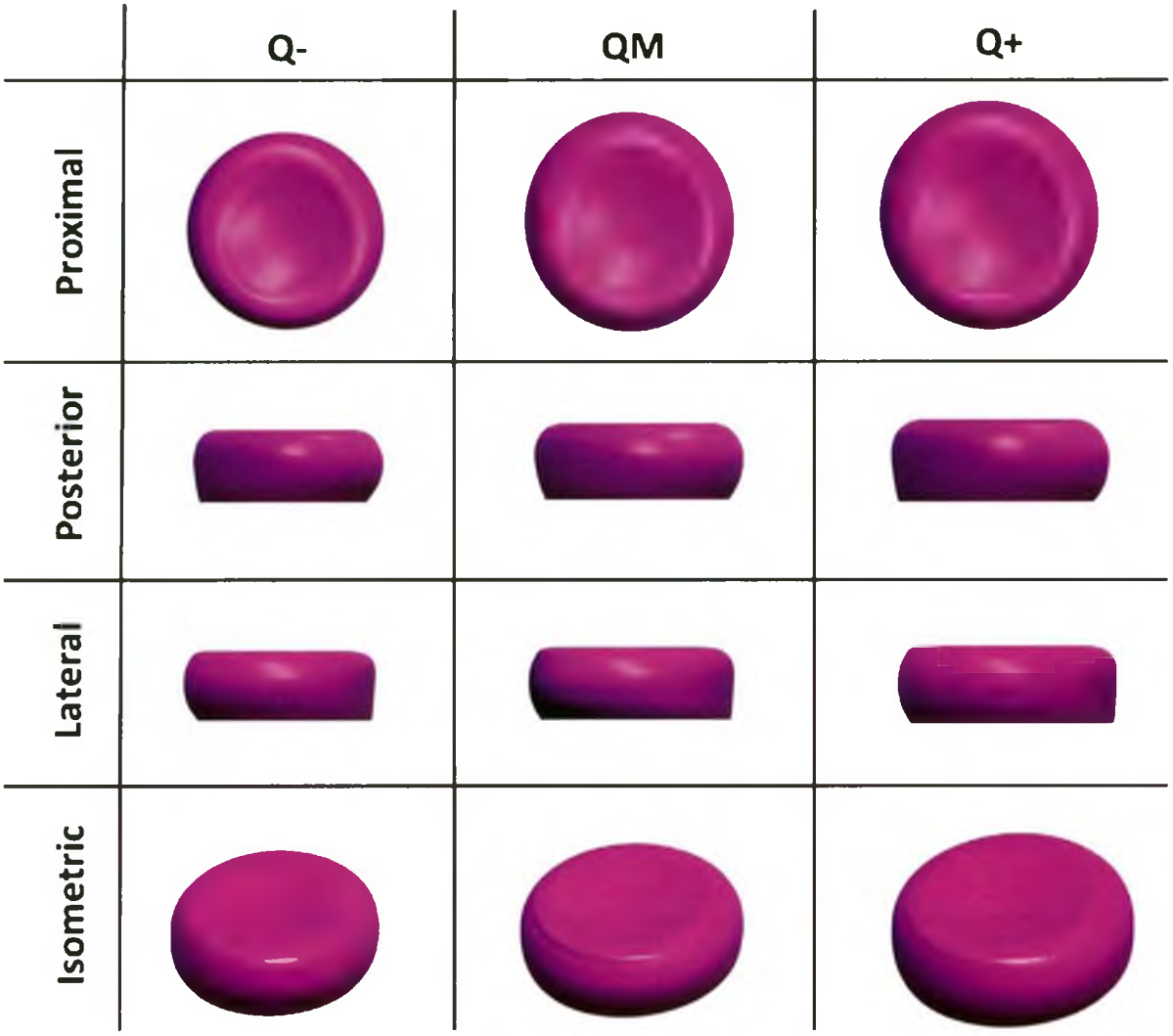

Figure 3.3: The quasi-anatomic implant series showing the small (Q-), mean (QM) and large (Q+) sizes.

3.2.4 PATIENT-SPECIFIC IMPLANT DESIGN

Patient-specific implants are commercially available using measurements obtained from radiographs to generate an axisymmetric implant[10]. This system, however, uses only overall diameter and height to determine the head shape. In the current study, three distinct patient-specific implant designs were compared—axisymmetric, elliptical and anatomic as detailed in Table 3.1 and Figure 3.4.

Table 3.1: The parameters used to define each of the patient-specific implant models.

Axisymmetric (3-parameter)	- Outer major diameter - Rim major diameter - Height
Elliptical (6-parameter)	- Outer major and minor diameters - Rim major and minor diameters - Height - Depth
Anatomic (82-parameter)	- Ellipse major and minor diameters and orientation as well as center offset for rim, outer and dish cross sections - Measurements taken at 5% increments of height until 20% and 10% thereafter - Head Height - Dish Depth

The same method used to assess the fit of the quasi-anatomic implants relative to the native anatomy was also applied for the three patient-specific models. Prior to fit assessment, the axisymmetric and elliptical models were first aligned using the ICP algorithm. The anatomic patient-specific implant did not require alignment as the CAD model was built in the same coordinate system as the CT and the ellipse fitted to each cross section included orientation relative to this coordinate system.

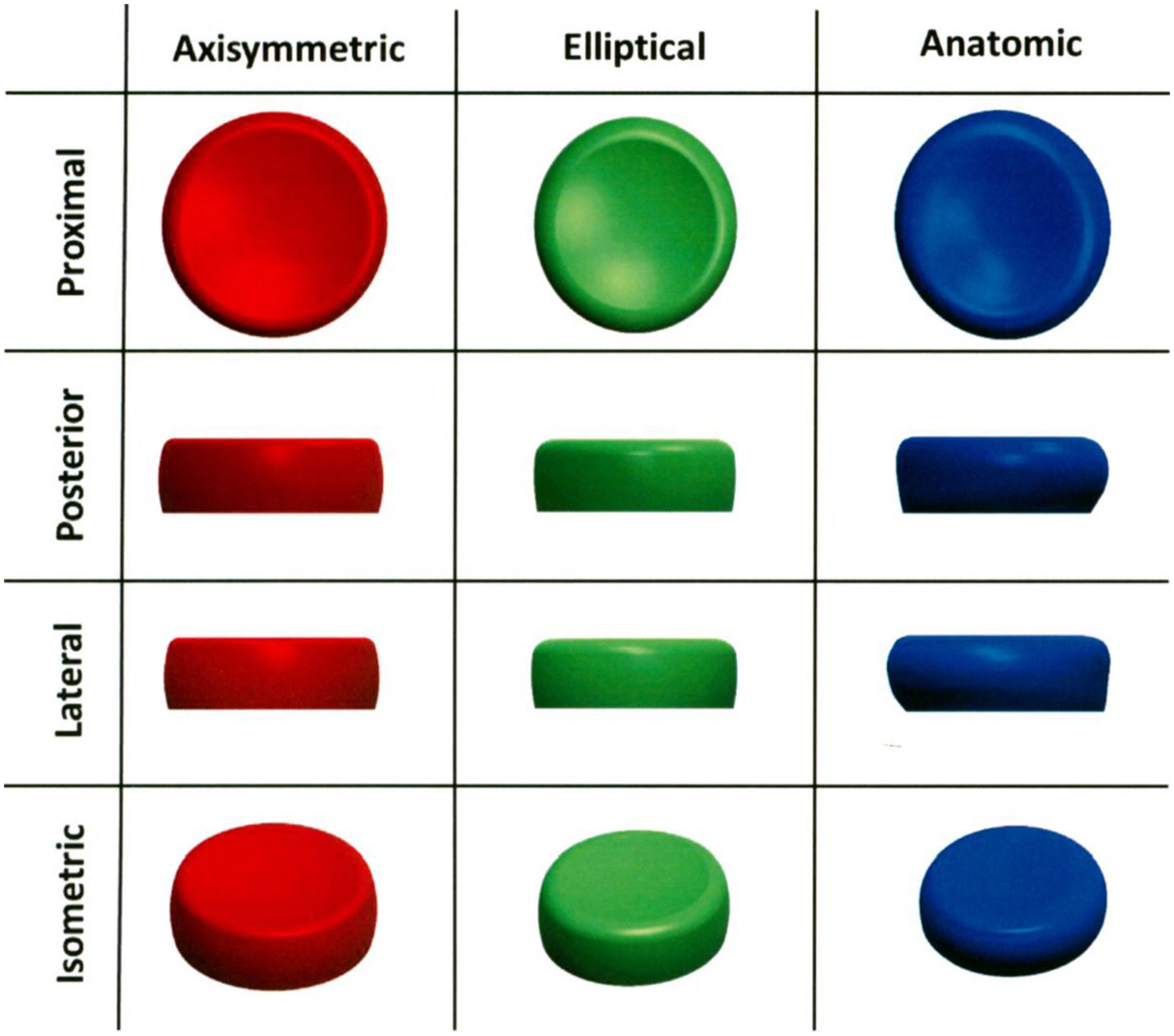

Figure 3.4: Comparison of the axisymmetric, elliptical and anatomic patient-specific implant models for one specimen.

3.2.5 Surface Mismatch

A custom program, previously described in the literature[13], created using the Visualization Toolkit (VTK, Kitware, Clifton Park, NY, USA) was used to determine surface mismatch. The implant models were first modified to limit the number of surface points to reduce processing time. An approximately even point distribution was ensured using a quadric clustering filter in VTK. Once this modified implant had been properly aligned to the model as described above, the distance between each point on the CAD

model and its nearest neighbor on the CT-obtained bone model was measured and the mean and distribution determined to quantify the surface mismatch of the existing axisymmetric, quasi-anatomic and patient-specific implants for each specimen. To calculate the mean mismatch, the absolute value at each point was used to eliminate direction so that the oversized and undersized regions of the implant did not cancel when averaged. The mean surface mismatch for each implant series was compared pair-wise using a one way ANOVA (SPSS, IBM Corporation, Armonk, NY, USA) at α=0.05.

3.3 RESULTS

All of the implants had statistically different means for distance mismatch via a one-way ANOVA at α=0.05. Figure 3.5 show the mean surface mismatch and its standard deviation for each implant series across all specimens.

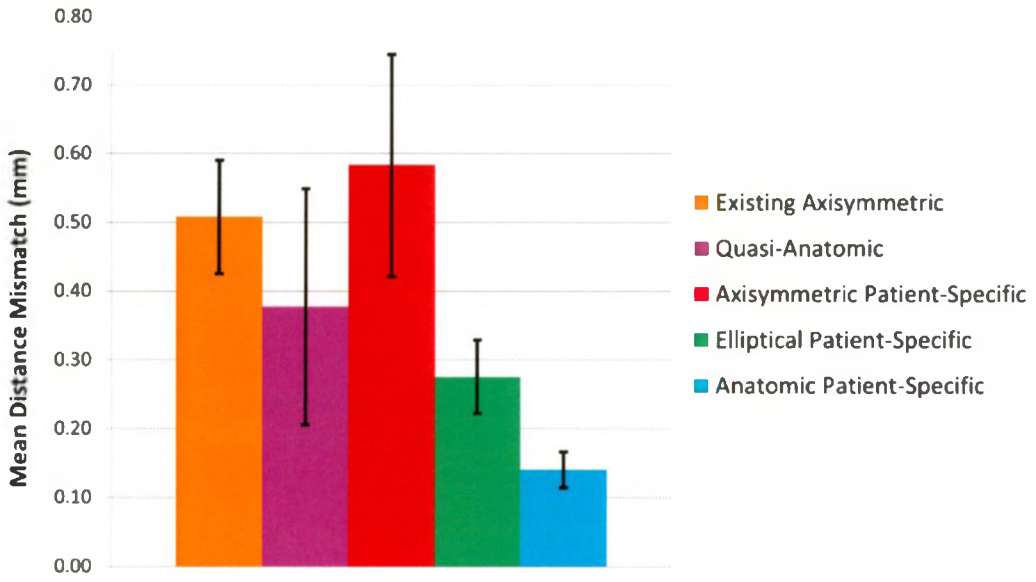

Figure 3.5: Comparison of mean surface mismatch across all five implant models.

Implant colors match those in the preceding images. Error bars show the standard deviation.

3.3.1 EXISTING AXISYMMETRIC IMPLANT

The outputs of the distance mapping program for the existing axisymmetric implant are shown for one specimen in Figure 3.6. The surface mismatch distribution for the existing axisymmetric implant across all specimens is shown Figure 3.7. The mean surface mismatch was 0.51±0.08mm. Approximately 43% of the implant surface was outside the ±0.5mm range and 11% was further than ±1mm.

For all but one specimen the determined ideal implant diameter for the existing implant series most closely matched the minimum outer diameter with a mean diameter difference of 0.25±0.57mm. The remaining specimen was matched to the implant closest to its maximum outer diameter which had an average difference of 1.57±0.72mm from the determined implant diameter across all specimens.

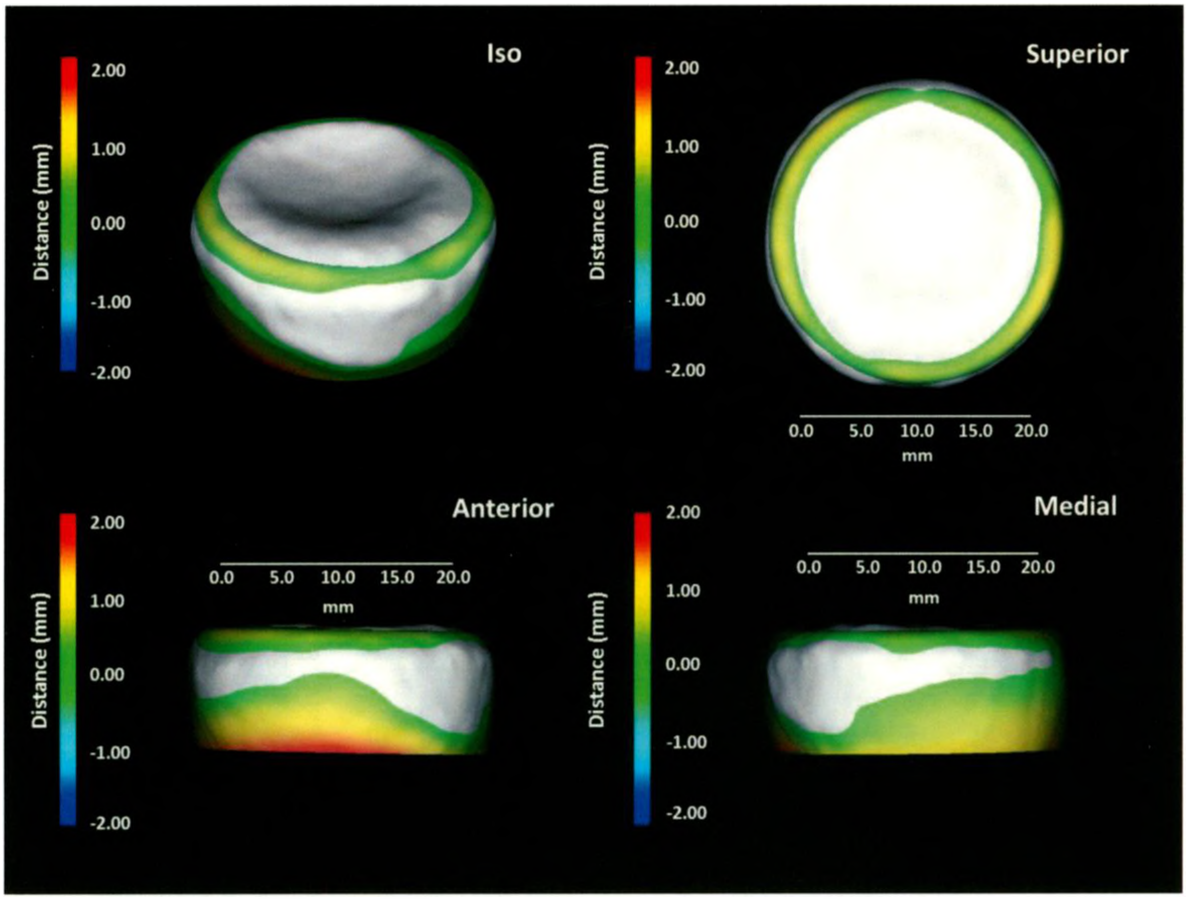

Figure 3.6: Distance Map of the Existing Axisymmetric Implant

The existing axisymmetric implant model (colored) overlaid on the specimen CT after ICP alignment, with distance mismatch mapped onto the implant surface using a scale of ±2mm.

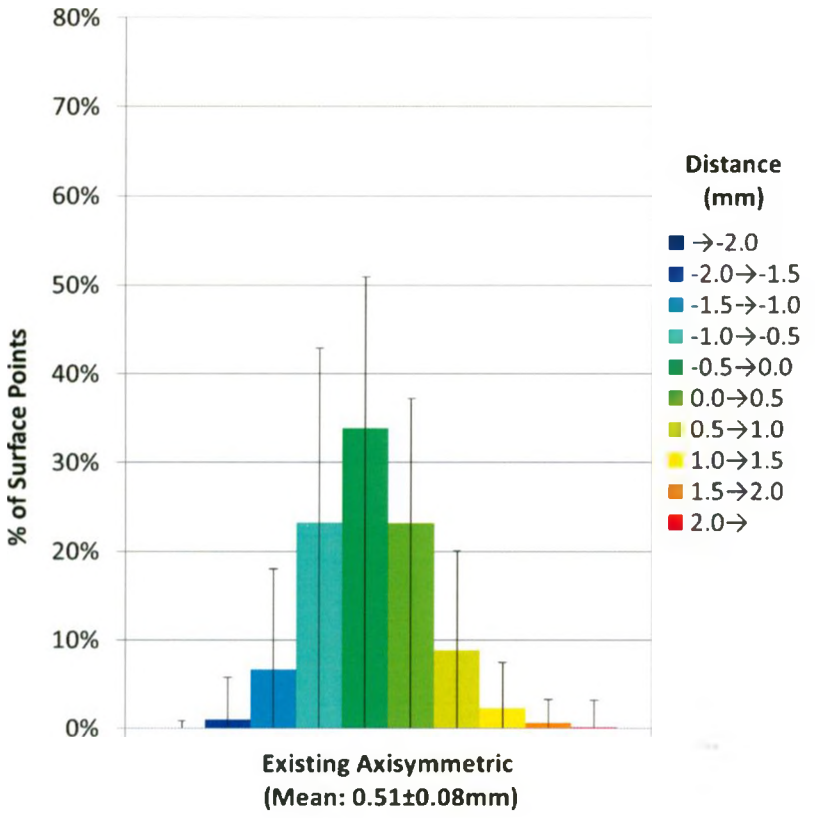

Figure 3.7: Surface mismatch histogram for the existing axisymmetric implant series using the most ideal size match.

Distance mismatch is grouped in 0.5mm increments from -2.0mm to +2.0mm. Verticle bars show the range of values.

3.3.2 QUASI-ANATOMIC IMPLANT

The outputs of the distance mapping program for the quasi-anatomic implant are shown for one specimen in Figure 3.8. The mismatch histogram for the quasi-anatomic implant across all specimens is shown Figure 3.9. The mean surface mismatch of the quasi-anatomic series was significantly lower than the existing axisymmetric implant series with a mean mismatch of 0.38±0.17mm ($p = 0.003$). Approximately 28% of the implant surface was further than ±0.5mm from the native head and only 3% was further than ±1mm.

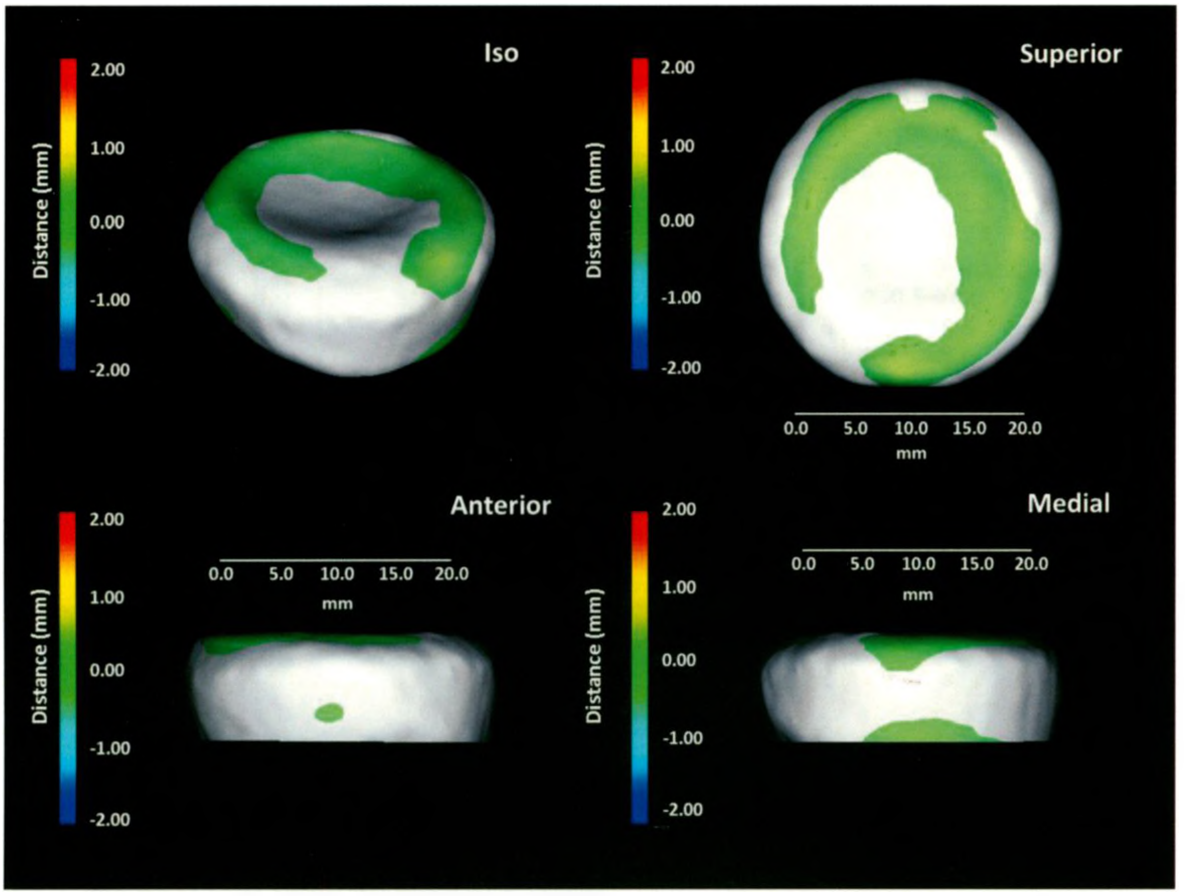

Figure 3.8: Distance Map of the Population-Based Quasi-Anatomic Implant

The "QM" quasi-anatomic implant model (colored) overlaid on the specimen CT after ICP alignment, with distance mismatch mapped onto the implant surface using a scale of ±2mm.

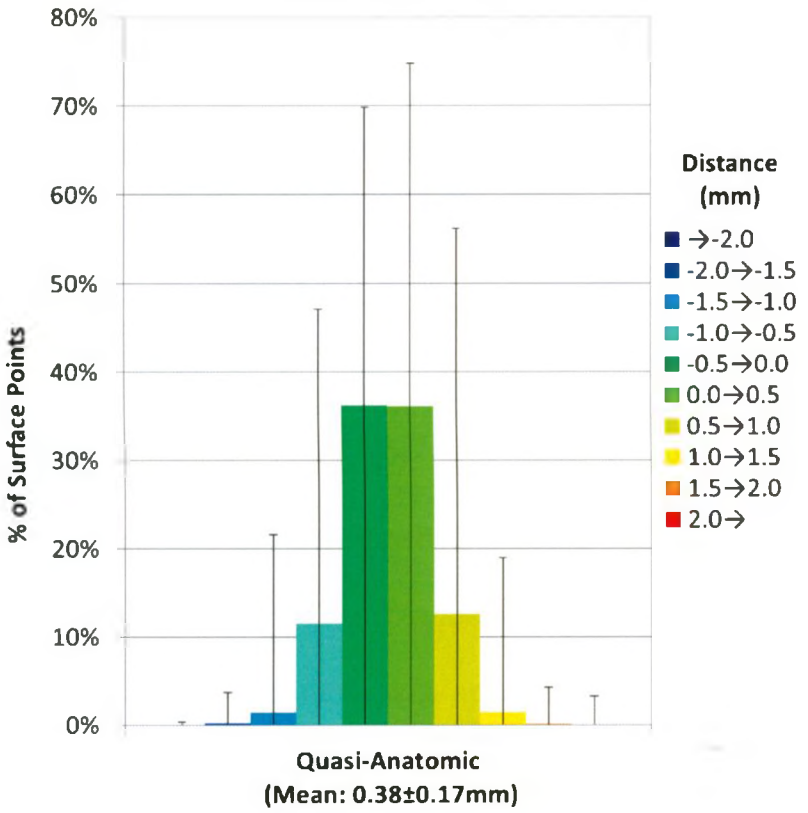

Figure 3.9: Surface mismatch histogram for the quasi-anatomic implant.

Distance mismatch is grouped in 0.5mm increments from -2.0mm to +2.0mm. Vertical bars show the range of values.

3.3.3 PATIENT SPECIFIC IMPLANTS

The outputs of the distance mapping program for each of the three patient-specific implant designs are shown for one specimen in Figures 3.10, 3.11 and 3.12. The distribution of surface mismatch for the patient-specific implants across all specimens is shown in Figure 3.13. The mismatch was significantly reduced as the number of parameters increased ($p<0.001$).

Of all the implant designs, the axisymmetric patient-specific design, using only three of the measured parameters, performed the worst, even when compared to the existing axisymmetric implants ($p=0.021$). The axisymmetric patient-specific models had a mean suface mismatch of 0.58±0.16mm with approximately 50% outside the ±0.5mm range and 16% outside the ±1mm range.

The elliptical patient-specific model, using only six of the measured parameters, performed better than the axisymmetric patient-specific implant with a mean mismatch of 0.28±0.05mm ($p<0.001$). Approximately 13% of the surface was outside the ±0.5mm range and only 2% was further than ±1.0mm.

The anatomic patient-specific model, using all 82 measured parameters, performed best with a mean mismatch of 0.14±0.03mm ($p<0.001$). Less than 1% of the surface, on average, was outside the ±0.5mm range and no part of the surface deviated more than 1mm from the native anatomy.

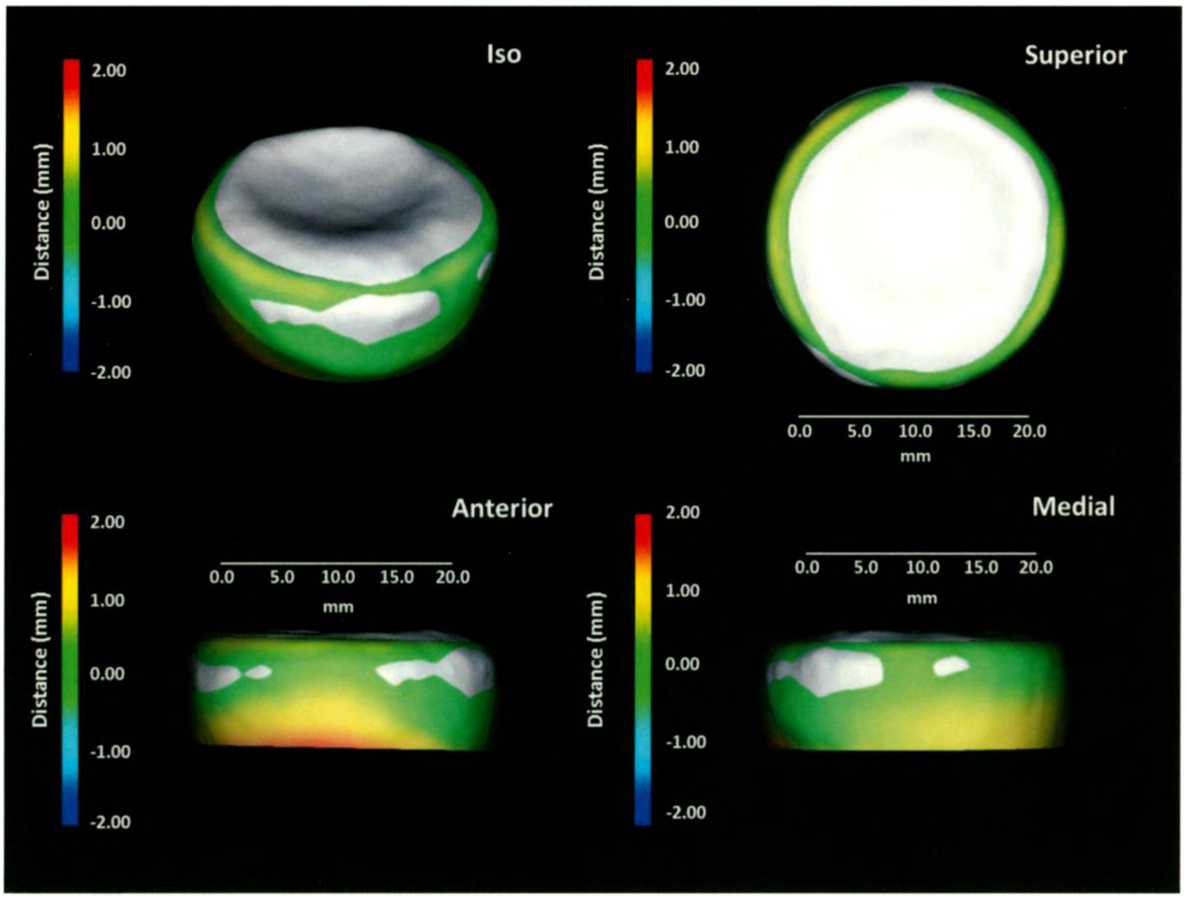

Figure 3.10: Distance Map of the Axisymmetric Patient-Specific Implant

The axisymmetric patient-specific implant model (colored) overlaid on the specimen CT after ICP alignment, with distance mismatch mapped onto the implant surface using a scale of ±2mm.

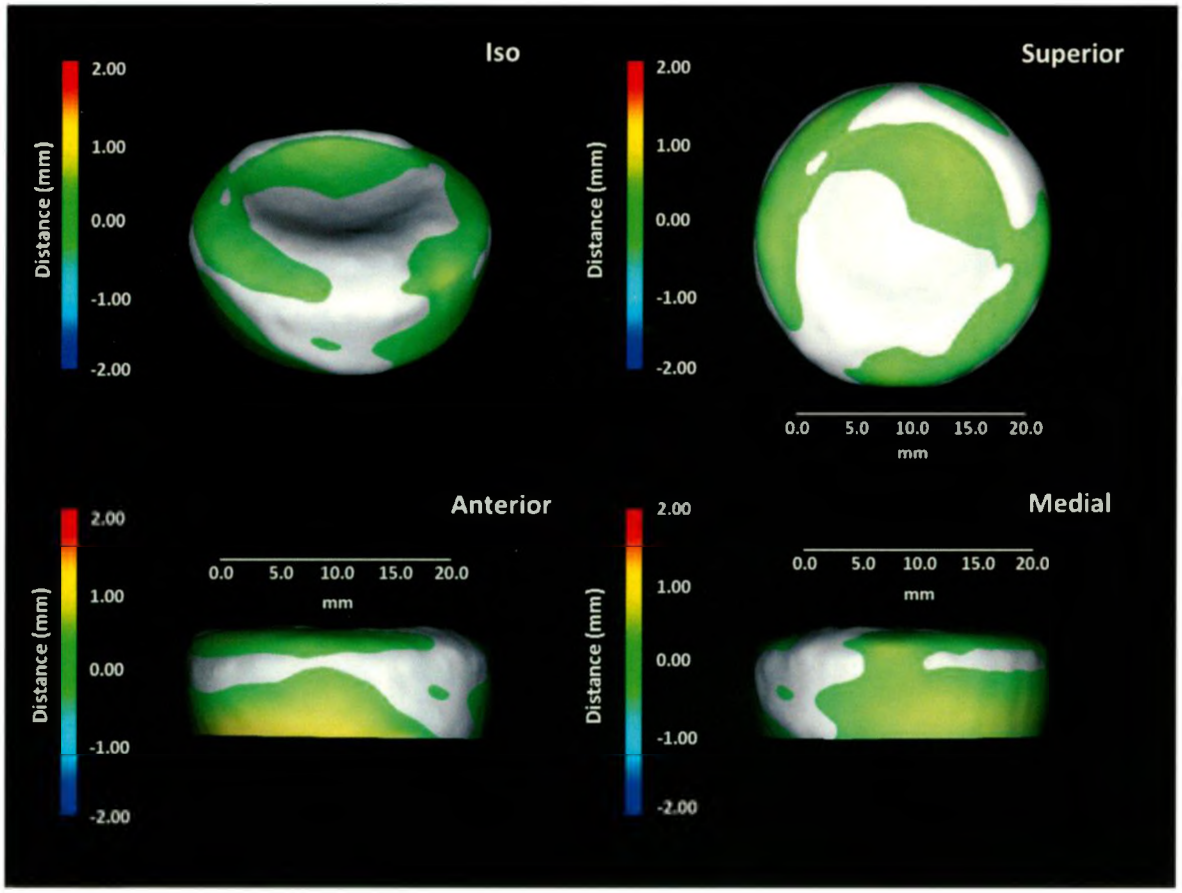

Figure 3.11: Distance Map of the Elliptical Patient-Specific Implant

The elliptical patient-specific implant model (colored) overlaid on the specimen CT after ICP alignment, with distance mismatch mapped onto the implant surface using a scale of ±2mm.

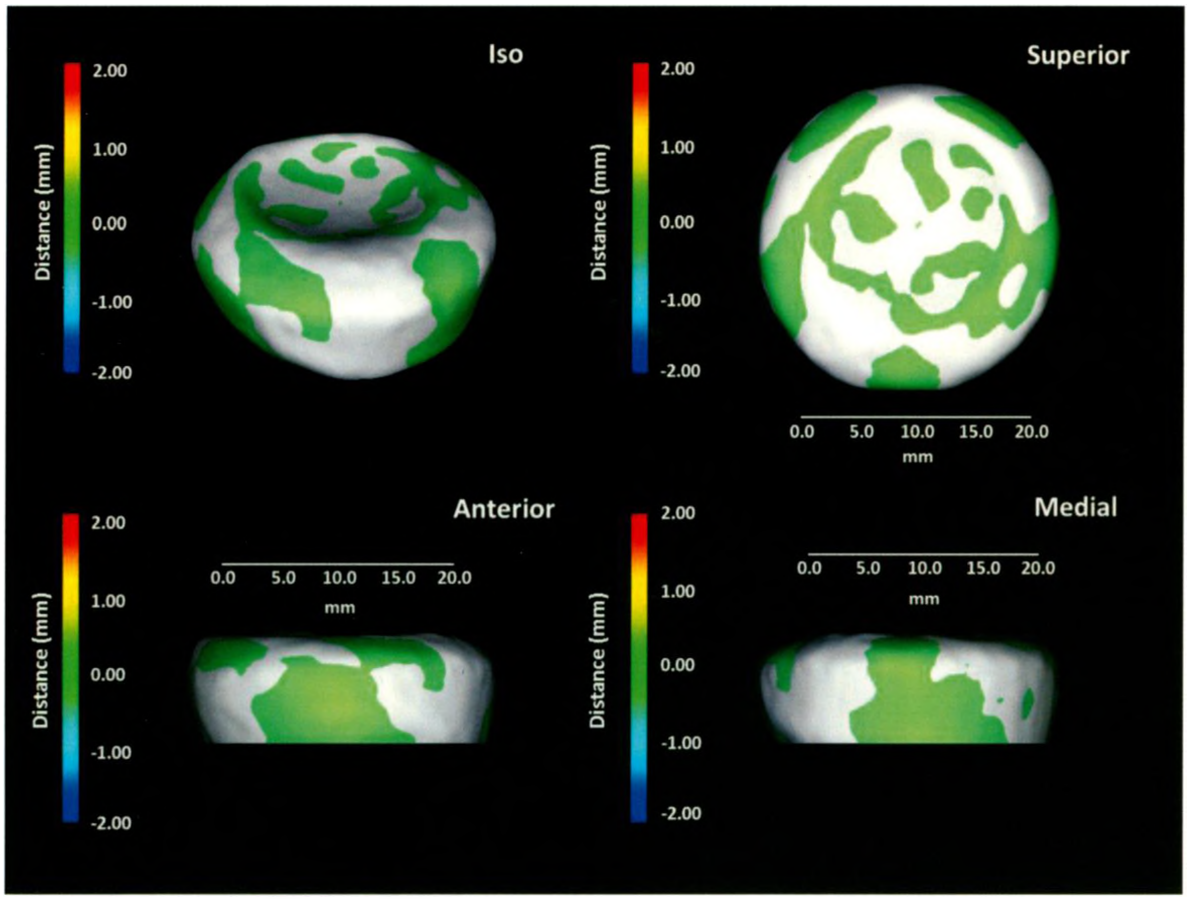

Figure 3.12: Distance Map of the Anatomic Patient-Specific Implant

The anatomic patient-specific implant model (colored) overlaid on the specimen CT (without ICP alignment), with distance mismatch mapped onto the implant surface using a scale of ±2mm.

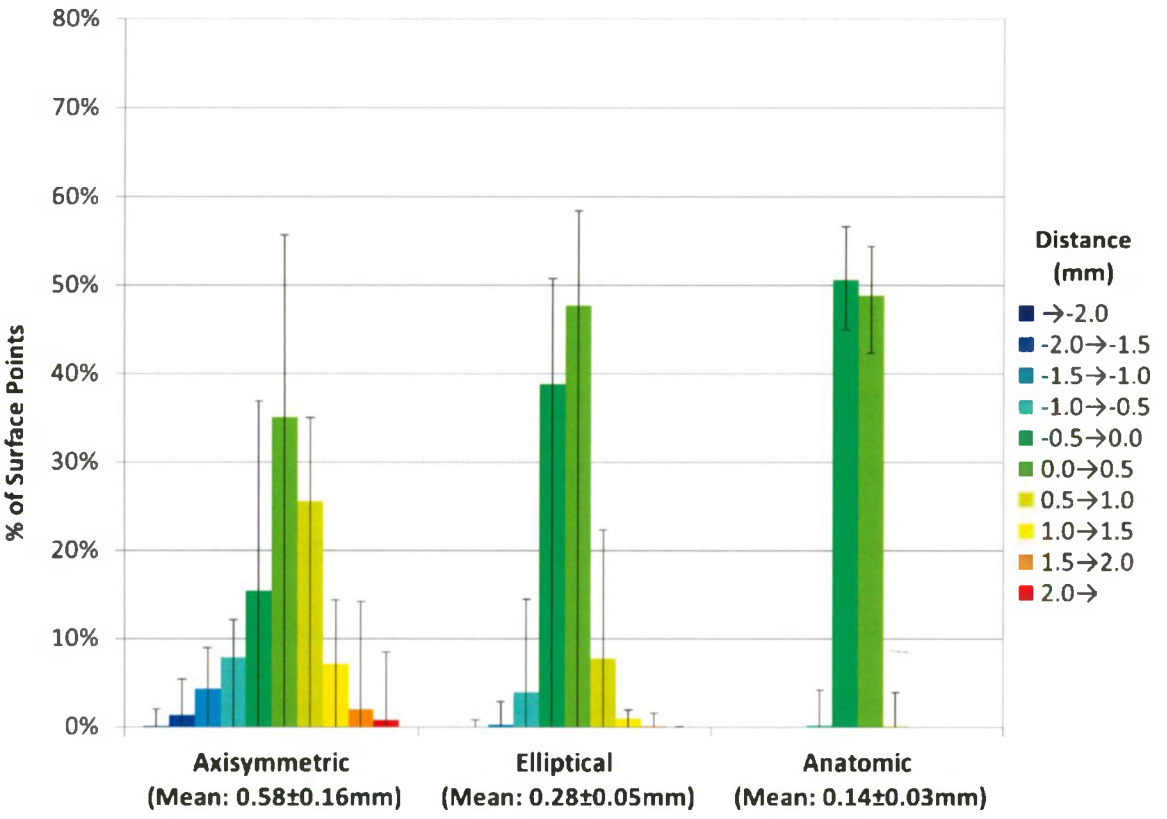

Figure 3.13: Surface mismatch histogram for the axisymmetric, elliptical and anatomic patient-specific implants.

Distance mismatch is grouped in 0.5mm increments from -2.0mm to +2.0mm. Vertical bars show the range of values.

3.4 DISCUSSION

The mean mismatch determined for the existing axisymmetric series of 0.58±0.08mm is suprisingly low considering their obviously non-anatomic shape. Each of the six sizes from 18mm to 28mm were fitted to at least one specimen whereas the quasi-anatomic design utilized only three implant sizes (and provided reduced mismatch). The data of Figure 3.7 further captures the non-anatomic shape of these implants in the wide range of mismatch values compared to the other designs (aside from the patient-specific axysymmetric implant). Comparison of the determined ideal size for the existing axisymmetric implant with the measured diameters for each specimen showed that the minimum outer diameter most closely matched the ideal implant size. However, it should be noted that these results assume fixed implant positioning which is not the clinical reality for this 'loose stem' implant design.

The population-based quasi-anatomic implants developed for this study showed significantly reduced surface mismatch when compared to the existing axisymmetric implants despite the reduced number of implant sizes. Performance of the quasi-anatomic series could be improved by addressing some of the observed shortcomings of the measurements used to determine the implant parameters as discussed in Chapter 2, particularly the poor reliability of the height measurement. Since the parameters at each cross section are dependent on the height of the implant, any inconsistencies could skew the averages used to determine the quasi-antomic implant shape. Additionally, as the Q+ and Q- implant groups had only five specimens each, an expanded specimen pool is needed to better capture the variability within the population. As larger female specimens

and smaller male specimens had similar diameters, expanding the implant series to include the complete range of male and female sizes may have resulted in better surface matching as the number of implants increased. Further study into the creation of population-based radial head implants should be conducted once the shortcomings of the measurement system have been addressed.

Increasing the number of input parameters of the patient-specific implants, resulted in significantly reduced surface mismatch. This is not unexpected as both the axisymmetric and elliptical models excluded known features of the radial head, specifically its elliptical shape and offset dish. However, it is worth noting that the elliptical shaped patient-specific implants based on only six measurements outperformed the quasi-antomic implant series which included averaged values of all 82 parameters measured. The anatomic patient-specific implant, as expected, had the lowest mean surface mismatch of any of the implants investigated. The anatomic implant did not suffer from the poor reliabilty in determining height as no parameters were averaged to create the model, unlike the quasi-anatomic series.

Surprisingly the existing axisymmetric implant series outperformed the patient-specific axisymmetric implants. As the patient-specific axisymmetric models were based on the three parameters, namely the maximum major outer diameter, depth and height, it appears that they were consistently oversized relative to the native anatomy. This is in agreement with our finding that the existing axisymmetric implant matched to the major outer diameter of the ellipse provided a poor fit. Using the minor instead of the major outer diameter would likely produce a better patient-specific axisymmetric model for future comparisons.

Both the population-based implants and the patient-specific models assumed ideal implant placement and therefore represent a best case scenario. It is likely that surgical errors when performing conventional axisymmetric and non-axisymmetric radial head arthroplasty using bony landmarks will result in some element of implant malalignment and hence a greater degree of surface mismatch than reported here. Further study into the effects of radial head implant mal-alignment on surface mismatch are warranted. The development of computer assisted techniques for placement of both population-based and patient-specific implants will likely improve their clinical success. A method for precise alignment of radial head implants using navigation is examined in the following chapter.

The current study is not without weaknesses. Although significant differences in the surface mismatch of varying implant models were identified, these differences may not be clinically significant in their effect on joint kinematics, force transmission and contact patterns. Further work is needed to determine the degree of surface mismatch which is clinically relevant. Additionally, the effect of surface mismatch may be region specific with increased sensitivity to mismatch at the articular surfaces as compared to the non-articular side of the radial head. The effect of poor reliability in height measurement in the previous morphology study has already been discussed. Additionally, the current study did not account for cartilage thickness at the radial head. Further investigations to quantify the thickness and distribution of articular cartilage are needed before this can be incorporated into the design and assesssment of radial head implants.

The distance mapping algorithm used in this study simply measured distance between nearest point pairs on the implant and bone model. This method relies on a sufficiently high point density to provide a reliable estimate of mean surface mismatch.

The value obtained will differ slightly depending on the direction the mismatch is calculated, either from implant to bone or from bone to implant due to the differing point densities of the bone and implant models. Future work would benefit from incorporating normal vectors to determine perpendicular distance between the surfaces. Modification of the mean mismatch calculation to compensate for variable point spacing on the implant surface would be worthwhile as it is difficult to ensure an even point distribution. Alternatively, a volume rather than surface based method could be employed to determine mismatch.

Finally, several studies have suggested that the radial head may have consistent but different shape types both in regard to the overall shape (elliptical vs. circular) and the height variation of the articular circumference[14,15]. Principal component analysis could be used to identfy these shape modes and categorize them using cluster analysis as decribed by Daruwalla et al.[16,17] with respect to clavicle morphology. Shape modes may be linked to other factors such as gender, age or ethnicity. This approach could be used in the design of a population-based implant series which represents each of these different modes, rather than blending them together with averaging as was the case in the current study. Further morphological investigation is warranted to determine if this approach is necessary. Additional FEA analysis of force transfer and contact mechanics should be conducted to validate any new implant designs produced using these methods.

Based on the results of the current study, the mean surface mismatch of radial head implants may be reduced through the use of reverse engineering technique to determine the required parameters for both population-based quasi-anatomic and patient-specific anatomic implant designs. Furthermore, by incorporating the complex shape of the radial

head into implant design, the range of mismatch can also be reduced by providing a more consistent shape match to the native geometry, thus eliminating outlier regions which increase mismatch present with axisymmetric implants. Although the current study showed a significant reduction in mismatch through the use of patient-specific implants, further study into the clinical significance of this finding is required to justify the added cost of using personalized custom-made implants.

3.5 REFERENCES

1. Beredjiklian PK, Nalbantoglu U, Potter HG, Hotchkiss RN. Prosthetic radial head components and proximal radial morphology: a mismatch. *Journal of Shoulder and Elbow Surgery*. 1999;8(5):471–475.

2. Popovic N, Djekic J, Lemaire R, Gillet P. A comparative study between proximal radial morphology and the floating radial head prosthesis. *Journal of Shoulder and Elbow Surgery*. 2005;14(4):433-40.

3. King GJW, Zarzour ZD, Patterson SD, Johnson JA. An anthropometric study of the radial head: implications in the design of a prosthesis. *The Journal of Arthroplasty*. 2001;16(1):112-6.

4. Swieszkowski W, Skalski K, Pomianowski S, Kedzior K. The anatomic features of the radial head and their implication for prosthesis design. *Clinical Biomechanics (Bristol, Avon)*. 2001;16(10):880-7.

5. Dotzis A, Cochu G, Mabit C, Charissoux JL, Arnaud JP. Comminuted fractures of the radial head treated by the Judet floating radial head prosthesis. *Journal of Bone and Joint Surgery - British Volume*. 2006;88(6):760-4.

6. van Riet PR, van Glabbeek F, Baumfeld J, et al. The effect of the orientation of the radial head on the kinematics of the ulnohumeral joint and force transmission through the radiocapitellar joint. *Clinical Biomechanics*. 2006;21(6):554–559.

7. Acumed. Anatomic Radial Head System. 2011:1-14. Available at: http://www.acumed.net/sites/default/files/literature/brochure-surgical-technique/anatomic-radial-head-system-brochure-surgical-technique.pdf.

8. van Glabbeek F, van Riet RP, Baumfeld JA, et al. Detrimental effects of overstuffing or understuffing with a radial head replacement in the medial collateral-ligament deficient elbow. *Journal of Bone and Joint Surgery*. 2004;86-A(12):2629-35.

9. Gupta G, Lucas G. Biomechanical and computer analysis of radial head prostheses. *Journal of Shoulder and Elbow Surgery*. 1997;6(1):37-48.

10. Kapp Surgical Instruments. Custom Radial Head Implants. 2011:1-4. Available at: http://www.kappsurgical.com/documents/Radial Head Rev 7-7-10.pdf?

11. van Riet RP, van Glabbeek F, Neale PG, et al. Anatomical considerations of the radius. *Clinical Anatomy*. 2004;17(7):564-9.

12. Besl P, McKay N. A method for registration of 3-D shapes. *IEEE Transactions on Pattern Analysis and Machine Intelligence*. 1992;14(2):239-56.

13. Lalone E, McDonald CP, Ferreira LM, et al. Development of an Image-Based Technique to Examine Joint Congruency at the Elbow. *Computer Methods in Biomechanics and Biomedical Engineering*. 2011:Article In Press.

14. Captier G, Canovas F, Mercier N, Thomas E, Bonnel F. Biometry of the radial head: biomechanical implications in pronation and supination. *Surgical and Radiologic Anatomy*. 2002;24(5):295-301.

15. Bartz B, Tillmann B, Schleicher A. Stress in the human elbow joint. *Anatomy and Embryology*. 1984;169(3):309–318.

16. Daruwalla ZJ, Courtis P, Fitzpatrick C, Fitzpatrick D, Mullett H. An application of principal component analysis to the clavicle and clavicle fixation devices. *Journal of Orthopaedic Surgery and Research*. 2010;5:21. Available at:

17. Daruwalla ZJ, Courtis P, Fitzpatrick C, Fitzpatrick D, Mullett H. Anatomic variation of the clavicle: A novel three-dimensional study. *Clinical Anatomy*. 2010;23(2):199-209.

CHAPTER 4 - Development of a Computer- and Image-Assisted Guidance System for Radial Head Arthroplasty

OVERVIEW:

The chapter describes the development and testing of a guidance system for computer-assisted radial head arthroplasty using pre-operative CT imaging. Navigation and registration errors were determined in a series of cadaveric specimens.

4.1 INTRODUCTION

Previous studies describing the complex shape of the radial head have identified the importance and difficulty associated with accurately positioning an anatomically shaped radial head replacement[1]. These difficulties are further exacerbated when the native anatomy is severely fractured or has been excised. Anatomic landmarks, such as the biceps tuberosity and radial styloid, have been shown to be highly variable between patients[2] increasing the potential error associated with surgeons using anatomic features. A current anatomic radial head replacement system, for example, aligns a mark on the implant head with the "lateral aspect of the radius in the neutral position"[3]. To date, no evidence has been provided on the typical alignment errors using this method or their associated complications. Previous studies have reported that radial head over- or under-lengthening of as little as 2.5mm can increase the risk of complications after radial head replacement[4]. No studies have examined the complications associated with other directions of radial head implant mal-alignment.

Computer-assisted orthopedic surgery has been previously applied at the hip and knee in order to guide implant alignment and reduce surgeon errors. Significant improvements in implant positioning have been demonstrated at both joints, although more recent studies have suggested that the long-term clinical outcomes may be no different than those obtained using traditional jigs[5-7]. As implant procedures involving the upper limb are less commonly performed, the potential for improved patient outcomes may be greater due to the inexperience of surgeons with these procedures.

Only one system for computer assisted placement of the radial head has been described[8]. The focus of this work was to quantify the effect of axisymmetric implant mal-alignment on elbow joint kinematics. The accuracy of implant placement, which was based on digitized bony landmarks, was never quantified and the effects of mal-alignment on joint kinematics have yet to be published.

In the current study, a computer- and image-assisted navigation system was designed to allow accurate implant placement during cadaveric kinematic based testing of the population-based and patient-specific anatomic implants detailed in Chapter 3. The specific objectives were to 1) develop a method for accurate surface-based registration of the radius, and 2) navigate a radial head implant within 2° and 0.25mm of the location determined using pre-operative planning. These values for target accuracy were based on results that showed the average improvement in surface mismatch between a quasi-anatomic design and patient-specific model was about 0.25mm (Chapter 3). Errors outside of this margin would negate the potential gains of a patient-specific design.

4.2 METHODS

4.2.1 IMPLANT DESIGN AND MANUFACTURING

The implant system devised for this study consisted of two components; a generic stem composed of a machined body and ball plunger, and the implant head which was patient dependent. The major features of the implant system are shown in Figure 4.1. The implant stem was designed to ensure that rigid fixation to bone could be achieved with cement. Eight divots located on the proximal section of the stem allowed for navigation tool calibration using a landmark based registration. After navigation, the stem could be easily disconnected from the tool using a single screw which had previously tensioned the tool around the top of the stem as shown in Figure 4.2. A square 6mm x 6mm profile was used to prevent rotation of both the implant head and the stem within the cement mantle. This profile also allowed for four possible stem positions with no effect on the final implant position. The distal portion of the stem was angled at 5° so that each of the four potential orientations would differ in the stem location to aid, along with its short length, in avoiding impingement upon the medullary canal. Implant assembly used a socket-like connection between the implant head and stem, while the ball plunger permitted interchange of the head component throughout testing.

Based on the parameterized CAD models, both the quasi-anatomic and patient-specific implant heads were created from ABS-M30 plastic using a fused deposition rapid prototyping machine with an accuracy of ±0.127mm (Stratsys Fortus 400MC, Eden Prairie, MN, USA). In order to ensure a smooth articular surface, the plastic was lightly sanded and treated with acetone which had a minimal effect on final shape.

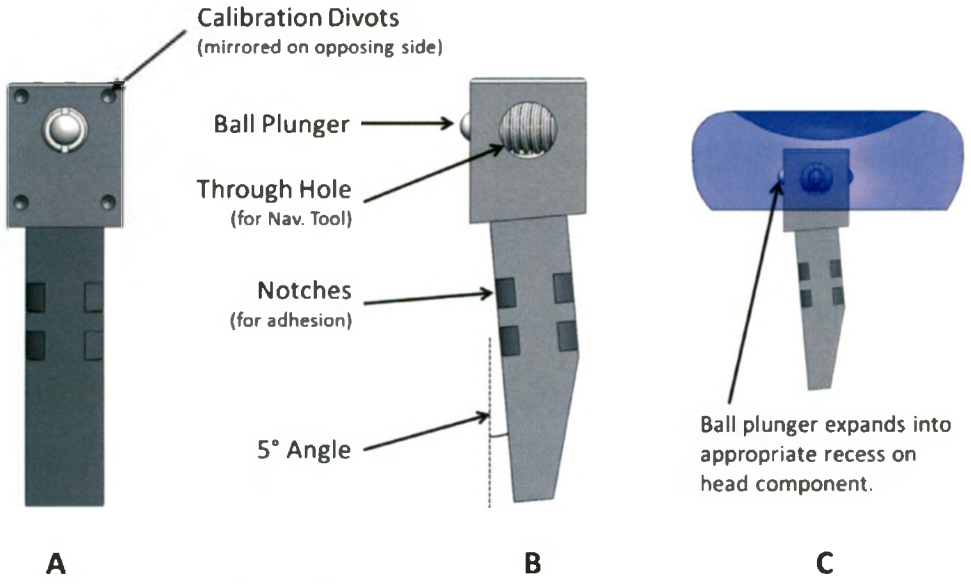

Figure 4.1: Overview of Stem Features

A) Front view of the implant stem
B) Side view of the implant stem
C) View of the assembled implant stem and head using transparency to show the ball plunger engaging on one of the four divots in the implant head.

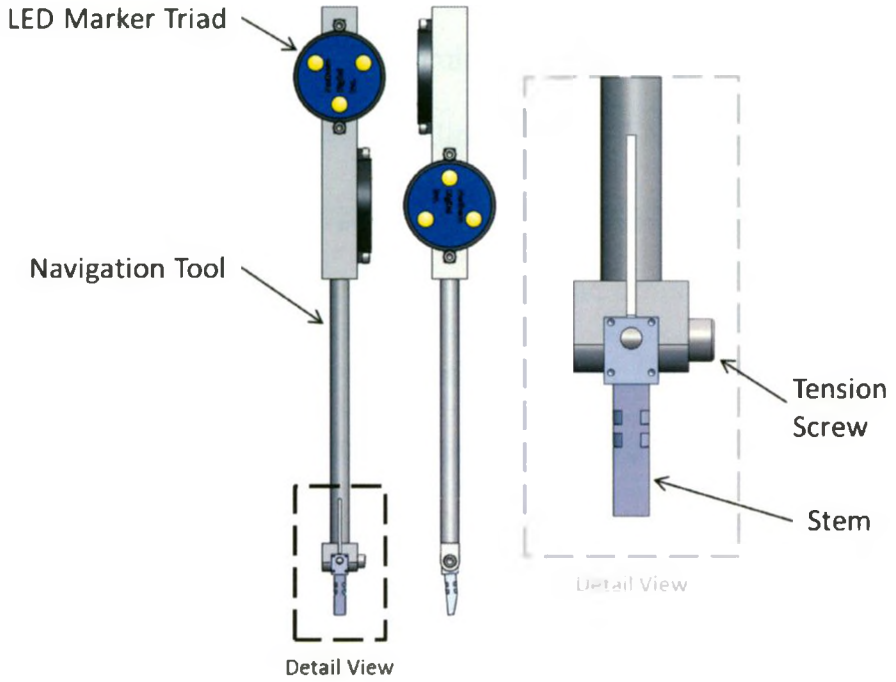

Figure 4.2: Overview of Navigation Tool

The tension screw pulls the two arms of the forked tool around the stem leaving the divots exposed for calibration to the attached markers.

4.2.2 PRE-OPERATIVE PLANNING

Images of the radius were obtained for seven male specimens, mean age 75.5 years (range, 57-84 years), before and after implant navigation using a 64-slice x-ray Computed Tomography (CT) scanner (GE Discovery CT750HD,Waukesha, WI) with a field of view of 20x20cm and a 512x512 reconstruction matrix (200mA, 120kVp) and saved as DICOM files. Voxel size was approximately 0.4x0.4x0.625mm. Only right male arms were used as a quasi-anatomic implant series had been previously designed for this population as detailed in Chapter 3. A 3D model was reconstructed via manual and automated segmentation using Mimics image processing software (Materialize, Leuven, Belgium). Models were processed to isolate the exterior bone surface using tools within the Mimics software.

Using a custom program created using the Visualization Toolkit (VTK) the 3D radial model was aligned to an anatomic coordinate system and morphological measurements obtained using automated ellipse fitting of cross sections as described in Chapter 2. As conceptualized in Figure 4.3, an ideal location for the implant stem was determined by identifying the center of the radial head cross section at the level of the proximal edge of the bicep tuberosity approximating the narrowest section of the medullary canal. This point was then projected proximally onto the best-fit plane of the radial rim to determine the stem orientation vector as well as the location of the stem recession on the bottom surface of each implant head.

In future clinical applications, this stem position could also be averaged across the quasi-anatomic implants allowing for a unified design. This was not a practical approach for the current study as this would have required stem removal and re-navigation to swap

between the quasi-anatomic model using the averaged stem position and patient-specific implant which would use the optimal position for the particular patient. To avoid this potential problem a customized quasi-anatomic implant of the correct size was manufactured for each specimen which shared a stem location with the patient-specific model.

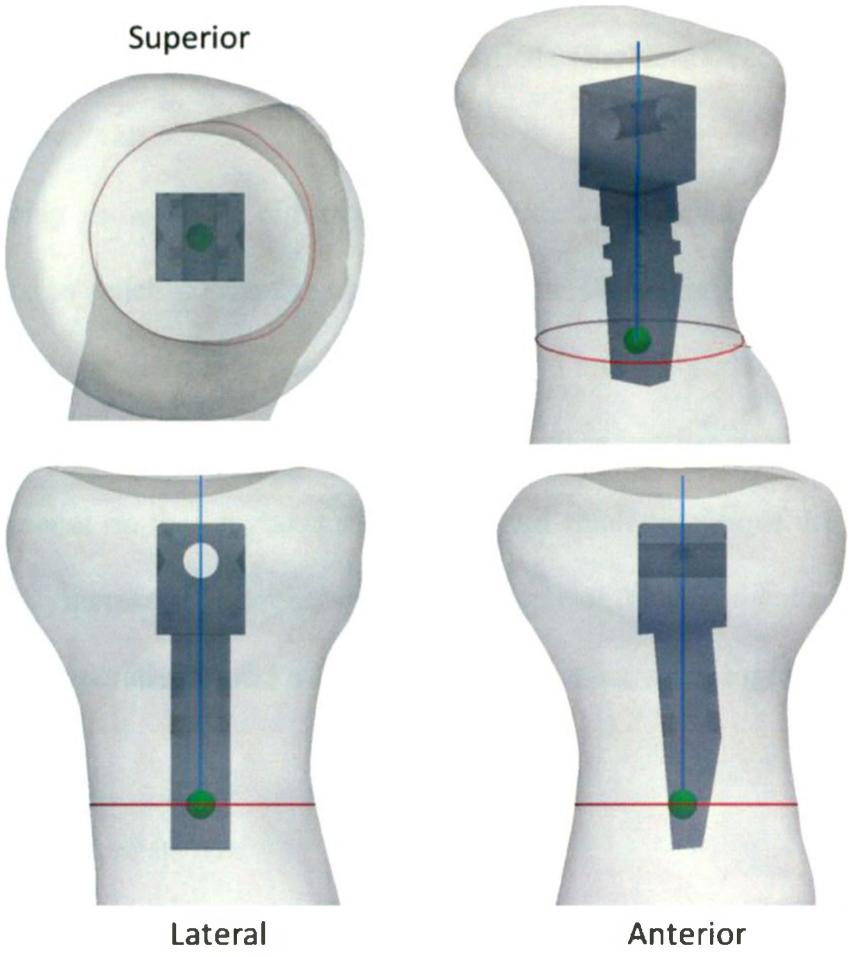

Figure 4.3: Determining the Stem Orientation Vector

The center (green) of the radial cross section (red) at the proximal edge of the tuberosity is identified in order to determine the stem orientation vector (blue) which is normal to the best fit plane of the rim.

4.2.3 SURFACE-BASED REGISTRATION

The surface-based registration between the pre-operative model and intra-operatively obtained digitizations was determined using VTK. An initial landmark based registration using three points (radial styloid, dorsal lip of the DRUJ and the center of the radial dish) was used to coarsely align the two datasets before final alignment using the iterative closest point (ICP) algorithm[9]. In order to generate surface models from the digitized points the fastRBF toolbox was used (FarField Technology Limited, Christchurch, New Zealand).

Pilot testing showed that digitizations of the dish and radial circumference alone were inadequate to reliably orient the radius using the ICP algorithm. It was suspected this was due to shape difference between the digitized and CT surfaces due to cartilage offset. The addition of distal landmarks, including surface patches accessible at the base of the tracker mount on the long axis of the bone and small patches of the radial styloid and dorsal DRUJ, increased ICP reliability. An example of the alignment between surface traces and the pre-operative model after ICP alignment is shown in Figure 4.4.

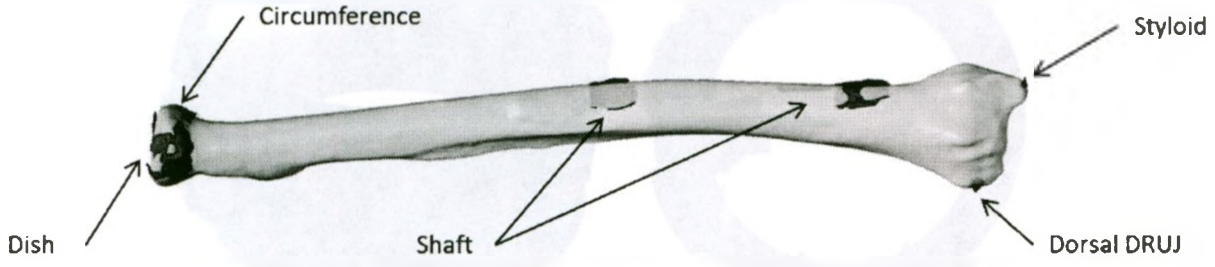

Figure 4.4: Surface-Based Registration of the Radius

Alignment of the pre-operative model (white) and intra-operative surface digitizations (red) after coarse alignment and ICP registration.

4.2.4 NAVIGATION

An active optical tracking system (Optotrak Certus, NDI, Waterloo, Ontario, Canada) paired with an interface in LabVIEW (National Instruments, Austin, Texas, USA) was used to provide real-time visual feedback to the operator during implant navigation. The 3D accuracy of the tracking system reported by the manufacturer is 0.1mm for a single light emitting diode (LED). The accuracy of a tracked rigid body has been reported as 0.5° and 0.2mm with 95% confidence within a range of 3.25m range from the camera system. However, this is dependent on the number and arrangement of LEDs affixed to the rigid body and the method used to calibrate them as trackers. Throughout navigation, the camera was kept well within the 3.25m optimal operating range to minimize tracking error. To allow the radius to be visible in multiple orientations 21 LEDs were fixed to a PVC ring and mounted concentrically to the long axis of the radius (Figure 4.5). The ring was calibrated using software provided by the tracking system manufacturer so that any visible LED triad could be used to determine its position and orientation.

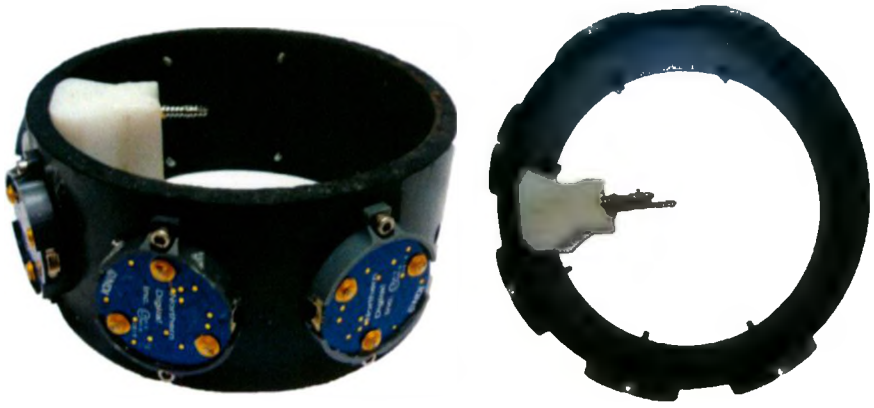

Figure 4.5: The "ring" used to track the position of the radius.

Marker triads (blue) arranged around a PVC pipe section were first calibrated and then attached concentrically around the radius using bone screws.

The navigation tool was initially calibrated using a tracked pointed stylus to obtain point readings of each of the eight divots on the implant stem relative to trackers on the navigation tool. A landmark-based method was used to register the average of five point readings of each divot to their matching partners on the virtual stem model.

In order to confirm that each implant head would be fully seated on the stem after radial head excision, the resection plane was digitized with a tracked stylus and compared to the registered pre-operative plan. Further resection was completed if the digitized plane intersected target implant positions. The height was further confirmed using surface digitizations after implant assembly.

Navigation was performed by aligning the stem model relative to the navigation tool with the matching model at the target location relative to the radius in real-time as shown in Figure 4.6. Coordinate axes were overlaid on each model to aid in placement. Two views were displayed simultaneously on the screen during navigation to give the operator a better understanding of the out of plane mismatch. PMMA bone cement (Surgical Simplex P, Stryker, Kalamazoo, MI, USA) was injected into the proximal radius. The stem was inserted slowly using the navigation tool and any excess cement removed. Using the feedback provided on the screen, the stem was aligned to the target location and held manually in place as the cement hardened. Before removing the navigation tool, its final position was recorded.

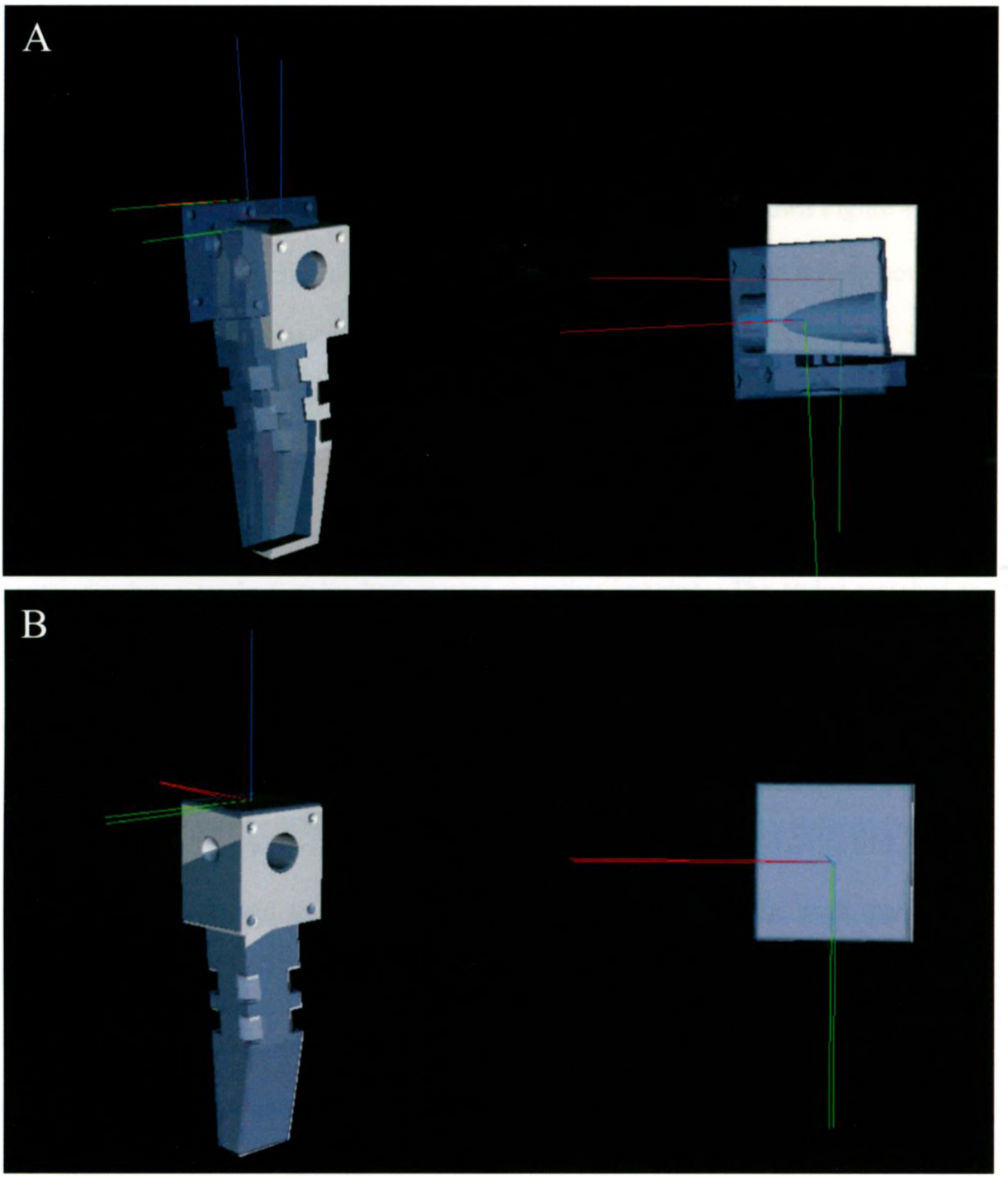

Figure 4.6: Stem Insertion Using Computer Guidance

Two views show the stem model with respect to the bone (lighter) and navigation tool (darker/transparent) and their coordinate axes in real-time to the operator. A) Shows the implant during navigation and B) shows the overlapped models after alignment.

4.2.5 ACCURACY

The error between the final stem position and the target position was determined. This quantified the human error in aligning the two models on the screen during navigation. The order of transforms used to determine this error is shown Figure 4.7. The position of this target included the intra-operative registration error so it does not reflect final accuracy of placement.

A landmark-based registration using fiducial markers provided the datum by which the accuracy of the intra-operative surface-based registration could be determined. Five 19mm delrin spheres were fixed rigidly to the denuded radius as shown in Figure 4.8 and digitized using a tracked stylus before post-operative imaging. The stylus matched the spherical surface of the markers and was calibrated so that the virtual stylus "tip" was located at the marker center. Recordings obtained as the stylus was pivoted about a marker were averaged to determine the 3D location of each center relative to the radius tracker. Four markers were used in the landmark-based registration and the fifth, located most proximally, served to quantify target registration error (TRE). Each marker was segmented and reconstructed using the Mimics software. Any obvious flaws in the reconstructed models were removed manually. The geometric centers of these models were then determined using a sphere fitting algorithm and registered to those previously digitized.

In order to determine the new target location, the pre-operative model was registered to the post-operative model directly using an initial point based alignment followed by ICP registration. As this was an intra-modality registration between two CT models of the same structure the error was assumed to be negligible. The registration

error was determined by comparing the stem position based on the intra-operative registration and the more accurate position determined using the post-operative fiducial method as shown in Figure 4.7. Combining the navigation and registration components allowed total error to be determined.

Both the tool calibration and post-operative registration were assumed to have negligible error for the purpose of determining accuracy as both employed obvious landmarks, divots and spheres respectively, which could be reliably digitized. In order to verify this assumption, the fiducial registration error (FRE) was determined for both the tool and post-operative registration for each specimen by calculating the RMS error between paired points after registration. The target registration error was also calculated for the post-operative fiducial registration using the additional "Target" sphere, shown in Figure 4.8, which was located as proximally as possible on the remaining radial neck.

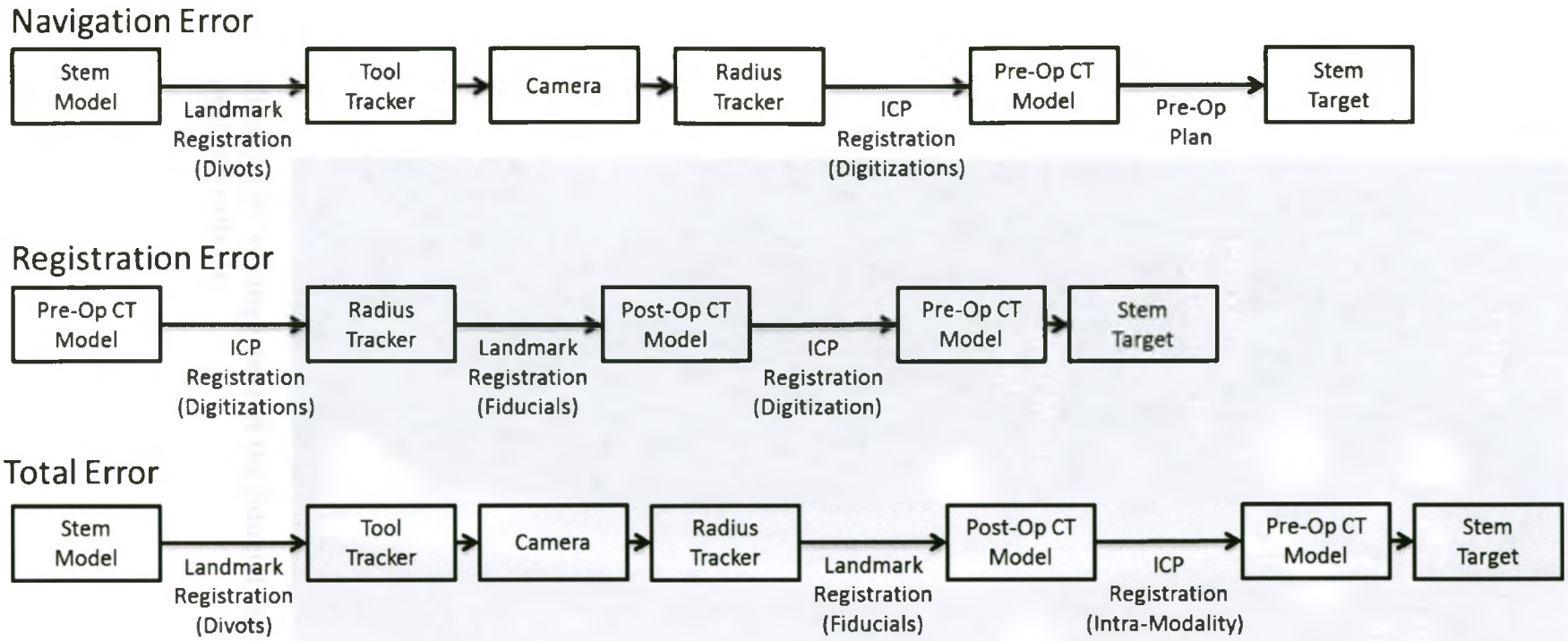

Figure 4.7: Overview of transformation matrix combinations used to determine the following:

Navigation Error - between the stem model relative to the navigation tool and target location seen by the operator determined using surface-based registration of the radius.
Registration Error - between the radial model aligned using surface-based ICP registration and the model determined post-operatively using the gold-standard fiducial registration
Total Error - between the stem model relative to the navigation tool and the target location as determined post-operatively using the gold-standard fiducial registration

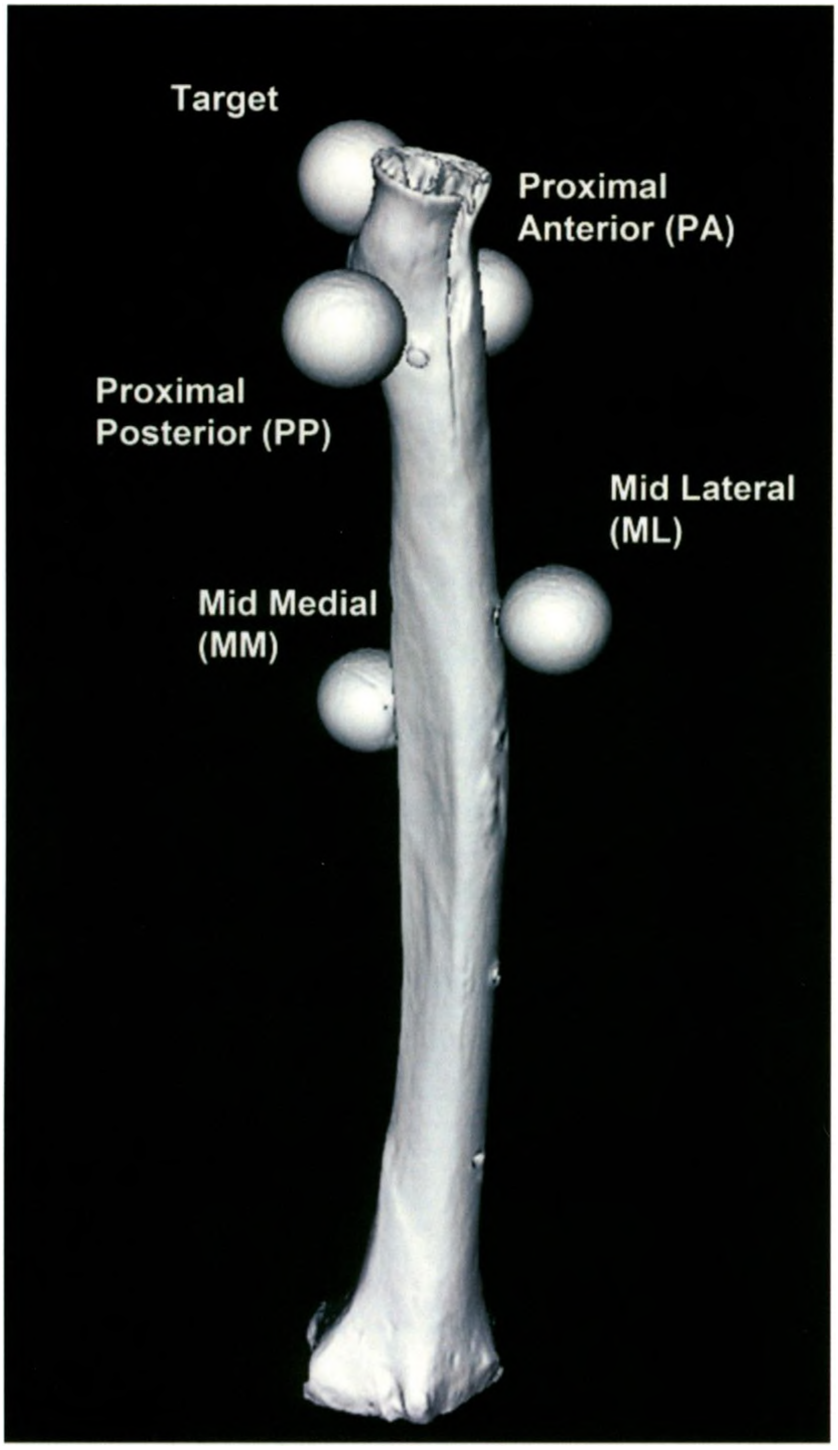

Figure 4.8: Arrangement of the fiducial markers used to register the radius post-operatively.

4.3 RESULTS

Navigated implant alignment was completed for seven specimens. Three of the specimens required stem removal and re-navigation due to either poor cement fixation or obvious mal-alignment when the cement set while attempting to hold the implant in the target location. Figure 4.9 visually compares the excised head of one specimen with the patient-specific and quasi-anatomic implants design to match it. Figure 4.10 shows the patient-specific design after stem navigation and implant assembly.

The navigation, registration and total error were determined for each specimen. Figures 4.11 shows the mean and maximum of each error type in translation and rotation relative to the anatomic coordinate system described in Chapter 2 (X,Y,Z = lateral, superior, proximal). Rotations where calculated using the fixed axis method[10].

The mean TRE and FRE for the post-operative fiducial registration was 0.7±0.4mm and 0.3±0.2mm, respectively. Tool calibration using the eight machined divots on the stem had an FRE of 0.3±0.1mm. TRE could not be calculated on the navigation tool.

Figure 4.9: Comparison of native anatomy (left) to patient-specific (middle) and quasi-anatomic (right) implant designs, before sanding and coating of the implant surface.

Figure 4.10: The patient-specific implant after stem navigation and implant assembly.

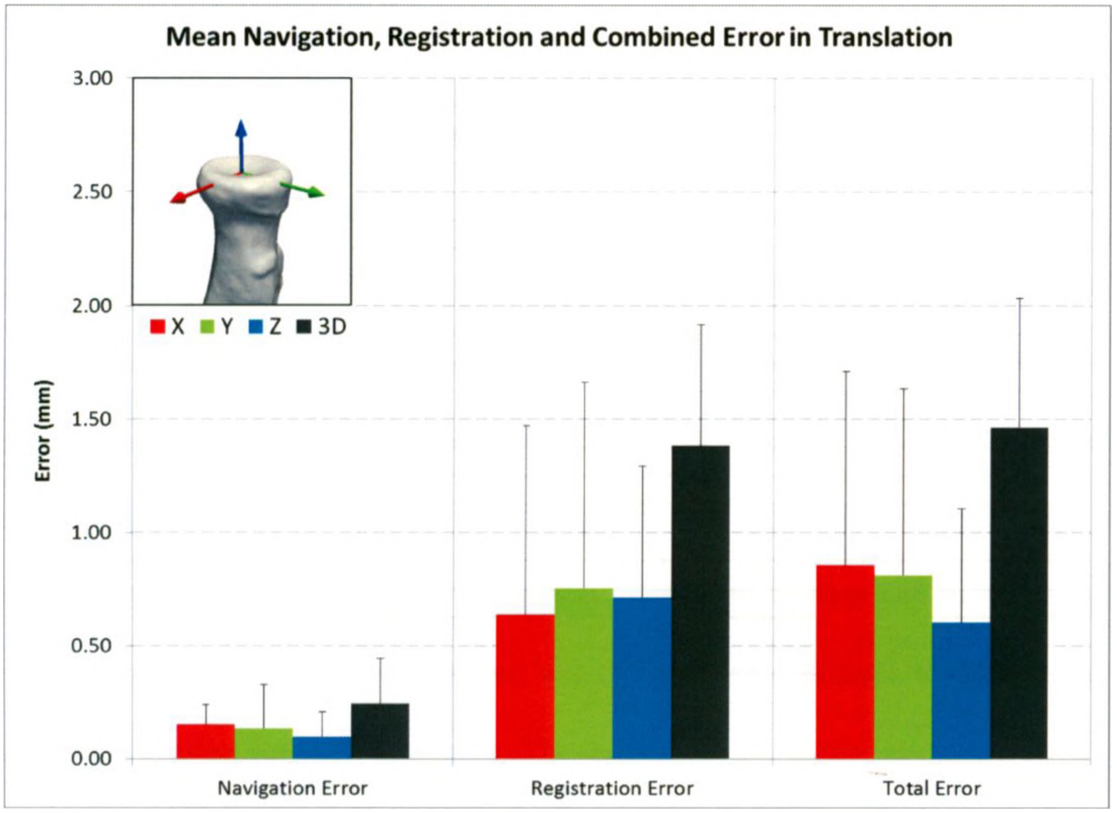

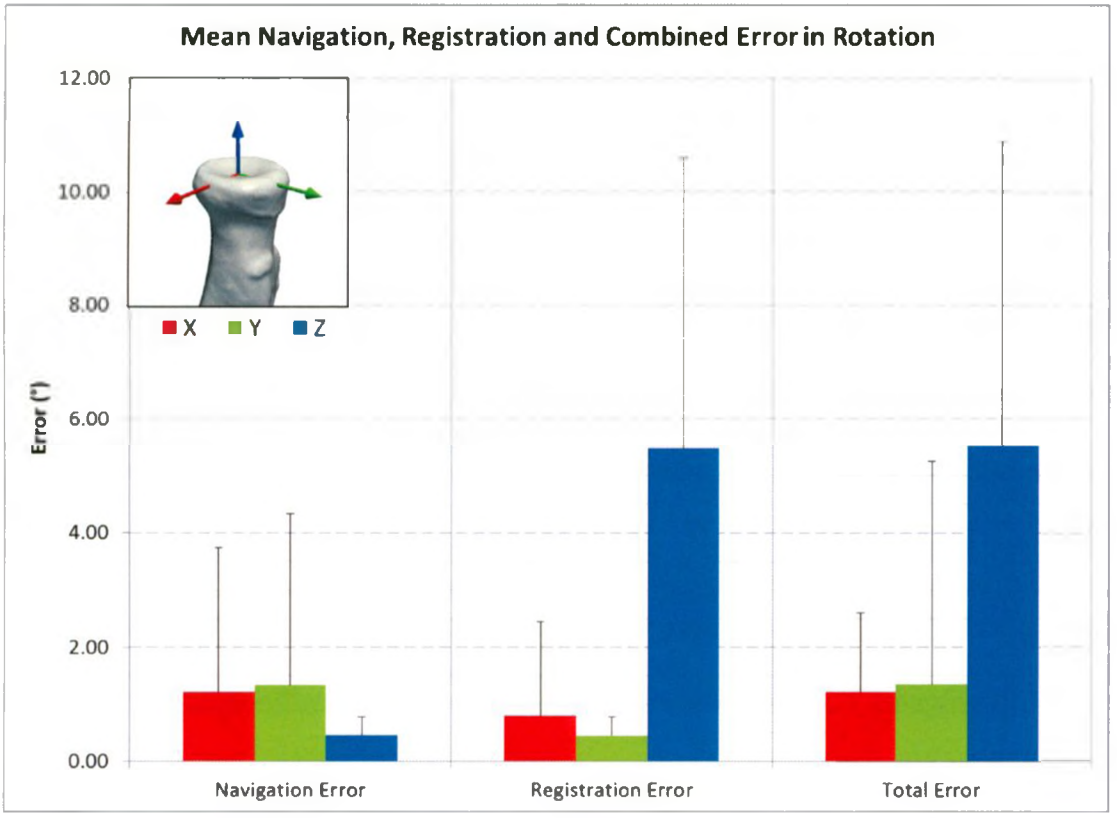

Figure 4.11: Mean and maximum navigation, registration and total error in translation (top) and rotation (bottom). Translation error included the equivalent 3D translation error (black bar).

4.4 DISCUSSION

The stem and head components designed for the current study were highly effective. The four potential stem orientations aided in avoiding impingement and ensuring that the navigation tool was visible to the camera system. The socket-like assembly mechanism of the stem and head simplified component swapping but did not disengage during elbow motion. The divots on the stem allowed for quick and accurate calibration with an FRE of 0.3±0.1mm. Though fixation required revision if voids were created from stem movement during navigation, once rigid fixation had been achieved it was maintained as the implant stem did not fail and was resilient to removal at the conclusion of testing for each specimen. The maximum navigation errors occurred with the first two specimens suggesting that mal-alignment was reduced with operator experience.

The error incurred during the manual alignment of the implant approached the desired threshold of 2° and 0.25mm. These target values were based on the previous chapter which showed a difference in mean surface mismatch between the quasi-anatomic and patient-specific implant models of ~0.25mm. Further to this, a 2° rotation about the center of the implant would incur a similar translation error. Intra-operative registration error of pre-operative imaging was larger than these target values, particularly about the z (proximal) axis. This was a foreseeable difficulty as digitizations included the cartilage offset, whereas the model obtained from CT imaging did not. Use of the ICP algorithm requires both models to be of similar shape and size to provide accurate alignment. The inclusion of mid-bone digitizations and small patches of both the radial styloid and dorsal DRUJ was meant to provide some resilience to mal-alignment

but ultimately this was not very effective, potentially due to the large number of proximal points. Further work is required to improve the accuracy or surface-based registration of the radius. Application of a cartilage offset to the articular surface of the CT model may improve registration accuracy, particularly in rotation about the proximal vector, but would require further information on articular cartilage distribution which has not yet been reported.

The accuracy of the datum fiducial based registration showed a low FRE at 0.3±0.2mm. However TRE was higher than FRE at 0.7±0.4mm. This is not unexpected as we were unable to follow some of the best practices recommended in the literature when determining the arrangement of fiducial markers[11]. The markers should surround the area of interest as the registration accuracy is highest near the centroid of their arrangement. This was not possible within the current study as the radial head itself is the most proximal part of the radius. Also, the target fiducial should be located as near to the area of interest as possible. In our case the radial head has been resected prior to navigation so we were limited to attaching the target fiducial as proximally as possible perpendicular to the radial neck. An improved measure of target registration error could be obtained by securing the fiducial with cement in the space occupied by the implant stem before its removal which would more closely approximate the region where the navigation is taking place. Alternatively, the fiducial registration could be avoided by including the stem in post-operative imaging so that its location could be determined directly. However, image artifacts caused by the metal in the implant may make segmentation difficult and unreliable. Due to relatively poor alignment associated with

the surface-based method, the use of the fiducial registration method as a gold-standard datum represents an acceptable loss of accuracy.

One flaw in the current study is the use of complete radial head digitizations in the registered dataset. In the clinical application the radial head would be fractured limiting the region available for digitization. Thus in some respects the registration achieved in the current study represents a best case scenario; registration error and hence the accuracy of implant placement would likely be worse clinically than achieved in this in-vitro study.

Another shortcoming is the use of ipsi-lateral imaging to generate the pre-operative plan. The radial head undergoing replacement would likely be fractured and unable to serve as the template to guide navigation. Previous studies have shown a lack of statistical side-to-side differences suggesting that minimal error would be incurred in shape between sides[12]. However, an accurate registration would likely be more difficult to obtain without the articular surfaces. Contra-lateral based planning for humeral component navigation has been investigated with a reported error of approximately 1.0° and 0.5mm[13]. Further work is required to assess the impact of this added step on radial head navigation accuracy.

Ultimately the current system represents an important first step in the development of a computer and image-assisted system for radial head implant navigation. Although the total rotational error about the proximal axis of 5.5±3.2° was larger than our target of 2.0° it may be an improvement on the accuracy of manual alignment which has never been quantified for an anatomic radial head system. Total rotational error about the lateral and anterior axes of 1.2±1.0° and 1.4±1.8° was below the target of 2.0°. Height mismatch of 2.5mm has been shown to effect kinematics of the joint with an axisymmetric design.

The current system had an average height mismatch of 0.6±0.3mm meeting this requirement although exceeding our target of 0.25mm. Translation errors in both the M/L and A/P directions were 0.9±0.5mm and 0.8±0.6mm respectively, which was larger than our target error of 0.25mm. The majority of this error can be attributed to registration rather than navigation suggesting that further improvements in registration techniques are needed. Translation error may be more provocative than rotational error due to the distortion of the rotational axis of the radial head. van Riet et al.[14] showed that a 90° rotation of the native radial head had limited impact on elbow kinematics and contact forces. However, the presence of MCL injuries may have masked the effects of irregular orientation in their study. Further work is required to determine the acceptable level of surface mismatch at radial head in order to define clinically relevant navigation targets.

4.5 REFERENCES

1. van Riet RP, van Glabbeek F, Neale PG, et al. Anatomical considerations of the radius. *Clinical Anatomy*. 2004;17(7):564-9.

2. Katchky RN, Johnson JA, King GJW, Athwal GS. Anatomic radial head arthroplasty: a lack of reliable landmarks for alignment. In: *COA/CORS Annual Meeting Abstract Supplement*.; 2011:164-165.

3. Acumed. Anatomic Radial Head System. 2011:1-14. Available at: http://www.acumed.net/sites/default/files/literature/brochure-surgical-technique/anatomic-radial-head-system-brochure-surgical-technique.pdf.

4. van Glabbeek F, van Riet RP, Baumfeld JA, et al. Detrimental effects of overstuffing or understuffing with a radial head replacement in the medial collateral-ligament deficient elbow. *Journal of Bone and Joint Surgery*. 2004;86-A(12):2629-35.

5. Jenny J-Y, Clemens U, Kohler S, et al. Consistency of implantation of a total knee arthroplasty with a non-image-based navigation system: a case-control study of 235 cases compared with 235 conventionally implanted prostheses. *The Journal of Arthroplasty*. 2005;20(7):832-9.

6. Barrett WP, Mason JB, Moskal JT, et al. Comparison of radiographic alignment of imageless computer-assisted surgery vs conventional instrumentation in primary total knee arthroplasty. *The Journal of Arthroplasty*. 2011:ARTICLE IN PRESS.

7. Sugano N, Nishii T, Miki H, et al. Mid-term results of cementless total hip replacement using a ceramic-on-ceramic bearing with and without computer navigation. *The Journal of Bone and Joint Surgery*. 2007;89(4):455-460.

8. Stacpoole RA, Ferreira LM, King GJW, Johnson JA. Development of computer-assisted radial head replacement. *Proceedings of MCCAI*. 2003;2879:199–206.

9. Besl P, McKay N. A method for registration of 3-D shapes. *IEEE Transactions on Pattern Analysis and Machine Intelligence*. 1992.

10. Craig J. *Introduction to robotics: Mechanics & control*. Reading, Mass.: Addison-Wesley Pub. Co. 1986:40-45.

11. West JB, Fitzpatrick JM, Toms SA, Maurer CR, Maciunas RJ. Fiducial point placement and the accuracy of point-based, rigid body registration. *Neurosurgery*. 2001;48(4):810-6.

12. Popovic N, Djekic J, Lemaire R, Gillet P. A comparative study between proximal radial morphology and the floating radial head prosthesis. *Journal of Shoulder and Elbow Surgery*. 2005;14(4):433-40.

13. McDonald CP, Peters TM, King GJW, Johnson JA. Computer assisted surgery of the distal humerus can employ contralateral images for pre-operative planning, registration, and surgical intervention. *Journal of Shoulder and Elbow Surgery*. 2009;18(3):469-77.

14. van Riet R, van Glabbeek F, Baumfeld J, et al. The effect of the orientation of the radial head on the kinematics of the ulnohumeral joint and force transmission through the radiocapitellar joint. *Clinical Biomechanics*. 2006;21(6):554–559.

CHAPTER 5 - General Discussion and Conclusions

OVERVIEW:

This chapter reviews each of the initial objectives and hypotheses presented and summarizes the work done to address them. The strengths and limitations of the studies presented are discussed along with the future directions of this work.

5.1 SUMMARY

Numerous studies have examined radial head morphology including the use of reverse engineering techniques on 3D models obtained from CT imaging or direct measurements with coordinate measuring machines. While there is some controversy, most studies have reported that the radial head is elliptical. In Chapter 2 it was shown that automated ellipse fitting allows for rapid and accurate parameterization of radial head shape (Objective, Chapter 2). Measurements obtained using this method showed correlations and magnitudes closely matching previous results in the literature. The major and minor outer and rim diameters showed significant differences, and were highly correlated, confirming the elliptical nature of the radial head. Unlike previous studies, a large number of parameters, suitable for highly specific anatomic implants designs, were measured over the entire height of the articular circumference and the depth of the radial dish in a common anatomically oriented coordinate system. The use of these techniques should allow for precise recreation of patient-specific implant shapes as well as providing the necessary data for the development of an 'off-the-shelf' anatomic design.

Many current radial head implant designs have an axisymmetric non-anatomic shape. However, recently there has been an interest in the possible benefits of an accurately shaped and oriented anatomic implant design to optimize both joint kinematics and force transmission. Chapter 3 detailed the creation of a population-based radial implant by grouping specimens based on their overall size, and averaging their parameters as measured in Chapter 2. As detailed, a novel system was created for comparing surface mismatch between ideally sized and placed implants and radial head models created from CT imaging (Objective 2, Chapter 3). This provided an automated method of quantifying the ability of each implant design to accurately match the head shape. Significant differences were identified between a currently available axisymmetric design and the population-based and patient-specific anatomic models developed in this study. Additionally, varying the number of parameters used to define the patient-specific models demonstrated that ideally sized implants based around simplified circular or elliptical radial head models were less accurate than the custom patient-specific model incorporating all measured parameters.

Computer navigated alignment of a radial head implant has only been detailed in one previous publication, albeit using an axisymmetric implant and without the use of pre-operative imaging. A novel system for registering a calculated target stem position from pre-operative imaging to allow for real-time guidance during implant placement was created, and its accuracy determined by comparison to the gold-standard fiducial method (Objectives 3-4, Chapter 4). Even with the addition of clinically unfeasible distal digitizations used in the current study and a complete digitization of the radial head, registration accuracy, particularly in the transverse plane, severely limited the total

accuracy of navigation. The error incurred by the user was below the target threshold of 0.25mm and 2° suggesting that, aside from the registration, the majority of the steps in the navigation process were successful. Approximately half of the specimens required revision due to poor fixation or mal-alignment caused by the inability of the operator to maintain an optimal manual alignment due to operator fatigue when holding the implant in position as the cement hardened. As anatomically based radial head replacement systems are becoming available, it is important to explore various methods of positioning, both manual and navigated, to ensure potential complications from mal-alignment can be consistently avoided.

5.2 STENGTHS AND LIMITATONS

The current work is not without limitations although many of the current shortcomings could be readily addressed in subsequent studies. Any limitations affecting the radial head measurements or implant design were propagated from the initial study through to subsequent studies which were based on that initial work. The most evident example of this is the lack of a cartilage thickness offset in the initial CT based measurements, affecting the final implant design parameters as well as the accuracy of registration during implant navigation. Another example is the poor reliability of radial head height measurements which skewed the averages used to generate the shape of the quasi-anatomic implants in Chapter 3. Finally, specimens used in this study were older than the typical patient undergoing radial head replacement. Future studies need to incorporate solutions to these shortcomings before generating a refined set of anatomic implants.

Some limitations, such as the use of distal and articular digitizations and ipsilateral rather than contralateral registration were self-imposed as these studies were meant to provide a preliminary feasibility analysis of the navigation of an anatomic radial head implant rather than provide a clinically applicable system. As such, the objective of this study was to assess registration using a best-case scenario and the results show that significant work is needed to ensure accurate registration at the radius.

The program used to determine the mismatch between each implant design and the CT bone models assumed ideal placement and ignored the possibility of implant movement effectively minimizing mismatch for the existing axisymmetric model which is not fixed in place when used clinically. Furthermore the results could be influenced by the point density of the models. Additional work to optimize the means by which mismatch is determined either using true perpendicular distances or volume based models should be conducted as this would provide a useful tool for comparing shapes of various implant designs.

Perhaps the most clinically relevant issue is the lack of knowledge as to what error in placement will create a worrisome effect on joint kinematics, contact pressures and implant wear post operatively. Some placement errors have been suggested to be more provocative than others such as height mismatch compared to implant rotation respectively, but little data exists, and virtually none in the case of anatomic radial head implants, demonstrating the effects of implant misalignment. This is significant as our largest error was in rotation about the proximal-distal axis which may be the least provocative in terms of post-operative patient outcomes. Although the error in this study exceeded target values they may still be acceptable when compared to the values

obtained clinically using current anatomic implants, which have never been examined. However, even the error in placement determined in this study relied on the datum fiducial registration which was not without its own error. Finally, with regard to implant placement both operator experience and fatigue had a role in the accuracy of placement.

The strength of these studies are that they are the first to document each stage of a radial head implant design from measurement of the morphological parameters through to navigated placement in cadaveric specimens using both a tracking system and image guidance. Only one previous study has included navigated radial head placement, this involved an axisymmetric implant where placement was based solely on digitizations and did not included an evaluation of placement accuracy. Although previous studies have suggested that reverse engineering techniques could be applied to more accurately model radial head implant, this is the first study to take data obtained from thorough characterization of the native shape and use it to generate personalized and highly accurate implant models. The ellipse fitting techniques detailed in Chapter 2 provide the basis for the generation of these parameters and show comparable results to previous morphological studies.

With regard to further testing of radial head implant shapes, this study creates the groundwork for how measurements can be quickly and consistently obtained and the mismatch between implant and bone models quantified. Furthermore, using the socket-like connection on the stem detailed in Chapter 4, each implant head can be easily swapped onto the same navigated stem allowing comparison of kinematic and contact data during testing on an elbow joint simulator.

5.3 CURRENT AND FUTURE DIRECTIONS

A primary objective moving forward is to examine the kinematic and contact differences between the existing axisymmetric, quasi-anatomic and anatomic patient-specific implant models based on the data obtained concurrently with the navigation study presented in Chapter 4. Additional studies examining cartilage thicknesses at the radial head are being conducted which should provide baseline data on the significance of this source of error.

Significant further study is required before a system for computer and image-assisted radial head replacement will be clinically viable. The accuracy of registering pre-operative imaging using surface digitizations, even with the inclusion of clinically inapplicable distal landmarks and the complete radial head, is the most obvious challenge with the current system. Efforts to define more suitable landmarks to improve the rotational registration accuracy are required. Data on the distribution and thickness of articular cartilage would provide valuable information in terms of both registration technique and implant design. The use of contra-lateral imaging for pre-operative planning and its effect on navigation accuracy is required to validate this unexplored step in the proposed system. Other registration techniques, including the use of intra-operative digitizations or imaging to guide placement, should be explored as they may circumvent some of the current difficulties. Secondary objectives include improvement of the measurement system, specifically with regard to the height and rim reliability, which would allow for a more accurate comparison between the population-based and patient-specific implants. The use of jigs or robotic assistance to maintain implant alignment during cement hardening would serve to avoid the issue of poor fixation and suboptimal

implant alignment due to operator movement during the curing of the cement. Finally, further work documenting the accuracy of manual alignment using anatomic radial head implants and the effects of implant mal-alignment on load transfer and kinematics may be the most crucial piece of information in determining if the potential benefits of the proposed anatomic based implants outweigh the current technical challenges.

5.4 SIGNIFICANCE

This study is the first to present results on the navigational accuracy of computer assisted radial head replacement using image guidance. Furthermore, this study is the first to utilize reverse engineered patient-specific radial head prostheses and provide comparison between different anatomical and axisymmetric designs. The results of this study will help identify future challenges in the development of clinically applicable systems for radial head navigation. The current system will allow for further comparison, through kinematic testing using a joint simulator, of the various implant designs after navigated placement.

Appendix A - Glossary

Anatomic	-	Relating to the structure of the body
Anterior	-	Towards the front of the body
Annular Ligament	-	A ligament which encircles the head of the radius ensuring contact between the radius and PRUJ
Arthroplasty	-	Surgical reconstruction or replacement of a joint
Articular	-	Relating to a joint
Axisymmetric	-	Having symmetry around an axis
CAOS	-	Computer-assisted orthopedic surgery
Capitellum	-	Smooth rounded surface on the lateral distal humerus which articulates with the radial dish
Cartilage	-	Smooth, firm connective tissue found on articulating surfaces of joints
CMM	-	Coordinate measuring machine
Comminuted	-	To break into several small fragments
Contact Area	-	Surface area in contact between two bones
Contralateral	-	Opposite side
Coronoid	-	Triangular anterior projection on the proximal ulna which articulates with the radius
CT	-	Computed tomography, method of x-ray imaging which produces cross section images of the body
Cubitus Valgus	-	Deformity of the elbow in the valgus direction
Digitization	-	Acquiring three-dimension location of points relative to an object
Dislocation	-	Displacement of a bone from its normal articulation
Distal	-	Away from the center of the body
DRUJ	-	Distal radioulnar joint, pivot-joint between the distal radius and ulna

Excision	-	Surgical removal
External Rotation	-	Rotation away from the body.
Fiducial	-	A fixed point of reference
Fossa	-	Shallow depression
FRE	-	Fiducial registration error, RMS error between homologous points used in registration
Humerus	-	Bone of the upper arm forming the shoulder and elbow
ICC	-	Inter class correlation
ICP	-	Iterative closest point, an algorithm used for surface registration
Inferior	-	Towards the feet
Internal Rotation	-	Rotation towards the body
Inter-Observer	-	Between measures made by different observers
Intramedullary Canal	-	Marrow cavity of a bone
Intra-Observer	-	Occuring between the same observer
Intra-Operative	-	During surgery
IOM	-	Interosseous membrane; fibrous connection between the radius and ulna which plays a role in load transfer and provides restraint against proximal radius migration
Ipsilateral	-	Same side
Landmark	-	Reliably identified feature
Lateral	-	Away from the middle of the body
Laxity	-	Looseness
LCL	-	Lateral collateral ligament; ligament composed of the LUCL and the RCL
LED	-	Ligh emitting diode

Lesser Sigmoid Notch	-	Depression on the lateral side of the coronoid which articulate with the radial head
Ligament	-	Fibrous connective tissue between two bones
LUCL	-	Lateral ulnar collateral ligament; extends from lateral epicondyle to the coronoid and serves as an important posterolateral rotational stabilizer
Medial	-	Towards the middle of the body
Modular	-	Constructed with standardized units allowing flexbility in assembly
MCL	-	Medial collateral ligament; extends from medial epicondyle of humerus to the coronoid providing primary valgus restraint
Morphology	-	Study of size, shape and structure
ORIF	-	Open reduction and internal fixation; method for surgically repairing fracure bone using plates and/or screws
Orthogonal	-	Perpendicular
Osseous	-	Relating to bone
Pedicle	-	Boney segment between the transverse process and body of a spinal vertebra
Posterior	-	Towards the back of the body
Post-Operative	-	After surgery
Pre-Operative Planning	-	Using medical imaging to determine surgical targets before operating
PMMA	-	Polymethylmethacrylate
Pronation	-	Rotation towards the midline
Prothesis	-	Artificial device extension replacing a missing body part
Proximal	-	Towards the center of the body

PRUJ - Proximal radioulnar joint, articulation between the lesser sigmoid notch of the ulna and the circumference of the radial head

Radial Dish - Concavity on the proximal end of the radial head which articulates with the capitellum

Radial Head - Complex anatomic structure forming the proximal end of the radial which articulates with both the humerus and ulna

Radial Neck - Narrow region of proxmal radius distal to the radial head

Radiolucency - Allowing the passage of x-rays

Radius - The lateral bone of the forearm articulating with the ulna, humerus and carpal bones

RCL - Radial collateral ligament; originates on the lateral epicondyle and inserts into the annular ligament serving as a primary varus stabilizer of the elbow

Registration - The process by which one dataset is aligned with another based on shared features

Reverse Engineer - Create a 3D CAD model of an existing part or in this study, bone. Involves measuring the object to construct the 3D model.

Rigid-Body - Solid body in which deformation is neglected

RMS - Root mean square; a statistical measure of magnitude

Segmentation - Process by which a 3D data set is transcribed from 2D slice information

Soft-Tissue - Tissues that connect, support or surround other structures, not including bone

Stereotactic - Precise surgical positioning in three-dimensional space using external frame of reference

Stylus - Penlike device used to obtain digitizations with respect to a tracking system

Subluxation - Incomplete or partial dislocation

Superior - Towards the head

Supination - Rotation away from the midline

Synovitis - Inflammation of the sinovial membrane or joint

TRE - Target registration error; distance error between homologous point not used in the registration located in the region of interest

Trochoginglymoid - Type of joint composed of hinge (ginglymus) and pivot joints (trochoid)

Tuberosity - Boney projection

Ulna - The medial bone of the forearm articulating with the radius, humerus, and carpal bones

Valgus - Displacement of the distal aspect of the bone away from the midline of the body

Varus - Displacement of the distal aspect of the bone towards the midline of the body

Appendix B - Comparison of ICP and Manual Implant Alignment

The use of the iterative closest point algorithm (ICP) to align various implants to bone models generated from each specimen's CT allowed for the distance mapping process to be automated. In order to quantify the difference between ICP and manually aligned implant a comparison study was conducted on seven specimens. Mean surface mismatch was determined for both cases as shown in Figure B.1 and compared using a paired t-test. Although the difference between the means was small at 0.04±0.02 mm there was a statistically significant (α=0.05) decrease in mean surface mismatch for the ICP aligned quasi-anatomic implant when compared to the manually aligned quasi-anatomic implant of the same size. As the mean surface mismatch was minimized using the ICP method, this represented the most ideal placement. Accordingly the ICP algorithm was used to align each of the implant models to determine surface mismatch with the exception of the patient-specific anatomic design.

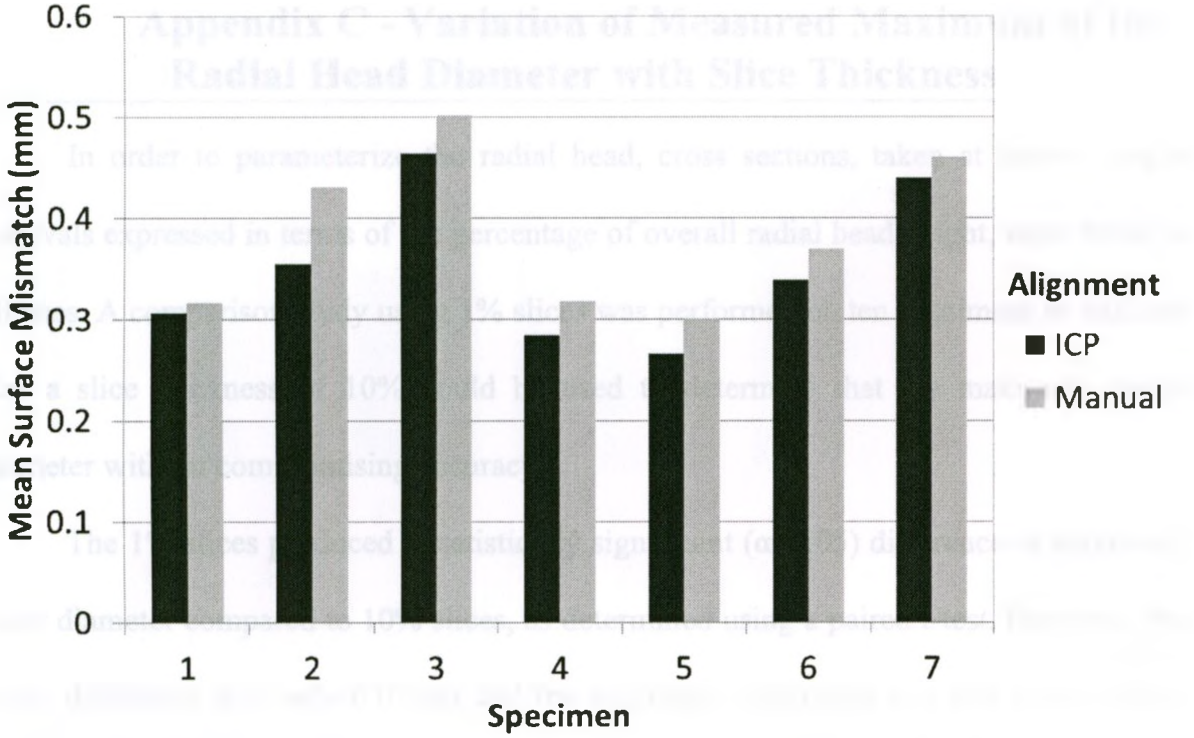

Figure B.1: Comparison of ICP and manual alignment for determining mean surface mismatch for a quasi-anatomic implant. (n=7)

Appendix C - Variation of Measured Maximum of the Radial Head Diameter with Slice Thickness

In order to parameterize the radial head, cross sections, taken at known height intervals expressed in terms of the percentage of overall radial head height, were fitted as ellipses. A comparison study using 1% slices was performed on ten specimens to validate that a slice thickness of 10% could be used to determine that the maximum radial diameter without compromising accuracy.

The 1% slices produced a statistically significant (α=0.05) difference in maximum outer diameter compared to 10% slices, as determined using a paired t-test. However, the mean difference was only 0.07mm and the maximum difference was less than 0.2mm. The 1% slices, as expected, consistently found a slightly larger maximum diameter. The results for all 10 specimens are shown in Figure C.1. This small difference was not considered clinically significant so 10% slices were used for the majority of the radial head height. At the proximal end of the radial head, 5% slices were used to capture the rapidly changing curvature in this region which was defined as the most proximal 20%.

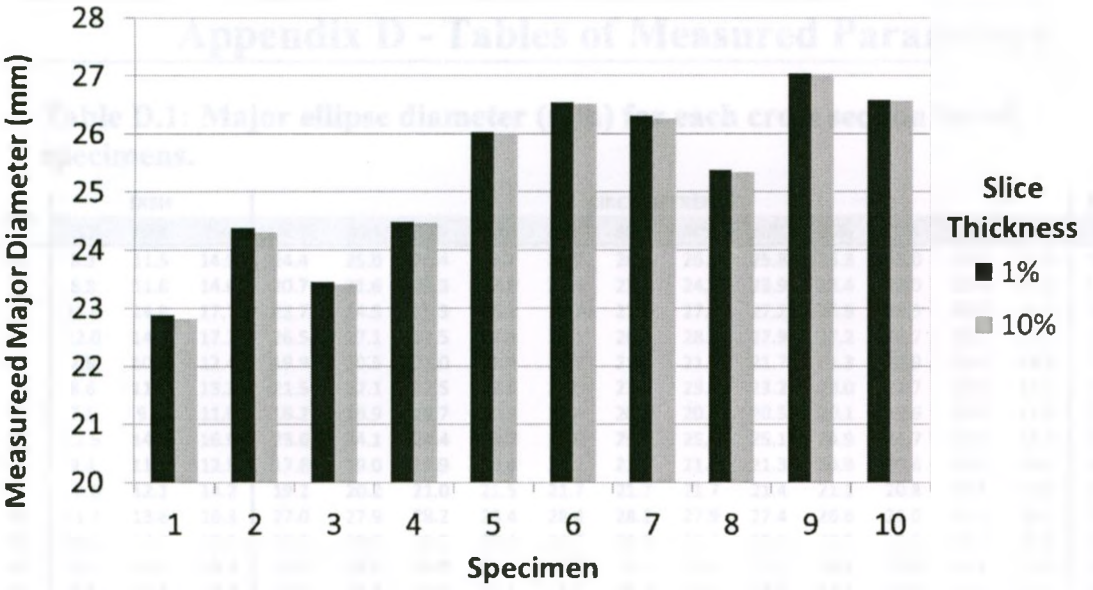

Figure C.1: Effect of slice thickness on the determined maximum outer diameter of the radial head using ellipse fitting of cross sections. (n=10)

Appendix D - Tables of Measured Parameters

Table D.1: Major ellipse diameter (mm) for each cross section for all specimens.

#	Sex	DISH			CIRCUMFERENCE												Rim
		15%	10%	5%	100%	90%	80%	70%	60%	50%	40%	30%	20%	15%	10%	5%	0%
1	M	8.3	11.5	14.9	24.4	25.0	25.4	25.7	25.9	26.1	26.1	25.8	25.3	25.0	24.7	23.8	18.8
2	F	8.8	11.6	14.6	20.7	21.6	22.3	22.9	23.6	23.9	24.0	23.9	23.4	23.0	22.4	21.4	17.6
3	M	11.9	14.8	17.7	23.7	24.5	25.3	26.1	26.7	27.1	27.2	27.2	26.9	26.5	25.9	25.1	21.7
4	M	12.0	14.7	17.2	26.5	27.1	27.5	27.8	28.1	28.3	28.2	27.9	27.2	26.7	26.1	25.2	22.1
5	F	7.8	10.3	12.4	19.9	20.5	21.0	21.4	21.7	21.9	21.9	21.7	21.3	20.9	20.4	19.5	17.0
6	F	8.6	11.0	13.3	21.5	22.1	22.5	22.8	23.0	23.2	23.3	23.2	23.0	22.7	22.3	21.5	17.9
7	F	7.5	9.8	11.9	18.2	18.9	19.7	20.2	20.4	20.6	20.6	20.5	20.1	19.6	18.9	17.9	15.0
8	M	12.5	14.6	16.9	23.6	24.1	24.4	24.7	24.9	25.0	25.1	25.1	24.9	24.7	24.4	23.8	21.3
9	F	9.4	11.2	12.9	17.8	19.0	19.9	20.6	21.1	21.3	21.4	21.3	20.9	20.6	20.1	19.5	16.6
10	F	10.0	12.1	14.2	19.2	20.2	21.0	21.5	21.7	21.7	21.7	21.4	21.1	20.8	20.4	19.8	17.3
11	M	11.3	13.8	16.3	27.0	27.9	28.2	28.4	28.4	28.2	27.9	27.4	26.6	26.0	25.3	24.1	21.0
12	M	14.2	16.7	19.1	28.5	28.7	28.7	28.6	28.7	28.8	28.6	28.0	27.5	26.9	26.3	25.3	24.1
13	M	9.5	12.3	15.2	23.7	25.0	26.0	26.8	27.2	27.5	27.6	27.2	26.3	25.5	24.5	23.3	19.3
14	M	8.9	11.6	14.2	25.1	25.4	25.5	25.5	25.5	25.5	25.3	24.9	24.2	23.8	22.9	22.0	18.0
15	F	7.9	10.5	12.9	20.6	21.4	22.0	22.6	23.0	23.1	23.0	22.5	21.7	21.3	20.6	19.7	16.1
16	F	0.7	8.2	11.6	19.6	20.8	21.6	22.6	23.3	23.5	23.6	23.4	23.0	22.7	22.3	21.4	15.6
17	M	8.1	12.0	14.8	21.2	22.1	23.0	23.5	23.8	23.9	23.9	23.7	23.3	23.1	22.7	21.8	18.2
18	M	3.4	10.1	13.5	22.9	24.2	25.4	26.1	26.7	27.2	27.4	27.1	26.2	25.5	24.5	23.1	17.4
19	M	9.8	12.7	15.7	23.8	24.4	24.8	25.2	25.5	25.8	25.9	25.8	25.5	25.0	24.2	23.3	18.7
20	M	9.0	12.2	14.6	23.2	24.5	25.4	26.1	26.6	26.9	26.9	26.5	25.7	25.0	24.1	22.8	18.0
21	M	7.0	9.8	12.2	19.0	20.0	20.8	21.3	21.8	22.3	22.5	22.5	22.1	21.6	20.8	19.8	15.8
22	M	7.4	11.1	14.3	24.1	24.8	25.5	26.2	26.9	27.4	27.6	27.4	26.4	25.6	24.7	23.6	17.8
23	M	9.5	12.4	15.8	23.8	24.2	24.4	24.5	24.6	24.6	24.4	24.1	23.6	23.1	22.6	21.7	18.4
24	M	11.2	13.8	16.0	25.9	26.6	26.8	27.0	27.0	26.9	26.8	26.7	26.2	25.9	25.4	24.4	19.7
25	F	6.4	9.3	11.7	18.7	19.2	19.7	20.2	20.5	20.5	20.5	20.2	19.7	19.3	18.8	18.4	15.3
26	F	9.3	11.3	13.7	19.3	20.3	20.9	21.4	21.8	22.0	22.2	22.1	21.9	21.7	21.3	20.6	17.2
27	F	10.6	12.7	14.7	18.5	19.7	20.2	20.7	21.1	21.4	21.5	21.5	21.2	20.9	20.4	19.6	17.6
28	M	8.6	11.5	14.3	22.2	23.2	23.9	24.4	24.8	25.2	25.4	25.4	25.1	24.8	23.9	22.7	17.9
29	F	7.4	10.5	13.2	19.6	20.0	20.3	20.3	20.4	20.5	20.5	20.3	20.1	19.8	19.5	18.9	16.0
30	M	11.2	13.7	16.3	23.9	24.3	24.6	24.8	25.0	25.0	24.9	24.7	24.4	24.2	24.0	23.6	19.3
31	F	9.8	12.1	14.0	21.3	22.3	22.8	23.0	23.2	23.3	23.3	23.2	22.9	22.6	22.1	21.3	17.1
32	F	4.1	8.2	11.0	19.9	20.7	21.3	21.7	21.9	22.2	22.3	22.1	21.6	21.2	20.7	19.9	15.6
33	M	11.4	13.5	15.6	24.1	25.0	25.4	25.6	25.8	25.9	25.9	25.8	25.3	24.9	24.6	24.0	19.6
34	F	8.5	10.9	13.1	19.7	20.4	20.9	21.3	21.5	21.7	21.7	21.7	21.4	21.2	20.8	20.2	16.3
35	F	8.2	11.1	13.0	19.1	20.0	20.5	20.8	20.8	20.7	20.8	20.7	20.6	20.3	19.7	18.8	15.5
36	M	10.5	13.0	15.7	23.4	24.0	24.5	24.8	25.1	25.3	25.4	25.4	25.2	24.9	24.5	24.2	20.1
37	M	7.4	11.4	14.4	24.9	26.0	26.5	26.6	26.7	26.7	26.5	26.1	25.4	24.8	23.9	22.6	18.9
38	M	8.4	11.4	14.5	21.9	22.4	22.7	22.8	22.8	22.8	22.6	22.5	22.2	21.8	21.4	20.5	18.1
39	M	8.9	11.3	13.5	22.8	23.4	23.8	24.1	24.3	24.3	24.2	24.1	23.7	23.3	22.8	21.8	17.3
40	M	9.9	12.5	14.9	20.7	21.5	22.2	22.6	23.0	23.2	23.4	23.3	22.9	22.5	22.1	21.2	18.3
41	M	12.5	14.2	16.2	22.2	23.5	24.4	24.9	25.3	25.4	25.6	25.5	25.1	24.7	24.2	23.3	19.4
42	M	9.2	11.7	14.4	22.5	23.1	23.7	24.1	24.3	24.5	24.4	24.1	23.4	22.9	22.2	21.3	17.8
43	M	8.3	11.6	14.4	25.2	25.8	26.0	26.0	26.0	26.0	25.8	25.5	25.0	24.5	23.9	22.9	18.7
44	M	8.1	11.7	14.3	24.1	24.9	25.4	25.9	26.2	26.4	26.5	26.4	25.6	25.0	24.1	22.9	17.9
45	M	16.9	18.6	20.1	25.3	26.2	27.0	27.3	27.3	27.4	27.5	27.4	27.1	26.9	26.6	26.0	23.2
46	M	9.4	12.6	15.3	24.8	25.4	25.9	26.1	26.3	26.2	26.0	25.6	24.8	24.4	23.9	23.1	19.1
47	M	9.5	12.1	14.5	23.4	24.0	24.5	24.9	25.2	25.3	25.3	25.1	24.4	23.8	22.9	21.7	17.7
48	M	10.0	12.9	15.8	24.3	25.5	26.3	26.6	26.9	27.0	27.0	26.9	26.4	25.8	24.8	23.6	19.4
49	M	10.2	13.3	16.6	25.6	26.1	26.3	26.5	26.5	26.6	26.5	26.2	25.7	25.3	24.9	24.3	20.1
50	M	10.1	12.4	14.6	24.2	24.5	25.0	25.3	25.7	26.0	26.1	26.0	25.4	24.8	24.0	22.7	19.3

*Grey percentages indicate the offset of the ellipse fitted cross section relative to proximal end of the radius expressed as a percentage of overall radial head height.

Table D.2: Minor ellipse diameter (mm) for each cross section for all specimens.

#	Sex	DISH			CIRCUMFERENCE												Rim
		15%	10%	5%	100%	90%	80%	70%	60%	50%	40%	30%	20%	15%	10%	5%	0%
1	M	6.2	10.4	13.0	22.7	23.7	24.4	24.8	25.1	25.1	24.8	24.3	23.3	22.1	20.4	19.7	15.9
2	F	7.9	10.5	12.8	18.0	19.0	20.0	20.6	21.1	21.5	21.6	21.6	21.2	20.8	20.2	19.0	16.5
3	M	11.5	14.1	16.2	21.6	22.8	23.9	24.7	25.2	25.5	25.6	25.3	24.7	24.1	23.3	22.0	19.0
4	M	10.8	13.5	16.2	23.9	24.8	25.4	25.9	26.2	26.4	26.4	26.1	25.3	24.8	24.1	22.9	20.3
5	F	7.0	9.6	11.9	19.3	19.8	20.2	20.4	20.7	20.8	20.7	20.4	19.7	19.3	18.5	17.6	15.3
6	F	8.3	10.8	12.7	19.4	20.2	20.7	21.2	21.5	21.7	21.7	21.4	20.8	20.2	19.5	18.4	16.1
7	F	7.2	9.6	11.4	17.7	18.6	19.1	19.5	19.9	20.2	20.2	19.9	19.3	18.9	18.2	17.2	14.8
8	M	12.3	14.2	16.1	22.5	23.1	23.6	23.9	24.1	24.2	24.1	23.8	23.3	22.9	22.3	21.3	19.0
9	F	9.0	11.0	12.6	16.5	17.6	18.6	19.4	19.9	20.1	20.2	19.8	18.9	18.3	17.7	16.6	15.1
10	F	8.8	10.7	12.5	17.3	18.5	19.3	19.9	20.3	20.5	20.4	20.2	19.6	19.3	18.8	17.9	16.1
11	M	11.2	13.5	15.5	24.6	25.5	26.1	26.6	27.0	27.3	27.2	26.7	25.6	24.8	23.8	22.6	20.0
12	M	11.6	13.7	15.5	24.9	26.1	27.3	27.9	28.4	28.4	28.2	27.9	27.1	26.4	25.5	24.6	20.8
13	M	8.8	12.2	14.5	21.6	22.6	23.6	24.4	25.2	25.7	25.8	25.5	24.7	24.0	23.0	21.6	18.8
14	M	8.6	11.0	13.0	22.5	23.0	23.4	23.7	23.8	23.7	23.4	22.8	22.0	21.2	20.4	19.2	16.4
15	F	7.5	10.0	12.0	19.7	20.6	21.2	21.6	21.8	21.9	21.7	21.3	20.4	19.7	18.9	17.5	14.6
16	F	0.7	7.8	11.1	15.9	17.6	18.8	19.9	20.7	21.4	21.9	22.2	21.8	21.3	20.3	18.9	15.1
17	M	5.5	9.7	12.6	19.1	20.0	21.1	22.0	22.5	22.8	22.9	22.7	22.0	21.5	20.8	19.7	16.1
18	M	2.4	9.2	12.6	20.9	23.0	24.6	25.4	25.9	26.1	26.1	25.7	25.0	24.5	23.6	22.1	17.0
19	M	9.1	11.5	13.7	22.4	23.3	23.9	24.3	24.4	24.5	24.4	23.9	23.0	22.3	21.3	19.9	16.3
20	M	7.2	10.6	13.4	21.2	22.5	23.8	24.5	24.9	25.4	25.5	25.2	24.0	23.2	22.1	20.7	16.5
21	M	6.4	9.6	11.8	17.0	18.3	19.4	20.1	20.5	20.7	20.7	20.3	19.7	19.2	18.5	17.4	14.3
22	M	6.6	10.6	13.6	21.5	22.5	23.4	24.1	24.5	24.8	24.9	24.8	23.9	23.2	22.2	20.7	16.7
23	M	8.1	10.4	12.5	22.2	22.7	23.1	23.4	23.6	23.7	23.8	23.6	23.1	22.6	21.8	20.7	16.3
24	M	10.1	13.2	15.9	23.5	24.5	25.3	25.7	26.0	26.0	25.9	25.6	25.0	24.4	23.7	22.7	19.0
25	F	5.5	8.9	11.1	16.8	17.8	18.5	18.9	19.1	19.3	19.4	19.4	19.1	18.8	18.2	16.9	14.6
26	F	8.7	11.0	12.7	17.0	18.2	19.1	19.7	20.1	20.3	20.4	20.3	19.8	19.3	18.6	17.3	14.8
27	F	10.0	12.1	14.1	16.7	17.7	18.9	19.8	20.2	20.4	20.6	20.6	20.5	20.3	19.9	19.3	16.9
28	M	8.3	11.2	13.7	20.7	21.8	22.7	23.2	23.6	23.7	23.7	23.3	22.6	22.0	21.2	19.6	16.1
29	F	7.2	10.3	12.9	19.2	19.7	19.9	20.0	19.9	19.6	19.4	19.2	19.1	18.9	18.7	18.2	15.4
30	M	10.2	12.8	14.9	21.8	22.6	23.1	23.2	23.2	23.1	23.1	23.0	22.5	22.1	21.5	20.2	17.5
31	F	8.7	11.3	13.7	18.9	20.3	21.1	21.6	21.9	22.0	22.0	21.9	21.6	21.2	20.5	19.4	16.1
32	F	3.6	8.2	10.6	18.4	19.4	20.0	20.3	20.5	20.5	20.2	19.6	18.4	17.6	16.6	15.6	12.4
33	M	10.9	13.0	15.2	22.9	23.9	24.5	24.9	25.0	25.0	24.8	24.5	23.9	23.5	22.8	21.4	18.0
34	F	7.9	10.3	12.2	18.2	19.2	19.8	20.3	20.6	20.8	20.8	20.7	20.2	19.8	19.3	18.1	15.1
35	F	5.9	9.3	11.9	17.4	18.6	19.6	20.2	20.5	20.6	20.4	20.2	19.8	19.4	19.0	18.1	15.2
36	M	9.7	12.1	14.2	21.6	22.5	23.1	23.6	24.0	24.3	24.5	24.1	23.3	22.7	21.7	19.7	18.4
37	M	6.7	10.0	12.7	23.1	23.7	24.3	25.0	25.5	25.9	26.0	25.7	24.7	24.0	23.0	21.5	18.1
38	M	7.4	10.0	11.9	21.0	21.4	21.7	22.0	22.3	22.4	22.5	22.4	22.0	21.6	21.0	20.3	16.7
39	M	8.8	11.1	13.1	21.9	22.6	23.0	23.4	23.7	23.8	23.5	22.7	21.7	21.0	19.9	18.8	15.2
40	M	8.2	10.9	13.4	19.5	20.3	20.9	21.5	21.8	22.1	22.1	21.9	21.5	21.1	20.5	19.6	17.5
41	M	12.1	13.9	15.6	21.4	22.5	23.4	24.1	24.6	24.9	25.0	24.9	24.2	23.5	22.6	21.3	18.0
42	M	8.5	11.0	12.8	20.8	21.7	22.2	22.5	22.8	22.9	23.0	22.6	21.6	20.8	19.8	18.1	16.2
43	M	8.2	10.5	12.4	23.3	23.7	24.1	24.4	24.7	24.8	24.7	24.0	22.1	21.1	19.9	18.6	16.0
44	M	7.1	11.2	14.0	22.9	23.7	24.4	25.0	25.4	25.8	25.9	25.7	24.8	24.0	22.8	21.0	17.0
45	M	15.5	17.0	18.6	24.3	25.8	26.4	26.7	26.9	26.9	26.9	26.7	26.1	25.5	24.6	23.4	20.6
46	M	7.9	11.5	14.3	23.5	24.1	24.5	24.8	24.9	24.9	24.9	24.6	24.3	23.7	22.9	21.4	18.9
47	M	8.5	10.9	13.1	21.8	22.7	23.4	23.8	24.2	24.4	24.3	23.8	23.0	22.5	21.8	20.6	16.8
48	M	9.6	12.5	14.9	22.5	23.5	24.4	25.2	25.8	26.3	26.5	26.1	25.2	24.4	23.4	22.0	18.6
49	M	9.8	12.4	14.6	23.5	24.2	24.6	24.8	24.9	24.8	24.6	24.2	23.5	23.0	22.3	21.2	19.4
50	M	9.8	12.1	14.4	23.2	23.8	24.2	24.5	24.8	25.0	25.0	24.5	23.5	22.8	21.9	20.9	18.4

* Grey percentages indicate the offset of the ellipse fitted cross section relative to proximal end of the radius expressed as a percentage of overall radial head height.

Table D.3: Lateral ellipse center offset (mm) relative to the deepest point for each cross section for all specimens.

#	Sex	DISH			CIRCUMFERENCE												Rim
		15%	10%	5%	100%	90%	80%	70%	60%	50%	40%	30%	20%	15%	10%	5%	0%
1	M	0.5	0.7	0.9	-0.4	-0.2	0.1	0.2	0.3	0.3	0.2	0.1	0.1	0.3	0.4	0.5	1.2
2	F	0.3	0.4	0.4	-0.3	-0.4	-0.3	-0.3	-0.1	0.0	0.2	0.3	0.4	0.4	0.4	0.5	0.6
3	M	1.3	1.3	1.2	0.6	0.8	1.0	1.2	1.2	1.1	1.0	0.9	0.9	0.9	0.8	1.0	1.0
4	M	-0.3	-0.3	-0.2	-1.1	-0.8	-0.6	-0.4	-0.3	-0.3	-0.3	-0.4	-0.6	-0.6	-0.6	-0.6	-0.7
5	F	0.3	0.4	0.5	-0.1	0.0	0.1	0.2	0.3	0.3	0.3	0.3	0.3	0.3	0.3	0.4	0.3
6	F	1.0	1.0	1.0	0.9	1.1	1.2	1.3	1.2	1.2	1.1	1.0	0.9	0.9	0.9	0.9	1.0
7	F	0.3	0.3	0.4	-0.1	0.1	0.2	0.3	0.4	0.4	0.4	0.4	0.4	0.3	0.4	0.4	0.5
8	M	-0.3	-0.2	-0.2	-0.8	-0.7	-0.7	-0.6	-0.5	-0.5	-0.6	-0.6	-0.6	-0.6	-0.5	-0.5	-0.5
9	F	0.4	0.5	0.5	-0.3	-0.1	0.1	0.2	0.3	0.3	0.3	0.3	0.3	0.3	0.3	0.3	0.3
10	F	0.1	0.1	0.1	-0.6	-0.3	-0.2	0.0	0.1	0.2	0.2	0.2	0.2	0.2	0.2	0.2	0.3
11	M	-0.7	-0.7	-0.8	-2.0	-1.8	-1.7	-1.7	-1.7	-1.7	-1.7	-1.8	-1.7	-1.7	-1.6	-1.5	-1.3
12	M	-1.4	-1.5	-1.4	-0.5	-0.4	-0.5	-0.5	-0.5	-0.5	-0.7	-0.9	-1.2	-1.3	-1.6	-1.7	-1.8
13	M	0.5	0.5	0.7	0.6	0.7	0.7	0.8	0.8	0.8	0.9	0.9	1.0	1.0	1.0	1.0	1.0
14	M	1.4	1.5	1.5	1.5	1.6	1.7	1.6	1.6	1.5	1.4	1.4	1.4	1.4	1.4	1.5	1.4
15	F	0.2	0.2	0.0	0.2	0.3	0.4	0.4	0.4	0.4	0.4	0.4	0.4	0.4	0.3	0.3	0.1
16	F	0.1	-0.2	-0.4	-0.8	-0.7	-0.5	-0.3	-0.1	0.1	0.2	0.3	0.3	0.2	0.2	0.2	-0.3
17	M	0.3	0.3	0.3	-0.5	-0.1	0.3	0.7	0.9	1.0	1.0	0.9	0.8	0.7	0.6	0.5	0.3
18	M	0.1	-0.6	-0.6	-1.5	-1.2	-1.0	-0.9	-0.9	-0.9	-1.0	-1.1	-1.1	-1.1	-1.2	-1.1	-0.8
19	M	0.3	0.2	0.6	0.5	0.6	0.7	0.7	0.6	0.5	0.4	0.2	0.2	0.1	0.2	0.2	0.5
20	M	0.2	0.4	0.7	0.7	1.0	1.2	1.2	1.2	1.2	1.1	1.0	0.9	0.8	0.8	0.9	0.8
21	M	0.1	0.3	0.2	-0.4	-0.1	0.1	0.2	0.1	0.1	0.0	-0.1	-0.1	-0.1	-0.1	0.1	0.1
22	M	0.3	0.2	0.3	0.2	0.3	0.4	0.4	0.4	0.3	0.2	0.2	0.2	0.2	0.3	0.3	0.4
23	M	-0.3	-0.3	-0.4	0.5	0.7	0.9	0.9	0.9	0.9	0.8	0.6	0.5	0.4	0.3	0.2	-0.2
24	M	-0.6	-0.6	-0.6	-1.1	-0.6	-0.4	-0.4	-0.3	-0.4	-0.5	-0.7	-0.8	-0.9	-0.9	-0.9	-0.6
25	F	-0.1	0.0	0.0	-0.3	-0.3	-0.3	-0.1	0.0	0.0	0.1	0.1	0.0	0.0	0.0	-0.1	-0.2
26	F	0.6	0.7	0.8	0.9	0.9	0.9	1.0	1.0	1.1	1.0	1.0	0.9	0.9	0.9	0.9	0.9
27	F	0.6	0.6	0.5	0.7	0.8	0.9	0.9	0.9	0.9	1.0	1.0	1.0	0.9	0.9	0.8	0.7
28	M	0.7	0.7	0.6	0.5	0.6	0.7	0.8	0.8	0.7	0.7	0.6	0.6	0.6	0.5	0.5	0.6
29	F	-0.2	-0.1	-0.1	-0.5	-0.3	-0.2	-0.2	-0.2	-0.2	-0.2	-0.2	-0.2	-0.2	-0.2	-0.2	0.0
30	M	0.1	0.1	0.2	-0.4	0.0	0.2	0.3	0.4	0.5	0.5	0.4	0.3	0.2	0.1	-0.1	0.0
31	F	0.9	1.1	1.3	1.1	1.5	1.6	1.7	1.6	1.5	1.4	1.3	1.2	1.2	1.2	1.2	1.4
32	F	-0.2	-0.3	-0.3	-0.8	-0.6	-0.6	-0.6	-0.6	-0.6	-0.7	-0.8	-0.8	-0.8	-0.8	-0.7	-0.6
33	M	0.1	0.2	0.2	-0.8	-0.3	-0.1	0.0	0.1	0.1	0.1	0.0	-0.1	-0.2	-0.2	-0.2	-0.2
34	F	-1.0	-0.9	-0.9	-1.3	-1.2	-1.1	-1.0	-1.0	-1.0	-0.9	-1.0	-1.0	-1.0	-1.0	-1.0	-0.7
35	F	0.4	0.4	0.5	-0.1	0.2	0.6	0.9	0.9	0.9	0.8	0.8	0.8	0.8	0.8	0.8	0.4
36	M	0.1	0.1	0.1	-0.7	-0.6	-0.5	-0.5	-0.4	-0.4	-0.4	-0.5	-0.6	-0.6	-0.6	-0.6	-0.2
37	M	0.1	0.2	0.0	-0.6	-0.3	-0.1	0.1	0.2	0.2	0.2	0.2	0.1	0.1	0.1	0.1	0.2
38	M	-1.0	-1.2	-1.3	-1.5	-1.5	-1.4	-1.3	-1.2	-1.1	-1.0	-1.0	-1.0	-1.0	-1.0	-1.0	-1.0
39	M	0.7	0.6	0.7	0.8	0.9	0.9	0.9	1.0	0.9	0.9	0.7	0.7	0.7	0.8	0.5	0.7
40	M	0.5	0.5	0.4	0.3	0.4	0.6	0.8	0.8	0.9	0.8	0.8	0.7	0.6	0.5	0.4	0.2
41	M	0.0	-0.2	-0.3	-0.4	-0.3	-0.3	-0.3	-0.3	-0.3	-0.3	-0.3	-0.2	-0.2	-0.2	-0.2	-0.4
42	M	-0.4	-0.7	-0.8	-0.9	-0.9	-0.8	-0.8	-0.7	-0.7	-0.7	-0.7	-0.7	-0.7	-0.7	-0.6	-0.6
43	M	0.3	0.5	0.0	-0.2	0.0	0.1	0.1	0.1	0.2	0.2	0.2	-0.1	-0.1	-0.1	0.1	0.1
44	M	-0.2	0.0	0.1	0.7	0.8	0.8	0.9	0.9	0.9	0.9	0.8	0.8	0.7	0.6	0.5	0.3
45	M	-0.3	-0.2	-0.2	-0.8	-0.2	0.2	0.5	0.7	0.7	0.7	0.6	0.3	0.2	0.1	-0.1	-0.2
46	M	-0.4	-0.3	-0.2	-0.6	-0.4	-0.3	-0.2	-0.2	-0.2	-0.3	-0.4	-0.4	-0.5	-0.5	-0.6	-0.2
47	M	-0.2	-0.2	-0.2	-0.6	-0.4	-0.3	-0.3	-0.3	-0.3	-0.4	-0.4	-0.4	-0.4	-0.4	-0.4	-0.4
48	M	-0.4	-0.4	-0.5	-1.4	-1.1	-0.9	-0.8	-0.7	-0.7	-0.7	-0.7	-0.7	-0.6	-0.6	-0.6	-0.7
49	M	-1.3	-1.4	-1.5	-2.0	-1.7	-1.6	-1.6	-1.6	-1.6	-1.7	-1.8	-1.9	-1.9	-2.0	-2.0	-1.7
50	M	-0.4	-0.5	-0.6	-0.8	-0.7	-0.6	-0.6	-0.6	-0.6	-0.6	-0.7	-0.8	-0.8	-0.8	-0.7	-0.7

* Grey percentages indicate the offset of the ellipse fitted cross section relative to proximal end of the radius expressed as a percentage of overall radial head height.

Table D.4: Anterior ellipse center offset (mm) relative to the deepest point for each cross section for all specimens.

#	Sex	DISH			CIRCUMFERENCE												Rim
		15%	10%	5%	100%	90%	80%	70%	60%	50%	40%	30%	20%	15%	10%	5%	0%
1	M	0.9	1.4	1.5	3.9	3.6	3.4	3.2	3.1	3.0	3.0	3.0	3.2	3.3	3.3	3.0	2.3
2	F	-0.2	-0.4	-0.6	1.7	1.7	1.5	1.3	1.1	0.8	0.7	0.5	0.3	0.3	0.2	0.0	-0.6
3	M	1.3	1.5	1.6	3.7	3.4	3.1	2.8	2.6	2.6	2.6	2.6	2.7	2.6	2.5	2.4	2.0
4	M	1.7	1.7	1.7	3.4	3.2	3.0	2.8	2.7	2.7	2.6	2.7	2.7	2.7	2.7	2.6	2.4
5	F	0.3	0.3	0.2	1.6	1.5	1.4	1.3	1.2	1.2	1.2	1.3	1.3	1.2	1.2	1.0	0.9
6	F	0.6	0.7	0.7	1.9	1.8	1.6	1.6	1.6	1.6	1.7	1.8	1.9	1.9	1.8	1.7	1.4
7	F	0.3	0.3	0.2	1.1	1.1	1.0	0.9	0.9	0.9	0.9	0.9	0.9	0.9	0.8	0.6	0.4
8	M	2.0	2.0	2.0	3.3	3.2	3.1	3.0	2.9	2.8	2.8	2.8	2.8	2.9	2.9	2.8	2.5
9	F	0.1	0.1	0.1	1.5	1.4	1.3	1.2	1.1	1.1	1.1	1.1	1.0	0.9	0.8	0.7	0.6
10	F	0.9	1.0	1.0	2.0	1.8	1.6	1.4	1.4	1.3	1.3	1.3	1.3	1.3	1.4	1.4	1.3
11	M	0.8	0.8	1.2	3.1	2.8	2.8	2.9	3.0	3.1	3.2	3.4	3.4	3.3	3.1	2.6	2.4
12	M	1.0	1.0	1.1	3.2	2.8	2.5	2.5	2.5	2.5	2.6	2.7	2.8	2.8	2.8	2.2	2.8
13	M	1.2	1.6	1.6	4.4	3.9	3.5	3.2	3.0	2.9	2.7	2.7	2.7	2.6	2.5	2.3	2.1
14	M	0.9	0.9	1.0	2.6	2.5	2.4	2.3	2.3	2.4	2.4	2.4	2.4	2.3	2.1	1.9	1.4
15	F	-0.2	0.0	0.1	1.3	1.1	1.0	0.9	0.9	0.9	0.8	0.8	0.8	0.7	0.6	0.5	0.2
16	F	0.0	-1.1	-1.2	1.4	1.2	0.8	0.4	0.2	0.1	0.1	0.1	0.3	0.3	0.4	0.2	-0.7
17	M	-0.9	-1.1	-1.0	0.1	-0.2	-0.5	-0.7	-0.8	-0.8	-0.8	-0.6	-0.4	-0.3	-0.3	-0.4	-0.7
18	M	0.3	0.1	0.1	2.4	2.1	1.7	1.5	1.4	1.4	1.5	1.6	1.6	1.6	1.5	1.2	0.6
19	M	0.2	0.1	0.1	0.5	0.3	0.3	0.3	0.3	0.4	0.5	0.6	0.6	0.7	0.6	0.4	0.2
20	M	0.0	-0.1	0.0	1.6	1.3	1.1	0.9	0.9	1.0	1.0	1.0	0.8	0.7	0.5	0.4	0.3
21	M	0.3	0.2	0.2	1.6	1.3	1.1	1.0	1.1	1.1	1.2	1.2	1.3	1.2	1.0	0.8	0.4
22	M	0.4	0.2	0.1	0.9	0.6	0.5	0.4	0.4	0.4	0.5	0.6	0.6	0.6	0.5	0.5	0.2
23	M	0.1	0.1	0.5	1.7	1.7	1.6	1.5	1.4	1.4	1.4	1.5	1.6	1.7	1.6	1.6	1.1
24	M	0.6	0.7	0.8	1.9	1.8	1.6	1.5	1.6	1.6	1.7	1.8	1.8	1.9	1.9	1.9	1.3
25	F	0.6	0.8	1.0	2.0	2.0	1.9	1.8	1.7	1.6	1.6	1.7	1.7	1.8	1.8	1.7	1.5
26	F	1.0	1.1	1.1	2.0	1.9	1.8	1.8	1.7	1.7	1.8	1.8	1.8	1.8	1.8	1.6	1.2
27	F	-0.2	-0.1	-0.1	0.3	0.3	0.3	0.2	0.1	0.0	-0.1	-0.1	-0.1	-0.1	-0.1	-0.1	-0.1
28	M	0.3	0.2	0.1	1.8	1.5	1.3	1.1	1.2	1.3	1.3	1.4	1.5	1.5	1.3	1.0	0.4
29	F	0.2	0.2	0.1	1.5	1.3	1.1	1.0	0.9	0.9	1.0	1.1	1.1	1.0	1.0	1.0	0.5
30	M	1.5	1.5	1.7	2.5	2.2	2.1	1.9	1.9	1.9	1.9	2.0	2.0	2.1	2.1	1.9	1.8
31	F	0.5	0.5	0.7	1.8	1.5	1.3	1.3	1.3	1.3	1.4	1.4	1.5	1.5	1.5	1.3	1.0
32	F	0.4	0.6	0.6	1.8	1.5	1.4	1.3	1.3	1.3	1.4	1.5	1.5	1.4	1.4	1.3	1.0
33	M	1.6	1.6	1.7	2.9	2.7	2.5	2.3	2.3	2.2	2.2	2.3	2.4	2.4	2.5	2.4	2.1
34	F	0.5	0.5	0.5	1.3	1.2	1.0	1.0	0.9	1.0	1.0	1.1	1.2	1.2	1.2	1.2	0.8
35	F	-0.8	-0.8	-0.6	1.6	1.2	0.9	0.8	0.8	0.8	0.9	0.9	0.8	0.8	0.6	0.5	-0.1
36	M	1.5	1.4	1.3	2.6	2.4	2.2	2.1	2.0	2.0	2.0	2.0	2.1	2.2	2.2	2.2	2.0
37	M	0.5	0.6	0.6	2.5	2.2	1.9	1.7	1.6	1.7	1.8	1.9	2.0	2.0	1.9	1.6	1.2
38	M	-0.6	-0.7	-0.6	0.3	0.0	-0.3	-0.5	-0.5	-0.5	-0.5	-0.5	-0.4	-0.3	-0.2	-0.2	-0.3
39	M	-0.4	-0.3	-0.4	0.9	0.8	0.7	0.6	0.5	0.5	0.5	0.6	0.6	0.6	0.5	0.4	-0.3
40	M	0.6	0.7	0.6	1.9	1.6	1.4	1.3	1.2	1.2	1.2	1.2	1.3	1.3	1.3	1.2	0.9
41	M	0.6	0.6	0.7	2.6	2.4	2.3	2.2	2.1	2.1	2.1	2.1	2.0	1.9	1.8	1.6	1.3
42	M	0.4	0.5	0.5	2.3	2.2	2.0	1.9	1.9	1.8	1.8	1.7	1.7	1.5	1.4	1.2	0.9
43	M	0.3	0.5	0.9	1.8	1.7	1.7	1.6	1.6	1.6	1.7	1.7	1.6	1.6	1.5	1.4	1.0
44	M	-0.1	-0.2	-0.3	1.5	1.3	1.2	1.1	1.0	1.0	1.0	1.0	1.0	1.0	0.8	0.5	-0.1
45	M	0.1	0.1	0.1	2.6	2.1	1.6	1.3	1.1	1.0	1.0	0.9	0.9	0.8	0.7	0.6	0.5
46	M	-0.2	0.1	0.3	2.2	1.9	1.7	1.5	1.5	1.5	1.7	1.9	2.1	2.1	2.2	2.1	1.5
47	M	0.1	0.0	-0.2	0.9	0.7	0.6	0.5	0.5	0.5	0.6	0.7	0.6	0.6	0.5	0.4	0.0
48	M	0.1	0.0	-0.2	1.1	0.9	0.7	0.6	0.6	0.6	0.7	0.8	0.9	0.8	0.7	0.4	0.1
49	M	0.9	0.9	0.9	1.6	1.6	1.5	1.5	1.5	1.5	1.6	1.6	1.7	1.8	1.8	1.8	1.6
50	M	0.4	0.4	0.4	1.9	1.6	1.4	1.4	1.3	1.2	1.2	1.3	1.3	1.3	1.3	1.1	1.0

* Grey percentages indicate the offset of the ellipse fitted cross section relative to proximal end of the radius expressed as a percentage of overall radial head height.

Table D.5: Orientation angle (°) of major diameter relative to lateral vector for each cross section for all specimens.

#	Sex	DISH			CIRCUMFERENCE												Rim
		15%	10%	5%	100%	90%	80%	70%	60%	50%	40%	30%	20%	15%	10%	5%	0%
1	M	67	57	43	104	104	103	105	106	106	108	114	124	132	134	135	146
2	F	29	36	35	103	101	97	93	91	91	91	92	94	94	95	96	74
3	M	61	51	31	113	111	111	112	113	114	113	110	109	110	111	110	108
4	M	105	95	79	101	98	99	98	102	103	104	104	108	111	115	117	121
5	F	106	115	128	91	75	69	67	68	72	82	87	90	92	94	94	115
6	F	138	73	47	95	93	94	95	93	92	90	89	90	90	91	91	90
7	F	132	165	174	171	26	45	49	56	70	85	94	94	93	92	94	111
8	M	111	124	159	94	93	97	105	106	109	106	104	103	102	101	102	114
9	F	149	141	175	108	104	98	96	97	97	98	97	95	95	95	99	103
10	F	38	42	39	83	77	76	78	83	87	89	89	90	91	93	98	70
11	M	54	68	80	88	88	90	92	90	80	66	40	11	7	179	172	153
12	M	116	114	113	111	109	109	117	147	157	165	84	110	113	135	134	112
13	M	34	79	156	36	37	37	38	38	37	33	32	30	33	36	37	19
14	M	151	177	3	84	83	83	83	82	80	78	74	72	70	71	70	61
15	F	47	31	1	83	86	92	97	101	101	96	91	88	83	83	81	68
16	F	59	47	23	100	86	76	74	78	83	87	89	90	86	84	77	49
17	M	110	99	91	98	86	80	81	87	94	101	106	107	107	111	122	121
18	M	85	102	111	79	74	83	83	84	86	85	79	76	70	64	49	91
19	M	80	62	40	104	102	104	111	111	110	108	109	112	114	116	116	118
20	M	109	103	99	79	84	92	100	109	112	115	122	125	123	123	122	120
21	M	125	13	4	84	86	88	94	100	102	102	103	105	105	104	101	98
22	M	104	119	169	82	81	85	89	92	93	92	88	87	85	85	85	98
23	M	113	121	119	109	105	105	108	113	119	123	119	102	92	85	81	110
24	M	132	134	16	102	96	92	94	98	99	96	98	105	110	112	113	97
25	F	1	11	11	116	102	87	81	81	85	91	98	108	106	99	95	105
26	F	14	20	5	97	94	92	89	89	87	85	83	82	82	80	77	73
27	F	129	128	128	122	118	112	100	91	87	87	90	95	105	116	150	6
28	M	78	15	9	85	77	83	92	93	93	92	88	87	86	86	84	81
29	F	149	146	176	114	62	54	65	85	92	95	98	98	95	86	83	45
30	M	81	74	59	113	112	115	118	121	122	121	118	117	116	115	117	115
31	F	107	114	110	96	97	95	98	101	104	102	101	95	92	89	85	76
32	F	160	53	17	111	105	101	102	103	103	105	104	103	103	103	105	105
33	M	94	79	57	82	80	87	98	106	110	112	110	109	109	110	106	120
34	F	82	64	49	102	91	87	84	89	94	100	104	111	113	116	118	107
35	F	96	89	112	76	69	58	53	53	85	93	101	106	107	104	87	135
36	M	81	67	43	102	98	95	95	95	101	103	101	101	101	105	110	105
37	M	75	65	55	58	56	61	65	66	68	72	67	63	62	58	48	58
38	M	68	48	41	67	54	57	64	64	68	155	176	20	21	30	9	24
39	M	176	10	4	83	74	66	65	69	79	81	77	75	75	76	78	80
40	M	106	103	94	98	86	87	94	101	105	107	108	110	110	112	116	102
41	M	115	118	146	46	42	38	41	51	62	66	68	73	72	72	69	92
42	M	59	21	15	94	88	89	92	93	96	98	102	101	103	105	107	105
43	M	48	34	76	87	78	74	73	74	75	80	93	101	101	104	106	105
44	M	60	68	122	75	63	59	59	69	73	75	71	67	69	71	68	73
45	M	82	84	83	119	93	95	95	107	122	128	128	122	125	119	117	106
46	M	97	94	72	96	95	94	97	97	98	100	103	111	126	132	134	122
47	M	71	72	66	88	79	70	68	69	70	67	61	59	59	63	78	74
48	M	142	54	42	69	65	63	62	62	66	73	83	82	84	90	94	69
49	M	84	56	44	124	122	122	124	125	125	123	120	118	118	119	119	107
50	M	146	116	97	94	84	81	83	82	82	86	88	90	94	96	97	123

* Grey percentages indicate the offset of the ellipse fitted cross section relative to proximal end of the radius expressed as a percentage of overall radial head height.

Table D.6: Radial head height (mm) and dish depth (mm) for all specimens.

#	Sex	Height	Depth
1	M	1.7	9.50
2	F	1.8	8.25
3	M	2.2	9.75
4	M	2.5	10.00
5	F	1.7	7.75
6	F	1.7	8.25
7	F	1.7	7.75
8	M	2.4	8.75
9	F	2.1	8.25
10	F	2.0	8.25
11	M	2.2	9.00
12	M	2.9	9.50
13	M	2.0	9.25
14	M	1.7	8.25
15	F	1.9	8.50
16	F	1.5	10.25
17	M	1.6	9.00
18	M	1.6	10.50
19	M	2.1	9.25
20	M	2.1	10.50
21	M	1.7	8.75
22	M	1.8	9.75
23	M	1.9	8.50
24	M	2.4	10.50
25	F	1.5	7.50
26	F	1.9	8.00
27	F	2.2	8.25
28	M	2.0	9.00
29	F	1.8	9.00
30	M	2.2	9.00
31	F	1.9	8.50
32	F	1.4	8.50
33	M	2.1	8.50
34	F	1.7	8.00
35	F	1.7	9.00
36	M	1.9	8.75
37	M	1.9	9.75
38	M	1.6	7.75
39	M	1.9	8.25
40	M	1.8	8.00
41	M	2.6	9.00
42	M	1.9	8.25
43	M	1.8	8.00
44	M	1.8	9.25
45	M	3.5	10.00
46	M	1.7	8.50
47	M	2.0	8.75
48	M	2.2	9.50
49	M	1.9	8.50
50	M	2.2	9.00